Brownian Dynamics Simulation of Dusty Plasma: Comparison with Generalized Hydrodynamics

by

Nitin Upadhyaya

A thesis
presented to the University of Waterloo
in fulfillment of the
thesis requirement for the degree of
Master of Mathematics
in
Applied Mathematics

Waterloo, Ontario, Canada, 2010

I hereby declare that I am the sole author of this thesis. This is a true copy of the thesis, including any required final revisions, as accepted by my examiners.

I understand that my thesis may be made electronically available to the public.

Nitin Upadhyaya

Abstract

Brownian dynamics (BD) simulation method has been widely used for studying problems in dispersed systems, such as polymer solutions, colloidal suspensions and more recently, complex (dusty) plasmas. The main problem addressed with this simulation technique is that of time scale separation, which occurs when one form of motion in the system is much faster than the other. This can be a serious problem in Molecular dynamics (MD) simulation where very short time steps are needed to handle the fast motions and thus, requiring very long time runs for the proper evolution of slower modes making the simulation very expensive. More importantly, the fast motions may not be of much interest within themselves, as will be the case in a dusty plasma. The motion of neutral atoms or molecules comprising the plasma occurs at a very fast time scale with respect to the motion of dust particles, and is usually of very little interest, though a large number of such neutrals are present.

In such cases, an approximate method is usually adopted, whereby the neutral particles are omitted from the simulation and their effect upon the dynamics of dust particles modeled by a combination of random forces and frictional terms. This leads to a recasting of the Newton's Equation of motion solved in MD, to a Langevin equation, solved in BD. Adopting this approach, we simulate a system of charged dust particles interacting via Yukawa potential in a 2-Dimensional layer, and extract relevant equilibrium statistical features such as the radial distribution function, static structure factor and the low frequency dust wave modes.

We then propose the use of a Generalized Hydrodynamical (GH) approach to provide a semi-analytical model for the dust collective modes, which not only provides us with good predictions of the wave dispersion but also provides reasonable estimates for wave-number dependent wave damping, both of which will be compared against the results obtained from BD simulation.

Finally, through our simulations, we also observe the equilibrium configuration of dust particles in the presence of cold ions streaming perpendicularly into the 2-Dimensional layer of dust particles. This provides us with novel results in the regime of sub-sonic ion flow speeds.

Acknowledgements

Foremost, its a privilege to thank Professor Z. L. Mišković for all the guidance and support he has provided throughout my graduate studies. I will forever be grateful for his patience and kindness, in the process providing me with a new and exciting direction in life.

I would then like to thank the readers of this thesis, Professor Zoran Miskovic, Professor Matthew Scott and Professor Francis Poulin for sparing their time to be on the committee and provide valuable suggestions.

Next, I would like to thank Dr. L.J. Hou for some very useful discussions during the course of simulation work.

I was also fortunate to attend some very inspiring lectures by Professor Kevin Lamb, Professor Matthew Scott and Professor Robert Wickham as part of the courses I did under them.

I would also like to thank Miss Helen Warren, for her support right from the time of my application for graduate studies. Many thanks also to Miss Rina Salazar and Miss Helen Chen for all their help.

A special thanks to all the anonymous people who share their experience and expertise on the web, and help immensely in accomplishing a lot of work.

Finally, I would like to thank my long time friend Srinath, for his suggestion to apply to the University of Waterloo and for his company here.

To my Parents and Hanuman Ji.

Contents

List of Figures

Chapter 1

Introduction

This thesis will address the equilibrium collective behavior of a many body system with particles interacting via a continuous form of inter-particle potential. We will obtain and describe the particular collective modes of interest to us from two seemingly different points of view. On the one hand, we will treat the many body system as a collection of point particles interacting pair-wise with the given potential and conduct a numerical study of the system via Brownian dynamics (BD) simulation to extract its equilibrium collective behavior. On the other hand, for a theoretical study we will describe the many body system as forming a continuum medium (fluid) interacting pair-wise with the same form of potential as in BD, and subsequently attempt to describe its collective behavior using the hydrodynamic approach. Finally, we will compare the description of collective modes predicted by both the approaches.

The entire work will be carried out for a two dimensional system of dusty plasma with particles interacting via the Yukawa potential, although as motivated above, the work may be treated in a more general context. The simulation approach and the particular theoretical tools employed in our study of dust wave dispersion and damping may be regarded as being an extension (or application) of a rich body of work, originally developed and subsequently adapted in various forms by many illustrious people (as will be cited in appropriate places), for systems of Lennard-Jones fluids, colloidal suspensions, one component plasma (OCP) and ionic mixtures. Thus, an identical approach may be adopted to study a variety of similar systems. Needless to say, any successes are further indications of the strength of previous work done by the main contributors to this theory and any errors or misinterpretations, are solely mine.

We now proceed to introduce the particular system of dusty plasma and motivate the work to follow more specifically.

The term *Plasma* [2] represents a macroscopically neutral gas, consisting of many interacting charged particles (electrons and ions) and neutral atoms or molecules (neutrals). In most cases, a plasma coexists with external particles that are much more massive (typically sub-micron to micron sized) than the

constituent plasma particles, and these particles are referred to as dust particles. Depending on their interaction with the surrounding plasma environment, the dust particles acquire either a negative or positive charge. This mixture of charged dust (macro) particles, electrons, ions and neutrals is called a dusty (complex) plasma, where the presence of dust particles introduces several new features and complexities, particularly due to the vastly different length and time scales that they bring in[1].

Interest in the study of dusty plasmas arises due to their presence in a variety of conditions, ranging from astrophysical environments (such as planetary ring systems, meteoric dust), volcanic eruptions and in industrial applications, such as, in micro-electronics fabrication. Theoretically, complex plasmas are often characterized as a class of materials called soft matter, and the inherent complexity of such systems provides for rich physical behavior. In this particular case, many of the interesting properties belonging to this class of materials (such as collective modes, phase transitions [2]) becomes readily accessible to observation and study by the relatively greater ease with which the system of complex plasma can be setup in laboratory environment.

In many of the laboratory experiments, the dust grains acquire a very large negative charge (of the order of 10^3 electrons or more), and due to the small separation between dust grains, the ratio of their average electrostatic potential energy to the thermal energy exceeds unity. The resulting system is therefore called a strongly coupled dusty plasma (SCDP)[2], and the strong coupling leads to the formation of ordered structures, a characteristic of liquid and solid states.

The theoretical predictions, and subsequent verification through experiments, of low frequency dust collective modes known as the dust acoustic waves (DAW) and the Coulomb crystallization of dust particles, gave a major boost to the study of dusty plasma. The former were predicted by Shukla [3], and due to the low frequency (10-1100 Hz) nature of these wave modes, laboratory experiments were able to record these wave modes via video imaging. We will discuss more about these modes later in this work. For SCDP's, theoretical predictions of Coulomb crystallization of charged dust grains interacting through a form of short ranged shielded Coulomb potential, known in literature as Debye-Huckel or Yukawa potential, were first made by Izeka [3]. These were also verified later through laboratory experiments. As an example, a typical experimental setup discussed by Morfill *et al.* [4] consists of horizontally aligned planar electrodes, enclosing a plasma region, whereby dust particles in the form of formaldehyde spheres can be introduced into the plasma region. The dust particles are observed to form organized planar structures parallel to the electrodes (multiple layers together may form a thin disk shaped cloud), just over the lower electrode. The boundary region between the bulk plasma and lower electrode is known as the sheath region and the cloud of dust particles remains suspended in this region by a balance between the electrostatic force ex-

[1]Although the parameters vary a lot according to the experimental setups used, as an example, we may have plasma formed at a temperature of $\sim$ 2300K with singly charged Potassium ions (K^+, radius $\sim 150pm$) and dust particles composed of Aluminum Oxide (Al_2O_3) with charge $\sim 10^3$e and radius $\sim 10\mu$m [2] where e is elementary charge.

[2]In a typical *plasma*, the situation is opposite: The thermal energy of constituent particles is usually much greater that the average electrostatic potential energy

erted by the electrode and gravitational force. A pictorial representation of the setup is given in Figure 1.1.

The sheath region is often associated with high electric fields, plasma density gradients and ion flow perpendicular to the sheath. A study by Vladimirov and Nambu [5] analyzed the effects of this ion flow on the inter-particle potential between dust grains and reported that a finite speed of ion flow can cause attraction between dust grains in the direction of ion flow due to an oscillatory potential called Wake potential. In particular, they considered the dust particles as forming a static background with ions streaming down in the sheath region and showed that, if the velocity of ion flow exceeds a certain threshold, the dust particles vertically below may get trapped in the potential wells of the resulting oscillatory wake potential. Due to its long ranged nature, such a potential may dominate over the short ranged Yukawa potential in the interaction between dust grains in the vertical direction. This further complicates the analysis of 3D dust structures considerably.

For such laboratory generated dusty plasmas, the study of 2D SCDP's has thus been particularly favored in recent years, since this allows us to ignore the complications arising from downstream ion flows and focus on the inter-particle interaction between dust grains within a plane, which has so far been assumed to be governed by the short ranged Yukawa potential. Further, such a system is easier to simulate on a computer and therefore, complements experimental work very well.

Based on this brief background, in the major portion of the work to follow we shall focus on a 2D layer of dusty plasma governed by Yukawa type inter-particle potential. In the next chapter, we will briefly outline some basic features and important parameters of this system relevant to our work, and use those in our simulations and analytic work. However, towards the end of this work we will return to a simulation based analysis of the effect of ion flow with finite speed perpendicularly into a 2D layer of dusty plasma on the in-plane inter-particle potential between dust grains. This will be based on the theoretical developments reported by Hou *et al.* in 2001. [6, 7].

We next mention some relevant simplifications and assumptions made for the work to follow.

1.1 Assumptions

1.1.1 Simulation Assumptions

- The dust particles are modeled as point charge Brownian particles in a uniform, isotropic background of neutral atoms or molecules (neutrals).
- The charge on dust particles remains constant and the inter-particle interaction, assumed pair-wise, is governed by the Yukawa potential. Thus, the presence of ions and electrons is restricted to providing the static shielding via Yukawa potential, except when we explicitly model the effect of ion streaming and test the validity of using a Yukawa model for inter-particle potential in Chapter 6.

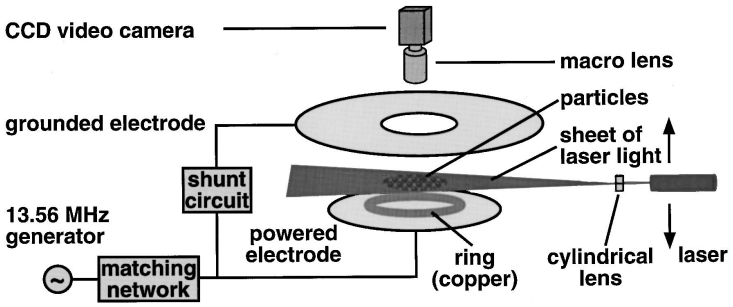

Figure 1.1: Pictorial representation of a laboratory setup to study 2D layer of dusty plasma suspended between horizontal electrodes. The region between the dust layer (being viewed through the cylindrical lens) and lower electrode is the sheath region. *Source*: Morfill *et al* [1].

- Dust waves are only a manifestation of the collective dynamics of dust particles, while the dynamics of collective modes of ions and electrons constituting the plasma, have no effect on them.
- Due to isotropy, statistical features, such as the static structure factor, current density and radial distribution function, only depend upon magnitude of wave-number k and magnitude of inter-particle separation r.

1.1.2 Theoretical Assumptions

- For the analytical models, the dust layer will be treated as forming a continuum, and the collective dynamics will be modeled by hydrodynamic equations. Thus, we will not be dealing with the kinetic theory description of plasma particles [8, 9, 10].
- We shall assume the existence of well defined transport coefficients, such as viscosity.
- We shall assume the existence of well defined thermodynamic properties, such as the isothermal compressibility [11].
- All random processes are assumed to be stationary and to satisfy the ergodic hypotheses [12].

1.2 Convention

- All bold face symbols signify vector quantities.
- All vector quantities, unless otherwise mentioned, are in Cartesian 2D (x, y) space.
- Whenever we explicitly switch from dimensional to non-dimensional variables, we will denote dimensional quantities with an overhead *bar*, while non-dimensional quantities as regular variables, without an overhead bar. This convention will thus be applied to all dynamical system variables and

dimensional tunable system parameters. Non-tunable system parameters and universal constants, both dimensional and non-dimensional will continue to appear as regular variables.

- Our use of the term Ordinary Hydrodynamics (OH) will refer to the continuity and momentum conservation equations, while Generalized Hydrodynamics (GH) will refer to the extension of OH that will satisfy frequency sum rules starting from the zeroth order frequency moment.
- Hydrodynamic model will also be referred to (but not developed) for charged species (to model charged dust particles in Chapter 2 and ion flow in Chapter 6). These have to be distinguished from any references to OH or GH.

1.3 Outline

The thesis will be organized as follows.

In Chapter 2, we will define the inter-particle Yukawa potential and present the relevant parameters characterizing the 2D system of dusty plasma. This will be followed by a brief discussion of the low frequency dust wave modes and a review of the theory of Brownian motion, including a derivation of the non-dimensional form of Langevin's equation to be used for the simulation work to follow.

Next, in Chapter 3 we will discuss the particular method used for the numerical integration of Langevin's equation. This will provide us with all the tools necessary to conduct a BD simulation study of the system of dusty plasma.

In Chapter 4, we will review the theory of hydrodynamics as used to obtain analytic estimates for the dust wave modes. This will motivate us to introduce Boon and Yip's theory of GH to obtain a more accurate semi-analytic formulation of not only the wave dispersion relation, but also for the wave-number dependent damping of these modes.

In Chapter 5, we will compare the results from BD simulation with those predicted from the GH approach.

Lastly, in Chapter 6 we will conduct a BD study of the effect of ion streaming into the layer of dusty plasma, and report the interesting new observations for subsonic ion flows.

Chapter 2

Background Work

In the following few sections, we will outline important features and parameters of the 2D layer of dusty plasma, and briefly review models for describing the dust particles collective dynamics providing the main motivations for our work. We will conclude with an overview of the theory of Brownian motion.

2.1 Yukawa Potential

When no external disturbance (force) is present, a plasma is macroscopically neutral, implying the absence of net electric charge in the system. Therefore the equilibrium charge neutrality condition reads

$$q_i n_{i0} = q_e n_{e0}, \tag{2.1}$$

where q_i, q_e are the charges on ions and electrons respectively, and n_{i0}, n_{e0} are the equilibrium number density of ions and electrons in the system. Consider now a single point charged dust particle. By this we mean that the size of the dust particle is much less than the screening length (to be defined shortly) and the average inter-particle separation between dust particles. Further, being highly charged with much greater size than the other constituent plasma particles, a dust particle has much greater inertia, and thus we can expect that it will attract opposite charges around it, forming a cloud of charged particles. Thus, if it is negatively charged (as is typically found), it will attract a cloud of mostly ions (assumed positive), which in turn will attract some electrons. The size of the cloud, i.e., its radial extent will typically be such that the particles at the edge of the cloud feel no electrostatic potential and have energies equal to their thermal energies. The Poisson's equation for this cloud is,

$$\nabla^2 \phi(\mathbf{R}) = 4\pi[q_e n_e(\mathbf{R}) - q_i n_i(\mathbf{R}) + q_d \delta(\mathbf{R})], \tag{2.2}$$

where ∇^2 represents the 3D Laplacian, $\mathbf{R}$ is 3D position vector and $\delta(\mathbf{R})$ denotes the location of point dust particle. Further, from equilibrium statistical mechanics, the density of electrons and ions in this cloud is governed by the Boltzmann distribution

$$n_e(\mathbf{R}) = n_{e0} e^{\frac{q_e \phi(\mathbf{R})}{k_B T_e}}, \tag{2.3a}$$

$$n_i(\mathbf{R}) = n_{i0} e^{-\frac{q_i \phi(\mathbf{R})}{k_B T_i}}. \tag{2.3b}$$

Assuming $\frac{q_e \phi(\mathbf{R})}{k_B T_e} \ll 1$ and $\frac{q_i \phi(\mathbf{R})}{k_B T_i} \ll 1$, we can expand the above equations in Taylor's series retaining up to first order terms, thus writing Eq. (2.2) as

$$\nabla^2 \phi(\mathbf{R}) = 4\pi \left[q_e n_{e0} \left(1 + \frac{q_e \phi(\mathbf{R})}{k_B T_e} \right) - q_i n_{i0} \left(1 - \frac{q_i \phi(\mathbf{R})}{k_B T_i} \right) + q_d \delta(\mathbf{R}) \right]. \tag{2.4}$$

Rearranging the terms and substituting Eq. (2.1), we obtain

$$\nabla^2 \phi(\mathbf{R}) = 4\pi \left(\frac{q_e^2 n_{e0} \phi(\mathbf{R})}{k_B T_e} + \frac{q_i^2 n_{i0} \phi(\mathbf{R})}{k_B T_i} \right) - 4\pi q_d \delta(\mathbf{R}). \tag{2.5}$$

If we define electron and ion Debye lengths as

$$\lambda_e = \sqrt{\frac{k_B T_e}{4\pi n_{e0} q_e^2}}, \tag{2.6a}$$

$$\lambda_i = \sqrt{\frac{k_B T_i}{4\pi n_{i0} q_i^2}}, \tag{2.6b}$$

and the total Debye length via

$$\lambda_D^{-2} = \lambda_e^{-2} + \lambda_i^{-2}, \tag{2.7}$$

we obtain from Eq. (2.5)

$$\nabla^2 \phi(\mathbf{R}) = \lambda_D^{-2} \phi(\mathbf{R}) + 4\pi q_d \delta(\mathbf{R}). \tag{2.8}$$

This equation can be solved using Fourier transforms [13][1] to yield the solution

$$\phi(R) = \frac{q_d}{R} e^{-\frac{R}{\lambda_D}}, \tag{2.9}$$

where R is the magnitude of distance in spherical coordinates. As seen from Eq. (6.4), this result is also valid for the inter-particle interaction between dust particles in a 2D plane, as outlined by the theory in Chapter 6 [6].

2.2 Relevant Parameters

Given the dust particle number density in 2D, n_{d0}, we define the average separation between nearest dust particles as

$$a = \frac{1}{\sqrt{n_{d0} \pi}}, \tag{2.10}$$

[1] Hideki Yukawa carried a similar derivation to arrive at his predictions of the elementary particle meson that mediates the force of interaction between a proton and neutron in the nucleus. The force of interaction is thus named after him.

which specifies a length scale for our system. The plasma coupling parameter, Γ, is defined to be the ratio of two particle potential energy separated by a, (q_d^2/a), to the average thermal energy of dust particles (k_BT). Thus,

$$\Gamma = \frac{q_d^2}{ak_BT}. \tag{2.11}$$

Further, we characterize a time scale for our system by defining the plasma dust frequency [14] as

$$\omega_{pd} = \sqrt{\frac{2q_d^2}{ma^3}}, \tag{2.12}$$

where m is the mass of a dust particle. Lastly, we define the screening parameter as

$$\kappa = \frac{a}{\lambda_D}. \tag{2.13}$$

2.3 Collective Modes in Dusty Plasma

Of particular interest in the study of plasmas is the study of collective modes. There are a myriad of such modes even in simple plasmas where no dust particles [2] are taken into account. For the system of dusty plasma, our main interest is in the study of one particular low frequency mode that results from the coherent motion of only the dust particles. The phase speeds of the waves is much smaller than the thermal speed of either electrons or ions. Thus, the dynamics of the massive dust particles is so slow, that we may assume the electrons and ions have sufficient time to accommodate themselves to the instantaneous electrostatic potential so that their densities are approximately be given by the Boltzmann distribution Eq. (2.3).

The first theoretical predictions of these modes is by Rao *et al.*[15]. The essential idea used to obtain the wave dispersion relation, i.e., $\omega = \omega(k)$, (wave frequency ω as function of wave number k), was to consider the dust particles as forming a charged continuum medium, and find the wave behavior governed by continuity, momentum conservation and Poisson's equations,

$$\frac{\partial}{\partial t} n_d(\mathbf{r},t) + \nabla_{||} \cdot [n_d(\mathbf{r},t)\mathbf{v}_d(\mathbf{r},t)] = 0, \tag{2.14a}$$

$$\frac{\partial}{\partial t}\mathbf{v}_d(\mathbf{r},t) + \left[\mathbf{v}_d(\mathbf{r},t)\cdot\nabla_{||}\right]\mathbf{v}_d(\mathbf{r},t) = \frac{q_d}{m}\nabla_{||}\phi(\mathbf{R},t)|_{z=0}, \tag{2.14b}$$

$$\nabla^2\phi(\mathbf{R},t) = -4\pi\left[q_i n_i(\mathbf{R},t) - q_e n_e(\mathbf{R},t) - q_d n_d(\mathbf{r},t)\delta(z)\right], \tag{2.14c}$$

where $\mathbf{r}$ is 2D position vector, $\mathbf{R} = \mathbf{r} + z\hat{\mathbf{z}}$ and $\nabla_{||}$ represents the gradient operator in the plane of dust particles. Assuming Eqs. (2.3) to hold true, this set of equations is solved perturbatively for the dispersion relation [8] in the following way.

In the unperturbed state, $\frac{\partial}{\partial t} = 0$, $n_d \equiv n_{d0}$=constant, $v_d \equiv v_{d0}$=0, $n_e \equiv n_{e0}(z) \sim q_e n_{e0}\left(1 + \frac{q_e\phi(\mathbf{R})}{k_B T_e}\right)$ $n_i \equiv n_{i0} \sim q_i n_{i0}\left(1 - \frac{q_i\phi(\mathbf{R})}{k_B T_i}\right)$. From Eq. (2.14c) we obtain the following equation for the unperturbed potential $\phi_0(z)$ (perpendicular to the x, y-plane occupied by dust layer)

$$\frac{d^2}{dz^2}\phi_0(z) - \lambda_D^{-2}\phi_0(z) = 4\pi q_d n_{d0}\delta(z), \tag{2.15}$$

yielding the solution

$$\phi_0(z) = -2\pi q_d n_{d0}\lambda_D \exp(-|z|/\lambda_D). \tag{2.16}$$

We now assume a perturbed state, whereby a small external force (to a first order perturbation) $\mathbf{F}_{ext}(\mathbf{r}, t)$ is applied to the dust particles. In response to this force, we linearize Eqs. (2.14) using $\phi(\mathbf{R}, t) = \phi_0(z) + \phi_1(\mathbf{R}, t)$, $n_d(\mathbf{r}, t) = n_{d0} + n_{d1}(\mathbf{r}, t)$, $v_d(\mathbf{r}, t) \equiv v_{d1}(\mathbf{r}, t)$, $n_e(\mathbf{R}, t) = n_{e0}(z) + n_0\frac{q_e}{T_e}\phi_1(\mathbf{R}, t)$ and $n_i(\mathbf{R}, t) = n_{i0}(z) - n_0\frac{q_i}{T_i}\phi_1(\mathbf{R}, t)$. This yields the following set of equations, correct to first order perturbation expansion,

$$\frac{\partial}{\partial t}n_{d1}(\mathbf{r}, t) + \nabla_{||} \cdot [n_{d0}\mathbf{v}_{d1}(\mathbf{r}, t)] = 0, \tag{2.17a}$$

$$\frac{\partial}{\partial t}\mathbf{v}_{d1}(\mathbf{r}, t) = \frac{q_d}{m}\nabla_{||}\phi_1(\mathbf{R}, t)|_{z=0} + \frac{\mathbf{F}_{ext}(\mathbf{r}, t)}{m}, \tag{2.17b}$$

$$\nabla^2\phi_1(\mathbf{R}, t) = \lambda_D^{-2}\phi_1(\mathbf{R}, t) + 4\pi q_d n_{d1}(\mathbf{r}, t)\delta(z). \tag{2.17c}$$

Now by using partial Fourier transforms with respect to $\mathbf{r}$ and t dependencies and taking the propagation vector $\mathbf{k} = (k_x, k_y)$, we recast Eq. (2.17c) as

$$\frac{\partial^2}{\partial z^2}\phi_1(\mathbf{k}, z, \omega) - k^2\phi_1(\mathbf{k}, z, \omega) - \lambda_D^{-2}\phi_1(\mathbf{k}, z, \omega) = 4\pi q_d n_{d1}(\mathbf{k}, \omega), \tag{2.18}$$

giving the solution

$$\phi_1(\mathbf{k}, z, \omega) = \frac{-2\pi q_d n_{d1}(\mathbf{k}, \omega)\lambda_D}{\sqrt{k^2\lambda_D^2 + 1}}\exp(-\sqrt{k^2\lambda_D^2 + 1}|z|/\lambda_D). \tag{2.19}$$

Similarly, the Fourier transform of Eqs. (2.17a),(2.17b) yield

$$-i\omega n_{d1}(\mathbf{k}, \omega) + n_{d0}i\mathbf{k} \cdot \mathbf{v}_{d1}(\mathbf{r}, t) = 0, \tag{2.20a}$$

$$-i\omega\mathbf{v}_{d1}(\mathbf{k}, \omega) = i\mathbf{k}\frac{q_d}{m}\phi_1(\mathbf{k}, z, \omega)_{z=0} + \frac{\mathbf{F}_{ext}(\mathbf{k}, \omega)}{m}. \tag{2.20b}$$

Eliminating $\mathbf{v}_{d1}(\mathbf{k}, \omega)$ from the above two equations and using Eq. (2.19), we obtain the first order perturbation to density in response to the external perturbation applied

$$n_{d1} = i\frac{n_{d0}}{m}\frac{\mathbf{k} \cdot \mathbf{F}_{ext}(\mathbf{k}, \omega)}{\left[\omega^2 - \frac{2\pi q_d^2\lambda_D n_{d0}}{m\sqrt{k^2\lambda_D^2+1}}\right]}, \tag{2.21}$$

giving the dispersion relation from the zeros of the denominator, $\omega^2 = \frac{2\pi q_d^2 \lambda_D n_{d0}}{m\sqrt{k^2\lambda_D^2+1}}$. This can be re-written in terms of the parameters defined in the previous section to give

$$\omega^2 = \omega_{pd}^2 \frac{k^2 a^2}{\sqrt{k^2 a^2 + \kappa^2}}. \tag{2.22}$$

This is the basic dispersion relation obtained by considering the 2D dusty plasma as forming a incompressible charged fluid.

Carrying out a Brownian dynamics simulation study for a 2D layer of dusty plasma, Hou and Miskovic [8] have shown that Eq. (2.22) provides good comparison with the dispersion results obtained from simulation in the weak coupling regime, i.e., $1 \lesssim \Gamma \lesssim 10$, while it begins to break down at higher wave-numbers beyond this regime, especially when longer range structural effects begin to appear.

The influence of longer ranged ordering as a result of stronger correlations between dust particles at higher coupling strengths for a 3D system of dusty plasma using a version of Generalized hydrodynamics (GH), was studied in a very comprehensive manner in an excellent paper by Kaw and Sen [10]. Through the introduction of visco-elastic functions (of k and ω), i.e., functions that reduce to viscous coefficients at low frequencies while, modeling elastic effects at higher frequencies (which leads to restoring forces), they were able to predict regions of negative group speed $\left(\frac{\partial\omega(k)}{\partial k} < 0\right)$, a prediction that can be observed in simulations. Further, the model is valid over a wider range of coupling parameters; from $\Gamma \ll 1$ all the way up to $1 \lesssim \Gamma \lesssim \Gamma_c$, where Γ_c is the value of coupling parameter where crystallization occurs. For a 2D dusty plasma, this is typically $\Gamma_c \sim 160$. In addition, they were also able to predict wave number dependent wave damping, with a half width proportional to $\nu_l k^2$, where ν_l is the coefficient of longitudinal viscosity. Given the typical value of ν_l evaluated by various groups [16, 17], these predictions seem to overestimate the damping compared to what can be observed from simulation studies.

The most successful theoretical model for predicting the dispersion relation of these wave modes is due to Golden and Kalman [18], and is based on the theory of Quasi Localized Charge Approximation (QLCA). The physical picture behind this model suggests that, in the region of strong coupling particles are trapped in localized potential wells occupying randomly located sites and undergoing oscillations around them. At the same time though, the site positions keep changing and a continuous rearrangement of configuration takes place. Based on these ideas, the authors were able to provide a semi-analytical[2] model for wave dispersion (adopting linear response formalism and deriving the wave dielectric response function) over a wide range of coupling parameters without resorting to any phenomenological models. However, in its original form, the QLCA is applicable only in the strong coupling regime, and does not have any means to account for wave-number dependent damping.

[2]By semi-analytical models, we refer to theoretical models that require as input some data from either simulation or laboratory experiments. QLCA for instance, requires as input the pair distribution function $g(r)$, which is most easily obtained from simulation.

2.3.1 Qualitative description of the GH Approach

The model we will be working on will try to address both these issues, wave number dependent dispersion and damping of DAW's based on a hydrodynamical approach. These wave modes or collective modes are a result of spontaneous microscopic fluctuations that always occur in a fluid even at thermal equilibrium. A knowledge of these collective modes can also be obtained by studying the response of a fluid to small external perturbations, an approach we made some use of while deriving the dispersion relation in the previous section. That the two approaches lead to identical information concerning the dynamics of a fluid close to equilibrium, is implied by the celebrated fluctuation-dissipation theorem (originally given in terms of Onsager's regression hypothesis [19]).

A study of the collective modes resulting from spontaneous microscopic fluctuations is greatly aided when the problem is addressed in terms of space and time correlation functions, which in their most general context are defined as the equilibrium average of the product of two dynamical variables (such as number density, current density), each of which expresses the instantaneous deviations of a fluid property from its equilibrium value at particular points in space and time. Correlation functions are very important tools for both theoretical and experimental investigations of the dynamics of fluids [20]. For instance, light and neutron scattering of fluids can be used to obtain information about number density-number density correlations (also called the number density auto-correlations) with light scattering typically giving information about the low wave-number and low frequency regions, while neutron scattering allows experiments to probe regions of higher wave-number and frequency. As an example, the study of static or time independent density-density correlation function (called the static structure factor) and its inverse Fourier transform, called the pair distribution function reveals that fluids that were once considered to be devoid of any structures, actually have short range ordering, i.e., in the vicinity of a fluid molecule, one can observe local structures in the form of a regular arrangement of neighboring molecules. The spatial extent of this arrangement is much shorter than typically found in crystalline solids, but such arrangements clearly exist [21]. Computer simulations provide another invaluable tool for studying these correlation functions. In addition to providing direct information on the dynamical behavior of the system, as for instance the spectral density of current density auto-correlation function, that we will obtain during this work, the simulations also help us in obtaining static correlation functions, that are often used as inputs to formulate the theory behind dynamical behavior of fluids. As an example, we will obtain the static structure factor (it is a static quantity not dependent on time) from simulations and use that as an input to the theoretical model for power spectral density, obtained from longitudinal current density auto-correlation function (which is a dynamical variable, since it is dependent on both space and time).

Our work in this thesis will therefore use computer simulations to study the spontaneous longitudinal and transverse current density fluctuations for a 2D system of dusty plasma in equilibrium, expressed in terms of their corresponding spectral densities (see Appendix B). The simulations will allow us to probe a large region of wave-number and frequency space and naturally reveal information about short-range (for low coupling strengths) and long-range ordering (for higher coupling strengths) of particles in the

medium. In order to now obtain a theoretical model for these fluctuations, we will assume the dust layer as forming a medium of neutral fluid and obtain the space time correlation functions in the context of hydrodynamics. But by definition, a hydrodynamical description of these correlation functions in terms of the local thermodynamic and transport properties of the fluid, will only reveal information about the long-wavelength and low-frequency fluctuations of the fluid. This will in turn, motivate our extension of the Ordinary Hydrodynamical (OH) description of these fluctuations, to their Generalized Hydrodynamical (GH) description, that will allow us to probe regions of shorter wavelengths and higher frequencies.

As discussed in the context of work done by Kaw and Sen [10], the simulations will reveal regions in the frequency wave-number (ω, k) space, where the dispersion relation will deviate from an OH (continuum) description that predicts a linear frequency wave-number dependence, i.e, $\omega(k) \propto k$. We will observe that the dispersion curve reaches a maximum and then curves back to regions of negative slope. This behavior is not very unusual, especially in the context of study of vibrational modes in crystalline solids, where the discrete nature of particles along a periodic arrangement of lattice points is taken into account. This provides a simple model to calculate the normal modes of vibrations by taking into account microscopic structure of a solid, albeit an idealized one. In particular, we will observe later during the course of this work, that the medium of dusty plasma easily transitions from regimes of shorter range ordering (fluid-like behavior) to regimes of longer range ordering (crystal-like behavior) based on the coupling strength parameter Γ. In the fluid-like regime, the dispersion curve will deviate from a fluid based description only in smaller regions of the k space while it will tend to exhibit quasi-oscillatory (thereby extending to higher regions in k space) dispersion properties in its crystal-like state. We can attempt to understand this quasi-oscillatory behavior in terms of a simple description of lattice vibrations in solids, which we now describe.

Referring to Figure 2.1, we consider the particles in a one dimensional lattice as being coupled together in a large spring-mass system (assuming the same spring constant). The particles vibrate about their equilibrium positions due to thermal vibrations, and these vibrations ((a particle's displacement from its equilibrium position) are assumed to be small, so that one can use the Hooke's law for spring force. The dispersion relation is obtained by a study of the normal modes of vibration [22].

Writing Newton's equation of motion for the n-th particle,

$$m\frac{d^2}{dt^2}x_n = s(x_{n+1} - x_n) - s(x_n - x_{n-1}), \tag{2.23}$$

where m is the mass of the particle (all particles assumed identical), s is the spring constant, while x_{n-1}, x_n, x_{n+1} are longitudinal displacements of the particles $n-1, n$ and $n+1$ respectively. For a normal mode analysis, we will assume all particles are oscillating harmonically with the same frequency ω and same phase constant ϕ. The shape of the mode is given by ratios of amplitudes of the particles harmonic oscillations. Thus, we assume that in a given mode (there will be N modes for a N particle system), we have

$$x_n = A_n \cos(\omega t + \phi), \tag{2.24}$$

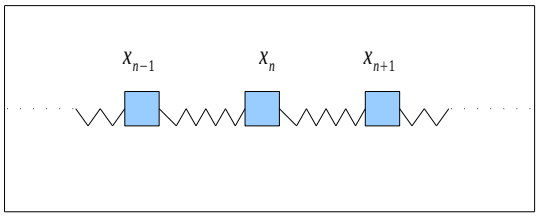

Figure 2.1: A simple one dimensional coupled spring mass system as a model to study lattice vibrations in a solid.

for $n = 1 \ldots N$. Therefore,

$$\frac{d^2}{dt^2} x_n = -A_n \omega^2 \cos(\omega t + \phi). \tag{2.25}$$

Substituting this into Eq. (2.23), we obtain

$$-m\omega^2 A_n = s(A_{n+1} + A_{n-1} - 2A_n), \tag{2.26}$$

yielding

$$A_{n+1} + A_{n-1} = A_n \left(2 - \frac{m}{s}\omega^2\right). \tag{2.27}$$

In order to proceed, the following solution is attempted,

$$A_n = A\sin(kna), \tag{2.28}$$

where a is equilibrium length of the spring. This solution is guessed based on the dependence of amplitude on the position for a continuous string fixed at both ends $A(x) = A\sin(kx)$, although dispersion relations can be shown to be independent of the boundary conditions [22]. Substituting Eq. (2.28) into Eq. (2.27), and after algebraic manipulations, we obtain,

$$2A_n \cos(ka) = A_n(2 - \frac{m}{s}\omega^2). \tag{2.29}$$

If we are away from any nodes, we can assume $A_n \neq 0$, thus giving us

$$\omega^2 = 4\frac{s}{m}\sin^2(\frac{ka}{2}). \tag{2.30}$$

We thus see, that a simple model like the above, predicts a dispersion curve that will be periodic in k. In the limit of small k, we obtain a linear dispersion relation $\omega(k) = ka\sqrt{\frac{s}{m}}$, as expected. Therefore incorporating the discrete nature of particles forming the system allows us to probe the dispersion relation into regions of higher wave-number, typically to the order of inter-particle spacing whereas in the continuum approximation, we are probing only the very long wavelength behavior.

The highly idealized and simple description above, however, provides an important insight for the development of our model. The data obtained from computer simulation also gives us information about smaller wavelengths, i.e., to the order of inter-particle spacing. As the coupling strength is increased, we move more and more into the elastic spring-like description above, and thus we can expect to observe a bending of the dispersion curves. On the theoretical side, this gives us indication to take the discrete nature of particles into account, and this will be our goal in the GH approach.

In the same context, it is useful to further explore a very simplistic description of a fluid particle that will help provide us with a physical picture [23] which we will use as a qualitative basis for the development of the GH model. A single fluid particle (a dust particle in our case) may be regarded as executing a simple harmonic motion (like the spring-mass system), around a point of its temporary equilibrium position. It can be considered to occupy this position, for a time duration say τ during which it will vibrate rapidly around this point. After τ time units, it will randomly jump to a new position and repeat the process. If a constant force is now applied to the fluid, it gives a preferred direction to the jumps of the particles along the direction of applied force and causes a net current or flow of particles. If the applied force is sufficiently small, the induced current is proportional to the applied force and provides a measure of the viscosity of the fluid.

Consider now an applied force, which is of very high frequency and short duration say, $t \ll \tau$. Thus the time is too short for a flow to be induced, and the reaction of the fluid particles to this force can be considered as an elastic deformation, as for instance in terms of a spring-mass system. In fact, such a picture also suggests transverse deformations in response to shear stress, and we will see later that computer simulations for dusty plasma can probe such shear waves with the GH model providing a reasonable theoretical model for the same.

In order to try and incorporate the ideas suggested by the above physical model, we now come back to our discussion of time correlation functions (we will ignore space correlations in this discussion for simplicity and consider time auto-correlation functions only). The long time behavior of these time correlation functions can be given in terms of macroscopic equations, i.e., the hydrodynamic equations for the fluid system. The equations are written in terms of thermodynamic and transport coefficients. In turn, Green-Kubo integrals[20, 21] allow us to effectively invert this relation and express a transport coefficient as long time integrals of an appropriate time auto-correlation function. That is, if σ is any transport coefficient, it may be expressed as the long time integral over a time auto-correlation function

$$\sigma = K \int_0^\infty dt\ C(t), \tag{2.31}$$

where $C(t)$ is an appropriate time auto-correlation function and K is any real constant. For instance, shear viscosity may be expressed as an integral over shear stress auto-correlation function [20]. Let us now consider a generalization of the above equation in the terms of the Fourier transform of the time

auo-correlation function,

$$\sigma(\omega) = K \int_0^\infty dt\ e^{i\omega t} C(t). \tag{2.32}$$

We see that the zero frequency limit of the above equation recovers the Green-Kubo integral Eq. (2.31). In fact, invoking the property that a classical time auto-correlation function is even in time, we can get a qualitative picture of what a zero frequency limit means. Let τ_c denote the relaxation time of $C(t)$ and scale Eq. (2.32) in terms of τ_c, i.e., let $\tau = t/\tau_c$. We thus obtain,

$$\sigma(\omega) \sim 2K\tau_c \int_0^{\tau_c} d\tau\ \cos(\omega\tau_c\tau) C(\tau). \tag{2.33}$$

For frequencies where $\omega\tau_c \ll 1$, Eq. (2.31) is recovered as the first term in the Taylor's series expansion of the cosine in terms of its argument. Consider now the opposite limit, i.e., $\omega\tau_c \gg 1$. Eq. (2.33) will be mostly 0 due to the many periods of the cosine term being elapsed before $C(\tau)$ changes its value, except in the vicinity of $\tau = 0$ allowing us to write the approximate short time behavior of the time auto-correlation function as

$$\sigma(\omega) \sim 2K\tau_c C(0). \tag{2.34}$$

Thus, the high frequency behavior of $\sigma(\omega)$ is mostly determined by the short time behavior of a time auto-correlation function $C(t)$. Let us now consider the specific example of shear viscosity in the context of its generalization in terms of the integral over shear stress auto-correlation function. Similar description can be given for longitudinal viscosity in terms of normal stress auto-correlation functions, although it is easier to interpret the former.

What the above descriptions suggest is that the generalized shear viscosity can be interpreted in terms of the Fourier coefficients of the shear stress auto-correlation function. The low frequency coefficients or low frequency stresses provide the constant viscosity coefficients we typically use in a hydrodynamic momentum conservation equation. A higher frequency coefficient or high-frequency stresses lead to generalized shear viscosity. But from our qualitative description pertaining to very high frequency stress and the elastic response of fluid particles to the same, we may interpret these frequency dependent generalizations as providing a natural transition from viscous to elastic response of a fluid element to applied or developed stresses. Further, from Eq. (2.32), we can re-write the generalized transport coefficient in terms of its real and imaginary parts as

$$\sigma'(\omega) = K \int_0^\infty dt\ \cos(\omega t) C(t), \tag{2.35a}$$

$$\sigma''(\omega) = K \int_0^\infty dt\ \sin(\omega t) C(t). \tag{2.35b}$$

For $\omega\tau_c \ll 1$, only the real part contributes, which essentially characterizes dissipative viscous process. For higher frequencies, both terms contribute, where the imaginary part may be regarded as the non-dissipative response of the fluid. In fact, if we assume the correlation function to have a simple exponential

form $C(t) = e^{-t/\tau_c}$, and solve Eq. (2.32) using Laplace transform evaluated as $s = i\omega$, we obtain,

$$\sigma(\omega) = \frac{K\tau_c}{i\omega\tau_c + 1}. \tag{2.36}$$

For $\omega\tau_c \ll 1$, $\sigma(\omega) = K\tau_c = \sigma$, giving a purely viscous response. For $\omega\tau_c \gg 1$, $\sigma(\omega) = \frac{K}{i\omega}$, given by the imaginary part, which we can now relate to the elastic response of the fluid. We will find such a splitting of the generalized viscosity coefficient into real and imaginary parts very useful later during this work. The real part will provide estimates of wave damping rate while the imaginary part will contribute to its elastic medium-like dispersion.

Since our main focus during the course of this work will be to study dynamic behavior of fluid in terms of its current density auto-correlation functions, our basic approach to probe the microscopic behavior of the medium of dusty plasma will be to extend the ordinary fluid based description by introducing generalized viscosity coefficients into the time evolution equation of the current density auto-correlation functions. Since the resulting dynamical equation for the relevant current density auto-correlation equation will generally have the form (though it will be further generalized to take into account spatial correlation)

$$\frac{\partial}{\partial t}C(t) = -\int_0^t dt' \; K(t')C(t-t'), \tag{2.37}$$

we will refer to such equations resulting from a generalization of the transport coefficients, as memory function equations, since as in the above equation, the time derivative of the current density auto-correlation function at an instant depends not only on the value of $C(t)$ at that instant, but also on its history from $t' = 0$ to $t' = t$. It is thus said to have memory.

Thus, in our attempt to describe the longitudinal and transverse wave modes, we will generalize the OH description by making use of non-local in time and space viscosity memory functions. In order to make use of this generalization, we will then use explicit phenomenological models for the appropriate memory function (just like the simple exponential model we introduced above for the shear stress auto-correlation function). This will allow us to obtain not only estimates of wave dispersion over a wide range of coupling parameters, but also theoretical prediction of wave damping[3] that will be compared with observations from simulation.

2.4 Overview of Brownian Motion

The theory of Brownian motion historically concerned itself with the irregular perpetual motions of colloidal particles in suspension in a liquid [24]. These motions have their origin in the collisions that the colloidal particles suffer with the molecules of the surrounding medium. In our system, we will model

[3]By damping we will be referring to wave-number k dependent damping rate of wave modes. These will be described via spectral widths, i.e., plotting the power spectral density as a function of ω for different values of k, and will often be referred to as profile plots.

the charged dust particles as Brownian particles, and treat the neutrals comprising the dusty plasma as forming the surrounding medium.

The first mathematical descriptions of Brownian motion were given independently by Einstein and Smoluchowski. Later, a more refined model was given by Langevin, that will be used in the rest of this work. Physically, Langevin's analysis of Brownian motion [25] is concerned with the motion of a sphere of mass m, moving with velocity $\mathbf{v}$ in a fluid at thermal equilibrium at temperature T. The sphere experiences a retarding force, which for small velocities can be modeled as $-\xi'\mathbf{v}$, where ξ' is called the drag coefficient. In the absence of any other forces, Newton's equation reads

$$m\frac{d}{dt}\mathbf{v}(t) = -\xi'\mathbf{v}(t). \tag{2.38}$$

Written in a time update form,

$$\mathbf{v}(t+dt) = \mathbf{v}(t) - \frac{\xi'}{m}\mathbf{v}(t)dt, \tag{2.39}$$

the equation represents the effect of average drag force exerted on the sphere by the surrounding medium in time dt. However, the medium will also exert random impulses to the sphere by frequent collisions, and if the size of the sphere is not too large, the effect of these collisions can be modeled by Gaussian white noise giving

$$\mathbf{v}(t+dt) = \mathbf{v}(t) - \xi\mathbf{v}(t)dt + \sqrt{\zeta^2 dt}\mathbf{N}_t^{t+dt}(0,1), \tag{2.40}$$

where ζ is an as yet undetermined coefficient, $\xi = \frac{\xi'}{m}$, $\mathbf{N}_t^{t+dt}(0,1) = \left[N_{t,x}^{t+dt}(0,1), N_{t,y}^{t+dt}(0,1)\right]$ is spatially independent and temporarily uncorrelated normal random variable with mean 0 and variance 1. This means that the Cartesian components $N_{t,x}^{t+dt}(0,1)$ and $N_{t,y}^{t+dt}(0,1)$ are independent of each other (spatially independent) and for each component, its time samples $N_{0,x}^{dt}(0,1), N_{dt,x}^{2dt}(0,1), \cdots, N_{t,x}^{t+dt}(0,1)$ are mutually uncorrelated. Thus, we are assuming the process to be a simple continuous Markov process. Henceforth, we will understand $\mathbf{N}_t^{t+dt}(0,1)$ written in an equation of the form Eq. (2.40) to have the subscripts t and superscript $t+dt$, and thus simply write it as $\mathbf{N}(0,1)$. It is the last term in Eq. (2.40) that attempts to model the effects of random fluctuations suffered by the sphere in a time dt[4].

It will be shown in a later section that the variance of any one component of velocity in the long time limit $t \to \infty$ can be given by $\langle v(t\to\infty)^2\rangle = \frac{\zeta^2}{2\xi}$. From physical reasoning, since in the long time limit the Brownian particle is expected to be in thermal equilibrium with the bath assumed at temperature T, we expect that the average kinetic energy per particle per degree of freedom will be given by the equipartition theorem [11]. We therefore have,

$$\frac{1}{2}m\left\langle v(t\to\infty)^2\right\rangle = \frac{k_B T}{2}. \tag{2.41}$$

Thus, in thermal equilibrium, we have

$$\frac{\zeta^2}{2\xi} = \frac{k_B T}{m}, \tag{2.42}$$

[4]The appearance of the term $(dt)^{1/2}$, as shown by Gillespie [25], can be attributed to the specific mathematical form required by a continuous Markov-process to propagate in time.

which is one form of the fluctuation-dissipation theorem [12, 26], relating dissipative transport processes (neutral drag friction) to the correlations of spontaneous fluctuations in the medium (diffusion).

2.5 Non-Dimensional Form of Langevin's Equation for a Single Dust Particle

We will now amend Langevin's Equation Eq. (2.40) to describe a single dust particle interacting via a pair-wise Yukawa potential Eq. (2.9) with another dust particle. Assuming for the time being that this interaction is occurring in one dimension (or equivalently, we may resolve the 2D interaction into its components and perform a similar analysis in each direction), we will show that we can express all relevant parameters of our system in terms of just three non-dimensional parameters which greatly simplifies simulation work.

In the following, dimensional variables appear with an overhead bar, and the non-dimensionalized variables appear without an overhead bar. In addition, tunable dimensional parameters (ξ, ζ), will be transformed to their equivalent non-dimensionalized parameters (γ, β). Other non-tunable dimensional and non-dimensional system parameters (that we will never explicitly vary) $\omega_{pd}, \lambda_D, a, m_{i,e,d}, q_{i,e,d}, T_{i,e,d}$ will continue to appear as regular quantities. Thus, we will be seeking to non-dimensionalize the following system varaiables.

Description	Dimensional System Variables	Non-Dimensional System Variables
time	$\bar{t}$	t
position	$\bar{r}(\bar{t})$	$r(t)$
velocity	$\bar{v}(\bar{t})$	$v(t)$
force	$\bar{F}(\bar{r})$	$F(r)$

Starting with the equations of motion for a particle in the presence of an external force [25, 26],

$$\frac{d}{d\bar{t}}\bar{r} = \bar{v}, \tag{2.43a}$$

$$\frac{d}{d\bar{t}}\bar{v} = -\xi\bar{v} + \frac{\bar{F}}{m} + \sqrt{\frac{\zeta^2}{d\bar{t}}}N(0,1), \tag{2.43b}$$

where $\bar{r} \equiv \bar{r}(\bar{t})$ is the inter-particle separation, $\bar{F} = -\frac{d}{d\bar{r}}\bar{\phi}(\bar{r})$ is the Yukawa force, $m \equiv m_d$ is mass of a dust particle and $\bar{v} \equiv \bar{v}(\bar{t})$ is the velocity of a dust particle. Notice, written in differential form, Eq. (2.43b) has a $(d\bar{t})^{-1/2}$ term and Langevin's equation in this form is usually called the white noise form of the Langevin Equation [25].

Non-dimensionalizing Eq. (2.43a) by $r = \frac{\bar{r}}{a}$, $t = \bar{t}\omega_{pd}$, we obtain

$$\frac{d}{dt}r = \frac{\bar{v}}{a\omega_{pd}}, \tag{2.44}$$

providing us the characteristic speed of the system $a\omega_{pd}$. Now, defining $v = \frac{\bar{v}}{a\omega_{pd}}, t = \bar{t}\omega_{pd}, r = \frac{\bar{r}}{a}$ and writing the explicit form of Yukawa force in Eq. (2.43b), we obtain

$$a\omega_{pd}^2 \frac{d}{dt}v = -a\omega_{pd}\xi v + \frac{q_D^2}{mr^2a^2} e^{-\frac{ra}{\lambda_D}} \left(1 + \frac{ra}{\lambda_D}\right) + \sqrt{\frac{\zeta^2\omega_{pd}}{dt}} N(0,1). \tag{2.45}$$

Dividing throughout by $a\omega_{pd}^2$, writing $\gamma = \frac{\xi}{\omega_{pd}}$ and noting that $\kappa = \frac{a}{\lambda_D}$ from Eq. (2.13) and $\omega_{pd}^2 = \frac{2q_d^2}{ma^3}$ from Eq. (2.12), we find

$$\frac{d}{dt}v = -\gamma v + \frac{e^{-\kappa r}}{2r^2}(1 + \kappa r) + \sqrt{\frac{\zeta^2}{a^2\omega_{pd}^3 dt}} N(0,1). \tag{2.46}$$

We know from the fluctuation-dissipation theorem Eq. (2.42) that $\zeta^2 = \frac{2\xi k_B T}{m}$. Making this substitution, and noting that $\gamma = \frac{\xi}{\omega_{pd}}$,

$$\frac{d}{dt}v = -\gamma v + \frac{e^{-\kappa r}}{2r^2}(1 + \kappa r) + \sqrt{\frac{2\gamma k_B T}{ma^2\omega_{pd}^2 dt}} N(0,1). \tag{2.47}$$

Now, writing $\omega_{pd}^2 = \frac{2q_d^2}{ma^3}$ and noting that $\Gamma = \frac{q_d^2}{ak_B T}$ from Eq. (2.11) we finally obtain

$$\frac{d}{dt}v = -\gamma v + \frac{e^{-\kappa r}}{2r^2}(1 + \kappa r) + \sqrt{\frac{\beta^2}{dt}} N(0,1), \tag{2.48}$$

where we have defined $\beta^2 = \frac{\gamma}{\Gamma}$. As can be seen, this equation is totally specified in terms of three non-dimensional parameters κ, γ and Γ, that will be the only inputs characterizing the system of dust particles that we require for our simulation. For convenience, a list of the relevant scaling used and the corresponding non-dimensional quantities appears in the glossary.

With this background, we now proceed to a more detailed study of how we will use Langevin's equation for the purpose of Brownian dynamics simulation.

Chapter 3

Numerical Integration of Langevin's Equation

Brownian dynamics (BD) simulation method may be regarded as a generalization of Molecular dynamics(MD) [27]. The MD method is based on Newton's equations of motion, whereas the BD method is based on its stochastic generalization, namely the Langevin equation Eq. (2.40). Here it is re-written for convenience in vector notation and includes the effect of external forces acting on the particle,

$$\frac{d\mathbf{r}(t)}{dt} = \mathbf{v}(t), \tag{3.1}$$

$$\frac{d\mathbf{v}(t)}{dt} = -\gamma\mathbf{v}(t) + \frac{\mathbf{F}(\mathbf{r},t)}{m} + \sqrt{\frac{\beta^2}{dt}}\mathbf{N}(0,1). \tag{3.2}$$

Here m, $\mathbf{v}$ and $\mathbf{r}$ are respectively the mass, velocity and the position of the Brownian particle, $\mathbf{F}$ is the deterministic force on the particle, resulting from external sources and/or inter-particle interactions and from Eq. (2.48), $\beta^2 = \frac{\gamma}{\Gamma}$.

Let us now consider how to numerically integrate such an equation. The above equations can easily be split into their components and for the time being let us consider one such component of velocity. As has already been discussed in the overview of BD, the random force is essentially a zero mean Gaussian white noise, that is uncorrelated with velocity. It is best to write the velocity in time update form as

$$v(t+dt) - v(t) = -\gamma v(t)dt + a(t)dt + \sqrt{\beta^2 dt}N(0,1), \tag{3.3}$$

where we denote by $a(t)$, the component of deterministic acceleration in the direction being considered[1]. A simple and powerful method to solve such an equation referred from Lemons [26], is as follows. Assuming that the time step dt is small enough such that the deterministic acceleration $a(t)$ is constant over this

[1] $a(t)$ will assumed to be dependent only on the position coordinates and independent of the velocity.

time, each variable in the sequence of random variables $v(dt), v(2dt), \cdots, v(t)$, is a linear combination of the independent normal variables $N_0^{dt}, N_{dt}^{2dt}, \cdots, N_{t-dt}^{t}$. Since, linear combinations of statistically independent normals are themselves normals, $v(t)$ is a normal random variable that can conveniently be expressed as

$$v(t) = N_0^t(\text{mean}[v(t)], \text{variance}[v(t)]). \tag{3.4}$$

Thus, the entire problem reduces to finding expressions for the mean and variance of $v(t)$.[2] In the following, angular brackets will denote ensemble averaging.

3.1 Mean and Variance of Velocity in One Dimension

Taking the expectation value on both sides of Eq. (3.3), we obtain

$$\langle v(t+dt) - v(t) \rangle = \langle -\gamma v(t) dt \rangle + \langle a(t) dt \rangle + \left\langle \sqrt{\beta^2 dt} N(0,1) \right\rangle. \tag{3.5}$$

Since the term $a(t)dt$ is deterministic, and the mean of $N(0,1)$ is 0, this reduces to,

$$\langle v(t+dt) \rangle - \langle v(t) \rangle = -\gamma \langle v(t) \rangle dt + a(t)dt, \tag{3.6}$$

which is essentially a deterministic ordinary differential equation in the mean value of velocity. In order to solve this equation, the systematic acceleration $a(t)$ is typically expanded into a Taylor's series about $t = 0$. This is justified, because in an actual simulation, the update equation is solved using very small time steps ($t \ll 1$), whereby $a(t)$ is reset to its new value before every time step. Thus, we write $a(t)$ as [27]

$$a(t) = a_0 + a_0^{(1)} t + a_0^{(2)} \frac{t^2}{2!} + a_0^{(3)} \frac{t^3}{3!} + \cdots + a_0^{(n)} \frac{t^n}{n!} + \cdots, \tag{3.7}$$

where $a_0^{(n)} = a^{(n)}(0)$ is the n^{th} derivative evaluated at $t = 0$. Writing Eq. (3.6) in differential form and making a change of variable $\langle v(t) \rangle' = e^{\gamma t} \langle v(t) \rangle$, we obtain the following differential equation

$$e^{-\gamma t} \frac{d\langle v(t) \rangle'}{dt} = \frac{d\langle v(t) \rangle}{dt} + \gamma \langle v(t) \rangle = a(t). \tag{3.8}$$

Now, writing $a(t)$ as a Taylor's series expansion, we obtain

$$e^{-\gamma t} \frac{d\langle v(t) \rangle'}{dt} = a_0 + a_0^{(1)} t + a_0^{(2)} \frac{t^2}{2!} + a_0^{(3)} \frac{t^3}{3!} + \cdots + a_0^{(n)} \frac{t^n}{n!} + \cdots. \tag{3.9}$$

Multiplying both sides of this equation by $e^{\gamma t}$ and integrating over time, one obtains

$$\langle v(t) \rangle' - \langle v(0) \rangle' = \frac{a_0}{\gamma}(e^{\gamma t} - 1) + \frac{a_0^{(1)}}{\gamma^2}(\gamma t e^{\gamma t} - [e^{\gamma t} - 1]) + \cdots. \tag{3.10}$$

[2] This approach may seem a bit round about since we can also integrate Eq. (3.3) directly and then update position by Eq. (3.1). However, having shown that the position and velocity are essentially normal random variables that can be completely specified by their means and variances, we have a lot more information about them which among other advantages provides for good check on simulation results, for instance, the convergence of equilibrium kinetic energy.

Next, rewriting $\langle v(t)\rangle' = e^{\gamma t}\langle v(t)\rangle$, multiplying both sides of the equation by $e^{-\gamma t}$ and writing $\langle v(0)\rangle = v_0$, we obtain,

$$\langle v(t)\rangle = e^{-\gamma t}v_0 + \frac{a_0}{\gamma}(1-e^{-\gamma t}) + \frac{a_0^{(1)}}{\gamma^2}(\gamma t - [1-e^{-\gamma t}]) + \cdots. \tag{3.11}$$

The above equation can be expressed in a more convenient form. From Eq. (3.10), the n^{th} term is the integral

$$T_n = \frac{a_0^{(n-1)}}{(n-1)!}\int_0^t ds\ s^{n-1}e^{\gamma s}. \tag{3.12}$$

Integrating once by parts, we obtain

$$T_n = \frac{a_0^{(n-1)}}{(n-1)!\gamma}\left[e^{\gamma t}t^{n-1} - (n-1)\int_0^t ds\ s^{n-2}e^{\gamma s}\right]. \tag{3.13}$$

Multiplying and dividing the integral term by $(n-2)a_0^{n-2}$, we can write the above expression in the form of a recursion relation

$$T_n = \frac{a_0^{(n-1)}}{(n-1)!\gamma}\left[e^{\gamma t}t^{n-1} - \frac{(n-1)!}{a_0^{n-2}}T_{n-1}\right]. \tag{3.14}$$

Now multiplying by $e^{-\gamma t}$ (identical to the step that led from Eq. (3.10) to Eq. (3.11)), we obtain,

$$e^{-\gamma t}T_n = \frac{a_0^{(n-1)}}{(n-1)!\gamma}\left[t^{n-1} - \frac{(n-1)!}{a_0^{n-2}}T_{n-1}e^{-\gamma t}\right]. \tag{3.15}$$

Defining the n^{th} coefficient as $c_n(t) = \frac{e^{-\gamma t}T_n}{a_0^{n-1}t^n}$, we therefore have

$$c_n(t) = \frac{1}{(n-1)!\gamma t}\left[1-(n-1)!c_{n-1}(t)\right]. \tag{3.16}$$

Thus, Eq. (3.11) may be expressed in the more convenient form

$$\langle v(t)\rangle = c_0v_0 + c_1a_0t + c_2a_0^{(1)}t^2 + \cdots c_na_0^{(n-1)}t^n + \cdots, \tag{3.17}$$

where $c_0(t) = e^{-\gamma t}$ and for all $n \geq 1$, $c_n(t)$ satisfies the recursion relation Eq. (3.16).

The time evolution of the variance of $v(t)$ can now be obtained starting from

$$d[v^2(t)] = v^2(t+dt) - v^2(t), \tag{3.18}$$

where $d[v^2(t)]$ signifies the differential. From Eq. (3.3), we can substitute the expression for $v(t+dt)$ as

$$d[v^2(t)] = [(1-\gamma dt)v(t) + a(t)dt + \sqrt{\beta^2 dt}N(0,1)]^2 - v^2(t), \tag{3.19}$$

obtaining

$$\begin{aligned} d[v^2(t)] = v^2(t)(1+\gamma^2dt^2-2\gamma dt) + \beta^2 dtN^2(0,1) + a^2(t)dt^2 + 2v(t)(1-\gamma dt)\sqrt{\beta^2dt}N(0,1) \\ +2\sqrt{\beta^2dt}N(0,1)a(t)dt + 2v(t)(1-\gamma dt)a(t)dt - v^2(t). \end{aligned} \tag{3.20}$$

Retaining terms of order dt and $dt^{1/2}$, the equation simplifies to

$$d[v^2(t)] = -2\gamma v^2(t)dt + \beta^2 dt N^2(0,1) + 2v(t)\sqrt{\beta^2 dt}N(0,1) + 2v(t)a(t)dt. \tag{3.21}$$

Taking mean on both sides of the above equation, we obtain the following relation

$$\begin{aligned} d\langle v^2(t)\rangle = -2\gamma\langle v^2(t)\rangle dt + \langle\beta^2 N^2(0,1)\rangle dt + 2\langle v(t)\sqrt{\beta^2 dt}N(0,1)\rangle \\ +2\langle v(t)a(t)\rangle dt. \end{aligned} \tag{3.22}$$

As chosen, $v(t)$ and $N(0,1)$ are statistically independent, and $a(t)$ is deterministic. Therefore,

$$d\langle v^2(t)\rangle = -2\gamma\langle v^2(t)\rangle dt + \beta^2 dt + 0 + 2\langle v(t)\rangle a(t)dt. \tag{3.23}$$

Dividing throughout by dt and re-writing the above in the form of an ordinary differential equation gives us,

$$\frac{d\langle v^2(t)\rangle}{dt} + 2\gamma\langle v^2(t)\rangle = \beta^2 + 2\langle v(t)\rangle a(t). \tag{3.24}$$

By definition, the variance of $v(t)$ is $\sigma_v^2 = \langle v^2(t)\rangle - \langle v(t)\rangle^2$. Differentiating this with respect to time, one obtains,

$$\frac{d\sigma_v^2}{dt} = \frac{d[\langle v^2(t)\rangle - \langle v(t)\rangle^2]}{dt}, \tag{3.25}$$

$$\frac{d\sigma_v^2}{dt} = \frac{d\langle v^2(t)\rangle}{dt} - 2\langle v(t)\rangle\frac{d\langle v(t)\rangle}{dt}. \tag{3.26}$$

Substituting expressions from Eq. (3.24) and Eq. (3.6), and again invoking the fact that $a(t)$ is a time dependent deterministic variable,

$$\frac{d\sigma_v^2}{dt} = \beta^2 + 2\langle v(t)\rangle a(t) - 2\gamma\langle v^2(t)\rangle - 2\langle v(t)\rangle a(t) + 2\gamma\langle v(t)\rangle^2. \tag{3.27}$$

Recognizing that $2\gamma\langle v(t)\rangle^2 - 2\gamma\langle v^2(t)\rangle = -2\gamma\sigma_v^2$, we finally arrive at

$$\frac{d\sigma_v^2}{dt} = \beta^2 - 2\gamma\sigma_v^2, \tag{3.28}$$

which can be solved to obtain

$$\sigma_v^2 = \frac{\beta^2}{2\gamma}(1 - e^{-2\gamma t}), \tag{3.29}$$

independent of the systematic acceleration, as expected. In the long time limit $t \to \infty$, $\sigma_v^2 \to \frac{\beta^2}{2\gamma}$, as had been used to arrive at the fluctuation-dissipation theorem Eq. (2.42).

3.2 Mean and Variance of Displacement in One Dimension

By following a similar logic as in the case of velocity $v(t)$, we can deduce that any component of position vector denoted by $x(t)$, will also be the sum of statistically independent normal random variables, and therefore a normal random variable itself. Thus, it can be written in the form

$$x(t) = N_0^t(\text{mean}[x(t)], \text{variance}[x(t)]). \tag{3.30}$$

Averaging both sides of Eq. (3.1) component wise, one obtains

$$\frac{d\langle x(t)\rangle}{dt} = \langle v(t)\rangle. \tag{3.31}$$

Integrating Eq. (3.17), one arrives at

$$\langle x(t)\rangle = x_0 + c_1 v_0 t + c_2 a_0 t^2 + \cdots + c_n a_0^{(n-2)} t^n + \cdots. \tag{3.32}$$

For the variance σ_x^2, solving as we did for velocity variance [26], we can write

$$d[x^2(t)] = x^2(t+dt) - x^2(t). \tag{3.33}$$

Substituting the position update expression into the above equation

$$d[x^2(t)] = [x(t) + v(t)dt]^2 - x^2(t), \tag{3.34}$$

and ignoring terms higher that order dt, this simplifies to

$$d[x^2(t)] = 2x(t)v(t)dt. \tag{3.35}$$

Averaging both sides and dividing by dt

$$\frac{d\langle x^2(t)\rangle}{dt} = 2\langle x(t)v(t)\rangle. \tag{3.36}$$

By definition of variance, on can write

$$\frac{d\langle \sigma_x^2\rangle}{dt} = \frac{d\langle x^2(t)\rangle}{dt} - 2\langle x(t)\rangle\langle v(t)\rangle, \tag{3.37}$$

arriving at

$$\frac{d\langle \sigma_x^2\rangle}{dt} = 2\mathrm{cov}(x, v), \tag{3.38}$$

where co-variance of position and velocity is written as $\mathrm{cov}(x, y) = \langle x(t)v(t)\rangle - \langle x(t)\rangle\langle v(t)\rangle$.

We now solve for the co-variance as

$$d[\mathrm{cov}(x, v)] = d[\langle x(t)v(t)\rangle - \langle x(t)\rangle\langle v(t)\rangle]. \tag{3.39}$$

Taking the differential of the right side, we obtain

$$d[\mathrm{cov}(x, v)] = \langle x(t)d[v(t)]\rangle + \langle d[x(t)]v(t)\rangle - \langle x(t)\rangle d[\langle v(t)\rangle] - d[\langle x(t)\rangle]\langle v(t)\rangle. \tag{3.40}$$

Substituting the expressions derived earlier for $\langle v(t)\rangle$ and $\langle x(t)\rangle$, we obtain

$$\begin{aligned} d[\mathrm{cov}(x, v)] = -\gamma\langle x(t)v(t)\rangle dt + \langle x(t)a(t)\rangle dt + \langle x(t)\sqrt{\beta^2 dt}N(0,1)\rangle + \langle v^2(t)\rangle dt + \\ \langle x(t)v(t)\rangle dt - \langle x(t)\rangle a(t)dt - \langle v(t)\rangle^2 dt, \end{aligned} \tag{3.41}$$

whereby the two terms containing the systematic acceleration $a(t)$ cancel out. Further, using the assumption that $x(t)$ and $N(0,1)$ are statistically independent and using definitions of variance and co-variance, the above equation simplifies to

$$d[\mathrm{cov}(x,v)] = -\gamma \mathrm{cov}(x,v) + {\sigma_v}^2. \tag{3.42}$$

Using the result for velocity variance Eq. (3.29) and multiplying by integrating factor $e^{\gamma t}$, we can solve the above differential equation to obtain

$$\mathrm{cov}(x,v) = \frac{\beta^2}{2\gamma^2}(1 - 2e^{-\gamma t} + e^{2\gamma t}). \tag{3.43}$$

Now, Eq. (3.38) can be solved to give

$$\sigma_x^2 = \frac{\beta^2}{\gamma^2}\left[t - \frac{2}{\gamma}(1 - e^{-\gamma t}) + \frac{1}{2\gamma}(1 - e^{-2\gamma t})\right]. \tag{3.44}$$

Thus, we have obtained the means and variances of each component of position and velocity that can be solved numerically as discussed in the next section. One point worth mentioning here is that, the variances for both position and velocity are independent of the systematic acceleration $a(t)$ under the condition that the systematic acceleration is only a function of time, and this may not be true in general. However, if we compare the actual analytical variances [26] for a typical position dependent systematic force, such as for the case of a harmonic oscillator, with the above variances as was done during the course of this work, one finds the difference is negligible, and to a good approximation we continue to use these expressions for the Brownian dynamic simulation for pairwise inter-particle interaction that depends only on inter-particle separation.[3]

As an additional note, we have just shown that each component of position $x(t)$ and velocity $v(t)$ is a normal random variable characterized by its mean and variance for which we have derived approximate analytic expressions, and these give us our principal working equations. Explicitly writing out each of the components, we thus have

$$v_x(t) = \langle v_x(t)\rangle + \sqrt{\sigma_{vx}^2} N_{v_x}(0,1), \tag{3.45a}$$

$$x(t) = \langle x(t)\rangle + \sqrt{\sigma_x^2} N_x(0,1), \tag{3.45b}$$

$$v_y(t) = \langle v_y(t)\rangle + \sqrt{\sigma_{vy}^2} N_{v_y}(0,1), \tag{3.45c}$$

$$y(t) = \langle y(t)\rangle + \sqrt{\sigma_y^2} N_y(0,1), \tag{3.45d}$$

where we make explicit use of subscripts x, y to denote the components in the respective directions. However, written in this form, the normal variables $N_{v_x}(0,1), N_x(0,1), N_{v_y}(0,1), N_y(0,1)$ are not necessarily statistically independent. In particular, while both $N_{v_x}(0,1)$ and $N_x(0,1)$ are independent of each

[3]Moreover, if we directly update the Langevin's Eqs. (3.1) and (3.2) for a typical case of say $\Gamma = 100$, and compare the velocity variance against the ones computed adopting the present approach, the results are identical up to three decimal places checked during this work. For a detailed comparison of different simulation schemes, refer to Hou and Miskovic [27].

of $N_{v_y}(0,1)$ and $N_y(0,1)$, $[N_{v_x}(0,1), N_x(0,1)]$ and $[N_{v_y}(0,1), N_y(0,1)]$ taken together, constitute sets of jointly distributed random variables. This follows from the definition of jointly distributed random variables, i.e., two variables are jointly normal if they are each a linear combination of independent normals. Since $x(t+dt)$ is obtained as a linear combination of $x(t)$ and $v_x(t)$, where $v_x(t)$ is obtained from an independent normal $N_{v_x}(0,1)$, we see that they constitute jointly normal random variables. Similarly for the y-components.

However, $v_x(t)$, $x(t)$ and $v_y(t)$, $y(t)$ can always be written in terms of independent normal random variables, which is very useful for the purpose of simulations. Thus, it is always possible to rewrite the above four equations as [26]

$$v_x(t) = \langle v_x(t)\rangle + \sqrt{\sigma_{v_x}^2}N_{1_x}(0,1), \tag{3.46a}$$

$$x(t) = \langle x(t)\rangle + I_{1_x}N_{1_x}(t) + I_{2_x}N_{2_x}(0,1), \tag{3.46b}$$

$$v_y(t) = \langle v_y(t)\rangle + \sqrt{\sigma_{v_y}^2}N_{1_y}(0,1), \tag{3.46c}$$

$$y(t) = \langle y(t)\rangle + I_{1_y}N_{1_y}(0,1) + I_{2_y}N_{2_y}(0,1), \tag{3.46d}$$

where

$$I_{1_x} = I_{1_y} = \frac{\mathrm{cov}(x,v_x)}{\sqrt{\sigma_{v_x}^2}} = \frac{\mathrm{cov}(y,v_y)}{\sqrt{\sigma_{v_y}^2}}, \tag{3.47a}$$

$$I_{2_x} = I_{2_y} = \sqrt{\sigma_x^2 - I_{1_x}^2} = \sqrt{\sigma_y^2 - I_{1_y}^2}. \tag{3.47b}$$

Here, $N_{1_x}(0,1), N_{2_x}(0,1), N_{1_y}(0,1), N_{2_y}(0,1)$ are statistically independent unit normal random variables and the equalities follow, since all the variances and co-variances are independent of the particular choice of coordinates. A method to generate statistically independent normal random variables from uniform random variables is given in Appendix C, and an excellent reference is Gillespie [25].

3.3 Time Stepping

Many different algorithms exist for the time stepping of finite difference [28] Eqs. (3.46) involving trade-offs in accuracy, time-stepping requirement, memory storage required and ease of implementation. In general, the methods may be classified into Verlet type methods and Prediction-Correction type methods [29]. However, for the purpose of this work we do not attempt to make any comparisons between the various methods and choose the predictor-corrector type method specifically tested and proven for high accuracy and stability (in terms of energy convergence) by Hou and Miskovic [27] for simulating a many particle system through Brownian dynamics simulation. We reproduce the basic steps [27] in Appendix G. In the following, we summarize all the steps needed to simulate our 2D system of dust particles.

- Initialize the simulation cell. In our case, we work in a 2D square cell with periodic boundary conditions [29](some details are also mentioned in the Appendix C), typically with $N = 4000$ particles. The particles are distributed randomly throughout the simulation cell at initialization.

- Evaluate position and velocity variances by using Eq. (3.38) and Eq. (3.29) once during the course of simulation, by setting $t \mapsto dt$, where dt is the time stepping used.

- Predict the position, velocity and all derivatives of acceleration for the particle, component wise using Eq. (G.1). For a multi-particle system, we do this for all particles in the simulation cell, and store the values in an array.

- Evaluate the external force acting on a particle. For a multi-particle system governed by pair-wise interaction only, evaluate the force acting on every particle by every other particle in the simulation cell, and store the resulting values in an array. Since this step is likely to be the most time consuming step of the simulation, we can use several ways to improve the performance. Some of these methods used during the course of this work have been illustrated in the Appendix C, while an excellent reference for the same is by Allen [29].

- Invoke the corrector step using Eq. (G.3) for every particle in the system.

- Finally, generate normal random variables and add random displacements using Eq. (3.46).

- These steps are repeated till the system reaches equilibrium, which can be checked by measuring the average kinetic energy of the system. Using Eq. (2.48), we expect the average kinetic energy per particle to reach $\frac{1}{2\Gamma}$. Further discussion on this can be found in Appendix C.

These are the general steps for simulation. In a later section, we will mention a few more details on how to extract collective wave modes and the static structure factor, once the system has reached equilibrium.

Chapter 4

Analytic Theory

As discussed in section 2.3.1, we will now obtain current density space-time auto-correlation functions within the framework of hydrodynamics and their generalization to incorporate the discrete nature of particles into account. In the process, we will make use of simple phenomenological models for the viscosity memory functions that will allow us to obtain estimates of dust wave dispersion and damping. These will then be compared with results from BD simulation in the next chapter.

4.1 Ordinary Hydrodynamic (OH) Equations

The fluid equations of continuity and conservation of momentum [30] that ignore any fluctuations in temperature of the system are,

$$\frac{\partial}{\partial t}\tilde{\rho}(\mathbf{r},t) + \nabla \cdot [\tilde{\rho}(\mathbf{r},t)\tilde{\mathbf{v}}(\mathbf{r},t)] = 0, \tag{4.1}$$

where $\tilde{\rho}(\mathbf{r},t) \equiv n_d(\mathbf{r},t)$ is the particle number density per unit area, and

$$\begin{aligned} m\tilde{\rho}(\mathbf{r},t)\frac{\partial}{\partial t}[\tilde{\mathbf{v}}(\mathbf{r},t)] + m\tilde{\rho}(\mathbf{r},t)[\tilde{\mathbf{v}}(\mathbf{r},\mathbf{t})\cdot\nabla]\tilde{\mathbf{v}}(\mathbf{r},\mathbf{t}) + \nabla\tilde{p}(\mathbf{r},t) = \eta_1\{\nabla^2\tilde{\mathbf{v}}(\mathbf{r},t) + \\ \nabla[\nabla\cdot\tilde{\mathbf{v}}(\mathbf{r},\mathbf{t})]\} + \eta_2\nabla[\nabla\cdot\tilde{\mathbf{v}}(\mathbf{r},t)], \end{aligned} \tag{4.2}$$

where m is the mass of a dust particle, $\tilde{p}(\mathbf{r},t)$ is the pressure, $\tilde{\mathbf{v}}(\mathbf{r},t) \equiv \mathbf{v_d}(\mathbf{r},\mathbf{t})$ is local velocity field, and η_1 and η_2 are coefficients of shear and bulk viscosity [30] respectively[1]. The above set of equations can be closed by expressing the pressure in terms of density, via the isothermal compressibility, as will be shown in the next section.

It is worthwhile to comment on how these equations compare with Eqs. (2.14), where the layer of dusty plasma was treated as an incompressible fluid of charged particles, and the set of equations were therefore

[1] We are following the 2D conservation of momentum equation as used by Nosenko and Goree [31] for a 2D Yukawa system.

completed by the Poisson's equation for charged dust particles. However, in this development we are considering the dust layer as forming a neutral compressible fluid [21], with particles interacting via the shielded Yukawa potential, analogous to the way Lennard-Jones fluid interact. The particular nature of the interaction potential influences the system pressure, in turn affecting the compressibility of the fluid, which will be explicitly incorporated in the development to follow. This approach may be regarded as analogous to the approach adopted by Hansen [32, 21] for the development of the theory of GH for a one component plasma and as suggested by Murillo [9] for dusty plasma.

Since our interest is in studying small deviations from local equilibrium[2], we will chose a reference frame moving with the fluid velocity, say $\tilde{\mathbf{v}}_{\mathbf{0}}$. We will linearize the above equations by considering small perturbations to first order, as follows

$$\tilde{\rho} = \tilde{\rho}_0 + \epsilon\tilde{\rho}_1 = \rho + \delta\rho, \tag{4.3a}$$

$$\tilde{p} = \tilde{p}_0 + \epsilon\tilde{p}_1 = p + \delta p, \tag{4.3b}$$

$$\tilde{\mathbf{v}} = \tilde{\mathbf{v}}_{\mathbf{0}} + \epsilon\tilde{\mathbf{v}}_{\mathbf{1}} = 0 + \mathbf{v}. \tag{4.3c}$$

Defining the current density as $\mathbf{j}(\mathbf{r},t) = \rho\mathbf{v}(\mathbf{r},t)$ and linearizing Eq. (4.1) and Eq. (4.2) with respect to small perturbations, one obtains to first order

$$\frac{\partial}{\partial t}\delta\rho(\mathbf{r},t) + \nabla\cdot\mathbf{j}(\mathbf{r},\mathbf{t}) = 0, \tag{4.4a}$$

$$m\frac{\partial}{\partial t}\mathbf{j}(\mathbf{r},\mathbf{t}) + \nabla\delta p(\mathbf{r},t) = \frac{\eta_1}{\rho}\{\nabla^2\mathbf{j}(\mathbf{r},t) + \nabla[\nabla\cdot\mathbf{j}(\mathbf{r},t)]\} + \frac{\eta_2}{\rho}\nabla[\nabla\cdot\mathbf{j}(\mathbf{r},t)]. \tag{4.4b}$$

Dividing the momentum conservation equation by m, and defining $\frac{\eta_1}{m\rho} = \nu_1$, $\frac{\eta_2}{m\rho} = \nu_2$, one obtains

$$\frac{\partial}{\partial t}\mathbf{j}(\mathbf{r},t) + \frac{\nabla\delta p(\mathbf{r},t)}{m} = \nu_1\{\nabla^2\mathbf{j}(\mathbf{r},t) + \nabla[\nabla\cdot\mathbf{j}(\mathbf{r},t)]\} + \nu_2\nabla[\nabla\cdot\mathbf{j}(\mathbf{r},t)]. \tag{4.5}$$

We now have two equations but three variables, $\mathbf{j}(\mathbf{r},t)$, $\delta p(\mathbf{r},t)$ and $\delta\rho(\mathbf{r},t)$. Recalling that we are working in a constant temperature ensemble with fixed number of particles N, we can now obtain a third equation from thermodynamics. Expressing variations in pressure in terms of variations in density,

$$\delta p = \left[\frac{\delta p}{\delta\rho}\right]_{N,T}\delta\rho, \tag{4.6}$$

we can identify the thermodynamic relation

$$\left[\frac{\delta p}{\delta\rho}\right]_{N,T} = \frac{1}{\rho\chi_T}, \tag{4.7}$$

where χ_T is the isothermal compressibility[21] of the system, assumed constant. We have thus completed our set of equations.

[2]By this process, we are studying small amplitude variations in a compressible fluid, which by definition is a *sound wave* [30] and therefore our interest in obtaining its dispersion relation and damping.

Let us now take the Fourier transform of Eqs. (4.4a) and Eq. (4.5) in position space, i.e., transform $\mathbf{j}(\mathbf{r},t) \rightarrow \mathbf{j}_{\mathbf{k}}(t)$, $\delta p(\mathbf{r},t) \rightarrow \delta p_{\mathbf{k}}(t)$ and $\delta\rho(\mathbf{r},t) \rightarrow \delta\rho_{\mathbf{k}}(t)$ and then assuming the system to be isotropic with no preferred direction of wave propagation, set $\mathbf{k} = (k,0)$ as the k-space vector[21]. Further, let us define components of the current density vector as $\mathbf{j}_{\mathbf{k}}(t) = (j_k^l(t), j_k^t(t))$, where $j_k^l(t)$ is the longitudinal part of the current density, pointing in the direction of k-vector (x direction in this case) and $j_k^t(t)$ is the transverse component, pointing in a direction perpendicular to k-vector (y-direction in this case). We thus obtain the following equations in Fourier space

$$\frac{\partial}{\partial t}\delta\rho_k(t) - ikj_k^l(t) = 0, \tag{4.8a}$$

$$\frac{\partial}{\partial t}j_k^l(t) - \frac{ik\delta p_k(t)}{m} = \nu_1[-k^2 j_k^l(t) - k^2 j_k^l(t)] - \nu_2 k^2 j_k^l(t), \tag{4.8b}$$

$$\frac{\partial}{\partial t}j_k^t(t) = -\nu_1 k^2 j_k^t(t). \tag{4.8c}$$

4.1.1 Longitudinal Current Density

Since our main interest lies in the longitudinal current density, we will now focus on Eq. (4.8a) and Eq. (4.8b) and drop the superscripts and subscripts l. A brief description of attempts to model the transverse current density using this theory is given in Appendix F.

First, Eq. (4.8a) may be written in integral form as

$$\delta\rho_k(t) = \delta\rho_k(0) + ik\int_0^t dt'\ j_k(t'). \tag{4.9}$$

Defining, $2\nu_1 + \nu_2 = \nu_l$, where ν_l is the longitudinal viscosity[3], we write Eq. (4.8b) as

$$\frac{\partial}{\partial t}j_k(t) - \frac{ik\delta\rho_k(t)}{m\rho\chi_T} = -\nu_l k^2 j_k(t). \tag{4.10}$$

Inserting Eq. (4.9) into the above equation, we obtain

$$\frac{\partial}{\partial t}j_k(t) = -\frac{k^2}{m\rho\chi_T}\int_0^t dt'\ j_k(t') - \nu_l k^2 j_k(t) + \frac{ik}{m\rho\chi_T}\delta\rho_k(0). \tag{4.11}$$

The longitudinal current density auto-correlation function[4] is defined as [20]

$$C(k,t) = \langle j_k^*(0)j_k(t)\rangle. \tag{4.12}$$

[3]There has been some debate recently as to the existence of some of these transport coefficients for 2D dusty plasma, for instance in Ref [33]. We will not be addressing these issues and, fortunately we also do not need to explicitly evaluate any of these transport coefficients !

[4]This can also be referred as *current density-current density correlation* or *current density auto-correlation.*

Multiplying Eq. (4.11) by $j_k(0)^*$ and ensemble averaging,

$$\frac{\partial}{\partial t}C(k,t) = -\frac{k^2}{m\rho\chi_T}\int_0^t dt'\ C(k,t') - \nu_l k^2 C(k,t), \tag{4.13}$$

where $\frac{ik}{m\rho\chi_T}\langle\rho_k(0)j_k^*(0)\rangle$ vanishes by symmetry [20], as can be seen by multiplying Eq. (4.8a) with $\rho_k(0)^*$ and ensemble averaging the resultant expression, evaluated at $t = 0$. As in Appendix E, $\langle\frac{\partial\rho_k(t)}{\partial t}\rho_k^*(0)\rangle_{t=0}$ vanishes, producing the desired result. The power spectrum of the longitudinal current density auto-correlation function can now be obtained as the Fourier transform of the longitudinal current density auto-correlation function or equivalently, as shown in Appendix B, the real part of the one sided Laplace transform [21] of the current density auto-correlation function, evaluated at $s = i\omega$, which we call $P(k,\omega) = \Re\{\mathcal{L}[C(k,t)]\}_{s=i\omega}$. Thus, we obtain

$$P(k,\omega) = 2v_{th}^2\frac{\omega^2\nu_l k^2}{[\omega^2 - \frac{k^2}{m\rho\chi_T}]^2 + [\omega(\nu_l k^2)]^2}. \tag{4.14}$$

Assuming χ_T is constant, this gives us a linear dispersion relation as

$$\omega = \frac{k}{\sqrt{m\rho\chi_T}}. \tag{4.15}$$

and the full width at half maximum as $\nu_l k^2$. We will now see in the next section that when we extend our model to GH, this same dispersion relation will be recovered in the limiting case of low wave-number k.

4.2 Extension to Generalized Hydrodynamics (GH)

In order to try and model the observed behavior of the power spectral density of the longitudinal current density auto-correlation function as observed from simulations, we now invoke the following zero and second frequency sum rules [20],

$$\frac{1}{2\pi}\int_{-\infty}^{\infty} d\omega\ P(k,\omega) = v_{th}^2, \tag{4.16a}$$

$$\frac{1}{2\pi}\int_{-\infty}^{\infty} d\omega\ \omega^2 P(k,\omega) = \langle\omega^2(k)\rangle, \tag{4.16b}$$

where v_{th} is the thermal speed contribution in the longitudinal direction and $\langle\omega^2(k)\rangle$ is called the longitudinal frequency or the second-moment of frequency. These rules are basically used to model the short time behavior of the correlation functions and will allow us to make comparisons with our introductory discussions in section 2.3.1. Consider for instance the current density auto-correlation function defined in Eq. (4.13) expressed in terms of its Fourier transform $P(k,\omega)$ as

$$C(k,t) = \frac{1}{2\pi}\int_{-\infty}^{\infty} d\omega\ e^{i\omega t}P(k,\omega). \tag{4.17}$$

Expanding $C(k,t)$ in Taylor's series around $t = 0$, we obtain

$$C(k,t) = C(k,0) + \frac{t}{1!}\left[\frac{\partial}{\partial t}C(k,t)\right]_{t=0} + \frac{t^2}{2!}\left[\frac{\partial^2}{\partial t^2}C(k,t)\right]_{t=0} + \cdots. \tag{4.18}$$

We can recognize from Eq. (4.17) that,

$$C(k,0) = \frac{1}{2\pi}\int_{-\infty}^{\infty} d\omega\ P(k,\omega),$$

$$\left[\frac{\partial}{\partial t}C(k,t)\right]_{t=0} = \frac{1}{2\pi}\int_{-\infty}^{\infty} d\omega\ \omega P(k,\omega) = 0,$$

$$\left[\frac{\partial^2}{\partial t^2}C(k,t)\right]_{t=0} = -\frac{1}{2\pi}\int_{-\infty}^{\infty} d\omega\ \omega^2 P(k,\omega),$$

and so forth for higher derivatives.(Note, all odd derivatives will vanish since $P(k,\omega)$ is an even-function [12] in ω, see Appendix B.2.) Denoting

$$\langle\omega^n(k)\rangle = \frac{1}{2\pi}\int_{-\infty}^{\infty} d\omega\ \omega^n P(k,\omega), \tag{4.20}$$

we call $\langle\omega^n(k)\rangle$ as the n-th frequency moment of $P(k,\omega)$, which satisfies the relation,

$$\langle\omega^{2n}(k)\rangle = (-1)^n\left[\frac{\partial^{2n}}{\partial t^{2n}}C(k,t)\right]_{t=0}. \tag{4.21}$$

Referring now to Eq. (4.8a), differentiating it once more with respect to time and substituting Eq. (4.8b), we obtain

$$\frac{\partial^2}{\partial t^2}\delta\rho_k(t) = -\frac{k^2}{m\rho\chi_T}\delta\rho_k(t) - \nu_l k^2\frac{\partial}{\partial t}\delta\rho_k(t). \tag{4.22}$$

Multiplying both sides of the above equation with $\delta\rho_k^*(0)$ and ensemble averaging at $t = 0$,

$$\left\langle\frac{\partial^2}{\partial t^2}\delta\rho_k(t)\delta\rho_k^*(0)\right\rangle_{t=0} = -\frac{k^2}{m\rho\chi_T}\left\langle\delta\rho_k(0)\delta\rho_k^*(0)\right\rangle - \nu_l k^2\left\langle\frac{\partial}{\partial t}\delta\rho_k(t)\delta\rho_k^*(0)\right\rangle_{t=0}. \tag{4.23}$$

As shown in Appendix E, we find that the last term on the right vanishes giving

$$\left\langle\frac{\partial^2}{\partial t^2}\delta\rho_k(t)\delta\rho_k^*(0)\right\rangle_{t=0} = -\frac{k^2}{m\rho\chi_T}\left\langle\delta\rho_k(0)\delta\rho_k^*(0)\right\rangle. \tag{4.24}$$

But by definition $\langle\delta\rho_k(0)\delta\rho_k^*(0)\rangle = S(k)$, where $S(k)$ is the static structure factor [21] defined in Appendix D. Therefore

$$\left\langle\frac{\partial^2}{\partial t^2}\delta\rho_k(t)\delta\rho_k^*(0)\right\rangle_{t=0} = -\frac{k^2}{m\rho\chi_T}S(k). \tag{4.25}$$

As shown in Appendix E, the left hand side of Eq. (4.25) can be written as

$$\left\langle\frac{\partial^2}{\partial t^2}\delta\rho_k(t)\delta\rho_k^*(0)\right\rangle_{t=0} = -\left\langle\frac{\partial}{\partial t}\delta\rho_k^*(t)\frac{\partial}{\partial t}\delta\rho_k(t)\right\rangle_{t=0}. \tag{4.26}$$

But from Eq. (4.8a), the right-hand side evaluates to

$$\begin{aligned}\left\langle \frac{\partial^2}{\partial t^2}\delta\rho_k(t)\delta\rho_k^*(0)\right\rangle_{t=0} &= -\left\langle \frac{\partial}{\partial t}\delta\rho_k^*(t)\frac{\partial}{\partial t}\delta\rho_k(t)\right\rangle_{t=0} \\ &= -k^2\left\langle j_k^*(0)j_k(0)\right\rangle. \\ &= -k^2 v_{th}^2 \end{aligned} \tag{4.27}$$

From the above equations and Eq. (4.25), we therefore infer that to be consistent with the zeroth sum rule, we must make the following replacement

$$\rho\chi_T \mapsto \frac{S(k)}{mv_{th}^2}. \tag{4.28}$$

In addition, following exactly the same derivation, we can find that there is no way we can satisfy the second frequency sum rule, since $\langle\omega^2(k)\rangle$ does not appear anywhere in our equations. Thus, in order to capture the short time behavior of the longitudinal current density auto-correlation function, we now invoke the results from our discussion on generalized transport coefficients (section 2.3.1) and as suggested in Refs [20], introduce a longitudinal viscosity memory function $\phi(k,t)$ in place of ν_l in the evolution equation for the current density auto-correlation function. Making this replacement in Eq. (4.13), we obtain

$$\frac{\partial}{\partial t}C(k,t) = -\frac{k^2v_{th}^2}{S(k)}\int_0^t dt'\ C(k,t') - k^2\int_0^t dt'\ \phi(k,t-t')C(k,t'). \tag{4.29}$$

Proceeding further with the model, we now try to see how the memory function helps us in satisfying the second frequency sum rule. Differentiating Eq. (4.29) with respect to time (following the chain rule for differentiating an integral),

$$\frac{\partial^2}{\partial t^2}C(k,t) = -\frac{k^2v_{th}^2}{S(k)}C(k,t) - k^2\int_0^t dt'\ C(k,t')\frac{\partial}{\partial t}\phi(k,t-t') - k^2\phi(k,0)C(k,t). \tag{4.30}$$

Setting $t=0$, this reads

$$\left[-\frac{\partial^2}{\partial t^2}C(k,t)\right]_{t=0} = v_{th}^2\left[\frac{(kv_{th})^2}{S(k)} + k^2\phi(k,0)\right]. \tag{4.31}$$

Matching with Eq. (4.16b), we obtain

$$\phi(k,0) = \frac{\langle\omega^2(k)\rangle}{v_{th}^2k^2} - \frac{v_{th}^2}{S(k)}, \tag{4.32}$$

which gives us the initial value of the longitudinal viscosity memory function as a function of second frequency moment Eq. (4.16b), the relation we were trying to obtain. Now, defining the memory kernel for convenience as

$$K(k,t) = \frac{(kv_{th})^2}{S(k)} + k^2\phi(k,t), \tag{4.33}$$

we find that we can rewrite Eq. (4.29) as

$$\frac{\partial}{\partial t}C(k,t) = -\int_0^t dt'\ K(k,t-t')C(k,t'). \tag{4.34}$$

Taking the Laplace transform

$$s\tilde{C}(k,s) - \tilde{C}(k,0) = -\tilde{K}(k,s)\tilde{C}(k,s), \tag{4.35}$$

where $\tilde{C}, \tilde{K}$ are Laplace transformed functions (s is the variable in Laplace transform space). We thus obtain

$$\tilde{C}(k,s) = \frac{\tilde{C}(k,0)}{s + \tilde{K}(k,s)} = \frac{v_{th}^2}{s + \tilde{K}(k,s)}. \tag{4.36}$$

The transform of memory kernel Eq. (4.33) reads

$$\tilde{K}(k,s) = \frac{(kv_{th})^2}{S(k)}\frac{1}{s} + k^2\tilde{\phi}(k,s). \tag{4.37}$$

Setting $s = i\omega$ in the above equation and separating the real and imaginary parts of the memory kernel, we obtain

$$\Re(\tilde{K}(k,\omega)) = K'(k,\omega) = k^2\phi'(k,\omega), \tag{4.38a}$$

$$\Im(\tilde{K}(k,\omega)) = K''(k,\omega) = -\frac{(kv_{th})^2}{\omega S(k)} + k^2\phi''(k,\omega), \tag{4.38b}$$

where $\phi'(k,\omega)$ and $\phi''(k,\omega)$ are the real (dissipative) and imaginary (non-dissipative) parts of the memory function. Substituting these values in Eq. (4.36) we obtain,

$$\tilde{C}(k,\omega) = \frac{v_{th}^2}{i[\omega + K''(k,\omega)] + K'(k,\omega)}. \tag{4.39}$$

Obtaining the power spectrum of the current density auto-correlation function[5] as the real part of Eq. (4.39) [21], and substituting for $K'(k,\omega)$ and $K''(k,\omega)$ as defined above,

$$P(k,\omega) = 2v_{th}^2\frac{\omega^2k^2\phi'(k,\omega)}{[\omega^2 - \omega_0^2(k) + \omega k^2\phi''(k,\omega)]^2 + [\omega k^2\phi'(k,\omega)]^2}. \tag{4.40}$$

In the above, we have explicitly defined

$$\omega_0^2(k) = \frac{(kv_{th})^2}{S(k)}. \tag{4.41}$$

Discussion

The entire derivation thus far has been carried out by treating the dust layer as being identical to a simple fluid[6], and therefore we have followed the transparent treatment for simple fluids outlined by Boon and Yip [20]. If we now try to make comparisons with our BD results, we notice that in our simulations the dust particles were treated as interacting Brownian particles in a background of neutrals whose effect we have completely ignored so far. The justification between our use of a hydrodynamics approach for our system of interacting Brownian particles and the link between this approach and the results from BD

[5]To be interchangeably referred as power spectral density or simply the spectral density [21]

[6]In the context used for instance, in references [20, 21].

simulation study, is provided by the work of Hess and Klein [34].

Beginning with the Fokker-Planck equation for a system of interacting Brownian particles, Hess and Klein [34] have derived an equivalent hydrodynamics equation by explicitly taking into account viscous effects, and the effect of friction drag exerted by background neutrals. In that context, their results lead to Eq. (4.34) as being correct even in the presence of neutral friction, provided the memory kernel $K(k,t)$ is considered to include the effects of both, non-local in time and space longitudinal viscosity memory function and non-local in time and space neutral friction memory function (hydrodynamic interaction)[7]. However, in the limiting case when any hydrodynamic interactions may be neglected, they have further shown that the effect of background neutral friction can be incorporated by adding the constant ξ to Eq. (4.34) as follows

$$\frac{\partial}{\partial t}C(k,t) = -\int_0^t dt'\ K(k,t-t')C(k,t') - \xi C(k,t). \tag{4.42}$$

Solving this equation by taking its Laplace transform, one obtains the following form of power spectral density

$$P(k,\omega) = 2v_{th}^2 \frac{\omega^2[k^2\phi'(k,\omega)+\xi]}{[\omega^2-\omega_0^2(k)+\omega k^2\phi''(k,\omega)]^2+\{\omega[k^2\phi'(k,\omega)+\xi]\}^2}, \tag{4.43}$$

which recovers Eq. (4.40) in the limit $\xi \to 0$.

Since we are focusing on a weakly damped system, we can also try to understand the inclusion of neutral friction from another point of view. That is, in order to extend the hydrodynamic model to higher frequencies, we can first apply the memory function formalism outlined by Boon and Yip [20] that incorporates the effects of viscous relaxation in the short time dynamics of dust collective modes by enforcing the low-order frequency sum rules upon the power spectral densities of such modes. This procedure can be completed by initially neglecting the neutral drag because, for typical dusty plasmas, the relaxation time due to dust collisions with neutral molecules is expected to be much longer than the viscous relaxation time. Once the initial value properties of the relevant memory functions are fixed by the sum rules, one may incorporate the effect of neutral drag by simply adding a local dissipative force into the fluid equations of motion and thereby make connection with the results from BD simulation. This thus allows us to treat the dust layer as a simple neutral fluid, and incorporate the effect of background neutral friction as a small modification to longitudinal current density auto-correlation as in Eq. (4.42). However, it is still best to regard this approach as an approximation in the limit of vanishing γ (which is consistent with the physical picture of a dusty plasma and our BD simulations), and in the spirit of suggestions made in Refs. [10, 9] for a system of dusty plasma.

[7] By hydrodynamic interactions we mean a non-local in time and non-local in space neutral friction in the form of a memory function, analogous to the longitudinal viscosity memory function. If a neutral friction memory function is considered, then the frequency moments will also have to re-evaluated and as shown in Refs [34], finite odd moments of the current density auto-correlation function will exist.

In addition, we notice that, and as has been suggested by the work in Refs [34, 32, 21], the inclusion of the static structure factor $S(k)$ (via the isothermal compressibility) into the current density auto-correlation equation helps us in incorporating all the microscopic details of the pairwise inter-particle potential into our equations. Thus, the entire dynamics for the power spectral density of the current density auto-correlation function for our system of charged dust particles is contained in Eq. (4.29). If we model our longitudinal viscosity memory function with a delta function modulated by ν_l, we will recover the case of constant viscosity, but the effect of inter-particle forces is still contained in the static structure factor.

The introduction of the longitudinal viscosity memory function can be regarded mathematically as an attempt to incorporate the second frequency sum rule into our equations. Physically, it can be seen in light of our discussion in section 2.3.1, where by we have modified the ordinary hydrodynamical equations to model the strong correlations between interacting dust particles by introducing a sort of elasticity to capture the response of the dust fluid to higher frequency stresses, by incorporating a finite time of relaxation of dust particles once displaced from equilibrium. The stronger the coupling between particles, the longer we can expect the relaxation time to be.

We next proceed to discuss three simple models for the longitudinal viscosity memory function, against which we will compare results from our BD simulation.

4.2.1 Simple Memory Function Models

If the longitudinal viscosity memory function is represented by $\phi(k,t) = \nu_l\delta(t)$, then $\phi'(k,\omega) = \nu_l$ and $\phi''(k,\omega) = 0$, giving us

$$P(k,\omega) = 2v_{th}^2 \frac{\omega^2(k^2\nu_l + \xi)}{[\omega^2 - \omega_0^2(k)]^2 + [\omega(k^2\nu_l + \xi)]^2}. \tag{4.44}$$

This gives us our first approximation to the dispersion relation as

$$\omega^2 = \omega_0^2(k). \tag{4.45}$$

Under the assumption of vanishing $\xi \to 0$, the form of Eq. (4.44) leads to a prediction of damping or half width at half maximum given by $\frac{1}{2}k^2\nu_l$, in agreement with the predictions of Kaw and Sen [10]. We can further note that, as $k \to 0$, Eq. (2.22) for the hydrodynamic dispersion leads to

$$\omega \sim \frac{k}{\sqrt{\kappa}}, \tag{4.46}$$

a linear dependence. Similarily, Eq. (4.45) yields

$$\omega \sim \frac{kv_{th}}{\sqrt{S(k\to 0)}}. \tag{4.47}$$

As shown in Eq. (D.9) (Appendix D), $S(k \to 0) = k_BT\rho\chi_T$. Further, $k_BT = v_{th}^2 = \frac{1}{2\Gamma}$. Thus, the approximate dispersion relation gives us

$$\omega \sim \frac{k}{\sqrt{m\rho\chi_T}}, \tag{4.48}$$

again a linear relation, reproducing the OH result Eq. (4.15) and also providing equivalence with the hydrodynamic (for charged species) dispersion relation for vanishing k, i.e., Eq. (4.46). Revisiting our earlier discussion on the effect of inter-particle forces being included in the isothermal compressibility, we notice from Eqs. (4.46) and (4.48) that

$$\chi_T \mapsto \frac{\kappa}{m\rho}. \tag{4.49}$$

We may try to understand this by considering some computed values of $S(k \to 0)$[8] for different values of κ. From simulation, the following can be observed.

κ	$S(k = 0.056)$
0.5	0.0038
1.0	0.0084
2.0	0.559

The table compares the value of $S(k \to 0)$ computed for $\Gamma = 100$ at the smallest value of $k = 2\pi/l$ accessible to the system, where l is the dimension of the square simulation cell in reduced units. The values suggest that, as κ increases, the compressibility can be expected to increase (possibly due to weakening of inter-particle repulsive forces), while at lower values of κ, the compressibility is expected to decrease (possibly due to the more long ranged inter-particle forces, making it more difficult for particles to pack closer together). A similar analysis was reported by Barrat *et al.* [32] for a Yukawa system.

To a next approximation, if we now choose an exponential longitudinal viscosity memory function $\phi(k,t) = \phi(k,0)e^{-\frac{t}{\tau_l}}$, (where τ_l will be assumed to be a constant relaxation time that we use as a fitting parameter, possibly as a function of Γ) we obtain,

$$\phi'(k,\omega) = \phi(k,0)\frac{\tau_l}{1+\omega^2\tau_l^2}, \tag{4.50a}$$

$$\phi''(k,\omega) = -\phi(k,0)\frac{\omega\tau_l^2}{1+\omega^2\tau_l^2}. \tag{4.50b}$$

To a good approximation, the dispersion relation can now be obtained from

$$\omega^2 - \omega_0^2(k) - \frac{k^2\phi(k,0)\omega^2\tau_l^2}{1+\omega^2\tau_l^2} = 0, \tag{4.51}$$

by solving for ω^2.

We can see that the idea of using an exponential model for the longitudinal viscosity memory function essentially stems from some physical reasoning. First consider using a delta function model for memory kernel in Eq. (4.34). This leads to an exponentially decaying current density auto-correlation function,

[8]The absolute values of $S(k \to 0)$ may not be taken to be strictly correct, as we found that an accurate evaluation of the low k behavior of $S(k)$ is fairly hard.

which we do not expect at stronger correlations, since previous results for the radial distribution function [8] clearly show an oscillatory behavior [8], a characteristics of dense fluids [19].

Suppose, we now use a constant value for the memory kernel. The differential equation Eq. (4.34) will now give purely oscillatory solutions, which is again unreasonable in a physical system.

Using a simple exponential model for the memory kernel however, allows us to provide a simple and physically more meaningful realization of the current density auto-correlation function. Moreover, an exponential model for the memory kernel can also be derived by using the techniques of Mori's [35, 34] yielding a continued fraction expansion on Eq. (4.34). Based on these grounds, if we now choose an exponential model for the longitudinal viscosity memory function as above, we will see in the next section that it provides us with a mathematically simple, yet a reasonable model for the system under consideration.

With equations Eqs. (4.32), Eqs. (4.40), (4.41) and (4.51) in hand, we can now compare the semi-analytic results with the results obtained from BD simulation.

4.2.2 Higher Order Moments

We can also attempt to extend the theory further by solving for higher order moments by proceeding the same way as for the second moment $\langle\omega^2(k)\rangle$, Eq. (4.29). Here, we attempt to solve for third and fourth frequency moments. As we will see, this will not only help us in avoiding the use of the relaxation time as a free parameter $\tau_l(\Gamma)$, but will also allow for another simple selection of the longitudinal viscosity memory function, based on conditions imposed by these higher order sum rules.

Differentiating Eq. (4.29) twice, to obtain the third derivative, we find

$$\begin{aligned}\frac{\partial^3}{\partial t^3}C(k,t) = -\frac{k^2 v_{th}^2}{S(k)}\frac{\partial}{\partial t}C(k,t) - k^2\int_0^t dt'\; C(k,t')\frac{\partial^2}{\partial t^2}\phi(k,t-t') - \\ k^2\left[C(k,t')\frac{\partial}{\partial t}\phi(k,t-t')\right]_{t'=t} - k^2\phi(k,0)\frac{\partial}{\partial t}C(k,t),\end{aligned} \tag{4.52}$$

which on evaluating at $t = 0$ yields

$$\left[\frac{\partial^3}{\partial t^3}C(k,t)\right]_{t=0} = -k^2\left[C(k,t')\frac{\partial}{\partial t}\phi(k,t-t')\right]_{t'=t=0}. \tag{4.53}$$

In the limit of vanishing γ, all odd frequency moments and hence the third frequency moment must vanish(Appendix A) [34]. Thus, we have the condition

$$-k^2 C(k,0)\left[\frac{\partial}{\partial t}\phi(k,t-t')\right]_{t'=t=0} = 0. \tag{4.54}$$

We therefore find that, the first derivative of longitudinal viscosity memory function must vanish at $t = 0$. Next, evaluating the fourth frequency moment we find,

$$\frac{\partial^4}{\partial t^4}C(k,t) = -\frac{k^2 v_{th}^2}{S(k)}\frac{\partial^2}{\partial t^2}C(k,t) - k^2\int_0^t dt'\ C(k,t')\frac{\partial^3}{\partial t^3}\phi(k,t-t') - k^2\left[C(k,t')\frac{\partial^2}{\partial t^2}\phi(k,t-t')\right]_{t'=t} - k^2\left[\frac{\partial}{\partial t}C(k,t)\frac{\partial}{\partial t}\phi(k,t-t')\right]_{t'=t} - k^2\phi(k,0)\frac{\partial^2}{\partial t^2}C(k,t). \tag{4.55}$$

Again setting $t' = t = 0$ we obtain,

$$\left[\frac{\partial^4}{\partial t^4}C(k,t)\right]_{t=0} = -\frac{k^2 v_{th}^2}{S(k)}\left[\frac{\partial^2}{\partial t^2}C(k,t)\right]_{t=0} - k^2 C(k,0)\left[\frac{\partial^2}{\partial t^2}\phi(k,t-t')\right]_{t'=t=0} - k^2\phi(k,0)\left[\frac{\partial^2}{\partial t^2}C(k,t)\right]_{t=0}. \tag{4.56}$$

Substituting for $\left[\frac{\partial^2}{\partial t^2}C(k,t)\right]_{t=0}$ from, Eq. (4.32) and writing $\left[\frac{\partial^4}{\partial t^4}C(k,t)\right]_{t=0} = \langle\omega^4(k)\rangle$, we obtain

$$\left[\frac{\partial^2}{\partial t^2}\phi(k,t-t')\right]_{t'=t=0} = \frac{\frac{\langle\omega^2(k)\rangle^2}{v_{th}^2} - \langle\omega^4(k)\rangle}{k^2 v_{th}^2}, \tag{4.57}$$

where as before, $v_{th} = \sqrt{\frac{k_B T}{m}}$ is the thermal speed.

We can now see that by choosing for $\phi(k,t) = c_1(k)e^{-c_2(k)t^2}$, we can establish conditions to satisfy all moments up to and including the fourth. Thus, we will get

$$\begin{aligned}\phi(k,0) &= c_1(k)\\ \left[\frac{\partial}{\partial t}\phi(k,t)\right]_{t=0} &= 0\\ \left[\frac{\partial^2}{\partial t^2}\phi(k,t)\right]_{t=0} &= -2c_1(k)c_2(k).\end{aligned} \tag{4.58}$$

where $c_1(k), c_2(k)$ can be obtained from simulation data using Eq. (4.32) and Eq. (4.57) respectively. Thus, by evaluating higher order frequency moments, we are able to obtain a model that does not involve any free parameters. This will constitute our Gaussian longitudinal viscosity memory function model.

Chapter 5

Results and Discussions

As mentioned briefly in the section on numerical integration of Langevin's equation, our simulation grid is a 2-Dimensional square array, typically containing $N = 4000$ particles with periodic boundary conditions. This grid is assumed to lie in the first quadrant of x, y plane, with area (in reduced units of a^2) such that from Eq. (2.10),

$$A = l^2 a^2 = N/n_d, \tag{5.1}$$

where l is the length of the side of the square simulation cell in reduced units. We further assume that, the wave number $\mathbf{k} = (k, 0)$ points in the x-direction which we now denote only by its magnitude k, and therefore the longitudinal mode is characterized by waves propagating in the x-direction. We now specify how we actually compute the power spectrum of the longitudinal current density auto-correlation function from simulation.

5.1 Wave Spectra from Simulation

- We first divide the simulation grid into thin slabs, labeled α (typically chosen as 2^9 slabs) along the longitudinal direction (x-direction in our case).
- After our system reaches equilibrium, we begin computing the current density using the following definition [8, 20]

  $$j(x,t) = \left[\frac{1}{\sqrt{N_\alpha}} \sum_{i=1}^{N_\alpha} v_{i,x} \right] \delta(x - x_\alpha), \tag{5.2}$$

  where $j(x,t)$ is the longitudinal current density, N_α is the number of particles in slab α, $v_{i,x}$ is the x-component of velocity of i^{th} particle, in slab α. At each time step, we compute the above sum for every slab, and record this data into a file. In a way, this provides us with a discrete sample of the current density, as a function of x. Recording this data over a period of time, we thus have discrete samples of current-density as a function of both position and time.

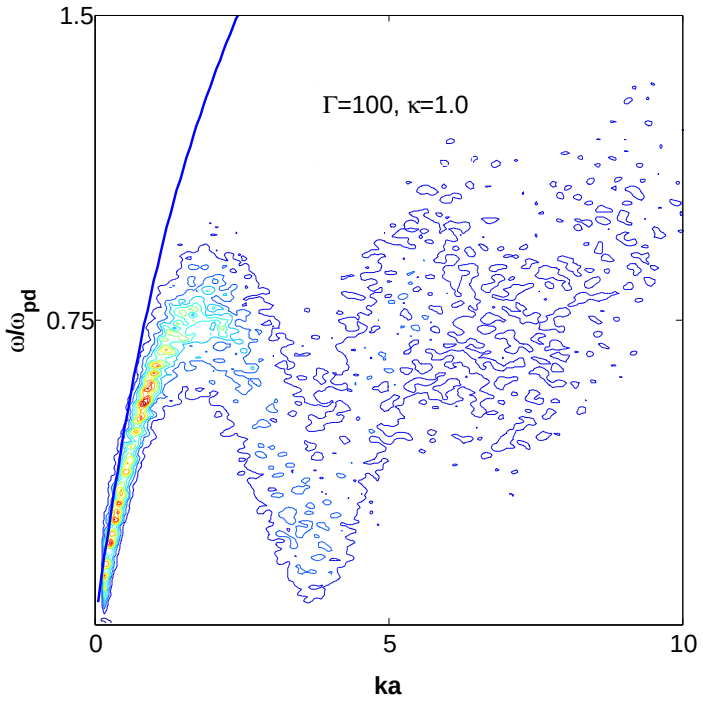

Figure 5.1: The solid blue curve represents the dispersion relation obtained by treating the dust layer as a charged incompressible fluid Eq. (2.22), while the contour plot is obtained from the power spectral density obtained from Brownian dynamics simulation of the dust particles, plotted for $\Gamma = 100$, $\kappa = 1.0$ and $\gamma = 0.06$.

- Finally, we compute a 2D Fast Fourier transform[1] of this data set, denoted as $F(k, \omega)$ and obtain the power spectral density as

$$P(k, \omega) = F^*(k, \omega) F(k, \omega), \tag{5.3}$$

  where $*$ signifies a complex conjugate. The power spectral density obtained this way can be shown to be equivalent to that obtained by taking a Fourier transform of the current density auto-correlation function $C(k, t)$ Eq. (4.13), up to a scaling factor [29, 36]. This has also been reproduced in Appendix B.

From the peak values of the power spectral density we can obtain the dispersion relation, $\omega = \omega(k)$. A typical plot so obtained, for the case of $\Gamma = 100, \kappa = 1.0, \gamma = 0.06$ is shown in Figure 5.1. In this plot, we also compare the dispersion relation obtained from simulation with the OH dispersion relation Eq. (2.22).

As we can see from the plot, the OH prediction is not able to model the bending of dispersion curve which is a result of stronger correlation effects between dust particles. Thus, while for very small wave

[1]For this work, all simulation was done in C-language while processing of data such as computation of FFT, was done using Matlab built-in routines.

numbers the hydrodynamic prediction matches with the results from simulation, we see that it begins to break down at higher wave numbers.

In order to use the results from GH, such as the dispersion relation obtained for the delta function model of the longitudinal viscosity memory function as given by Eq. (4.45), we notice that we require as input the static structure factor $S(k)$. In the present work, we directly use Eq. (D.5) given in Appendix D to compute $S(k)$ from simulation. Thus, once the system of dust particles attains equilibrium in time of the order of $\frac{10}{\gamma}$, we compute the sum given by Eq. (D.2) for one value of k, and use this sum in Eq. (D.5). We then repeat this process for different values of k, all at the same time step and record our result. The entire process is then repeated for several more time steps, giving the final result as an average over all these time steps. We thus replace the ensemble average with a long time average. A few representative plots of $S(k)$ for various values of coupling strengths Γ appear in Figure 5.2.

As can be observed, the magnitude of the first peak of the scattering intensity (where $S(k)$ has its first maximum), increases with an increase in Γ. Moreover, the oscillatory behavior at higher wave-numbers for higher Γ are suggestive of longer range ordering in the crystalline states. This behavior is further observed in the plots of radial distribution functions in Figure C.2.

We next proceed to perform comparisons between the results obtained from simulation with the predictions from GH, using the three simple memory function models described in the last section.

5.2 Comparison with Memory Function Models

In the following, all results will be shown for a standard value of $\gamma = 0.06$, along with the standard screening parameter $\kappa = 1$, for a set of coupling strengths $\Gamma = 20$, 60, 100, 200, 600, and 1000.

5.2.1 Dispersion Curves

Figure 5.3 shows plots of the dispersion curves obtained from GH for the three models of the longitudinal viscosity memory function discussed, i.e., delta function model (green), exponential model (red) and Gaussian model (black) against simulation data (contour plot) and predictions from OH (blue). First, a comparison between the GH models and OH reveals a much better match with the dispersion curves obtained from simulation using even the simplest delta function model for the longitudinal viscosity memory function. However, one can notice a mismatch between the delta function model and simulation data developing near the region of first dispersion peak, i.e., where $\frac{\partial \omega}{\partial k} = 0$, and this mismatch increases as we move to higher coupling regimes.

For the exponential model of the longitudinal viscosity memory function, the pertinent dispersion re-

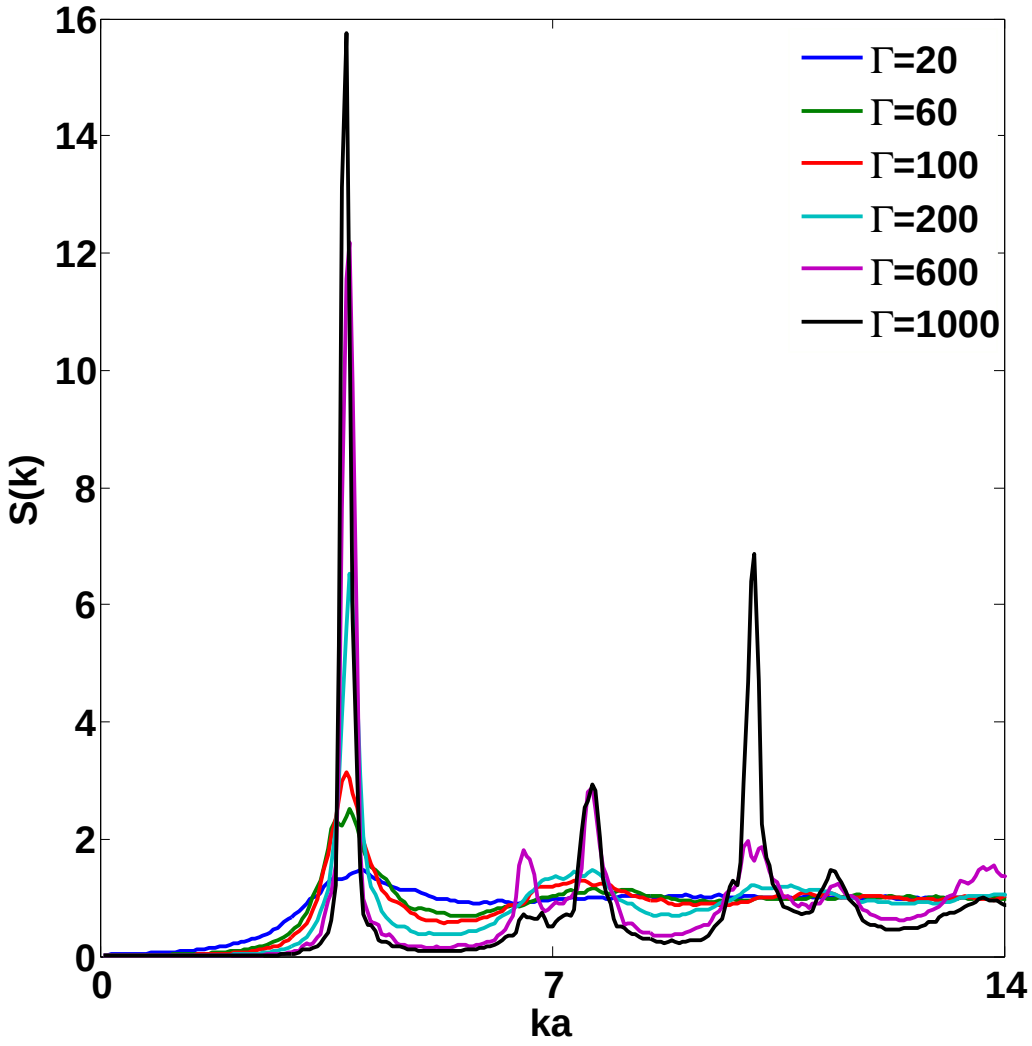

Figure 5.2: Static structure factors $S(k)$ as a function of reduced wave-number ka for $\Gamma = 20, 60, 100, 200, 600, 1000$ and $\kappa = 1.0$

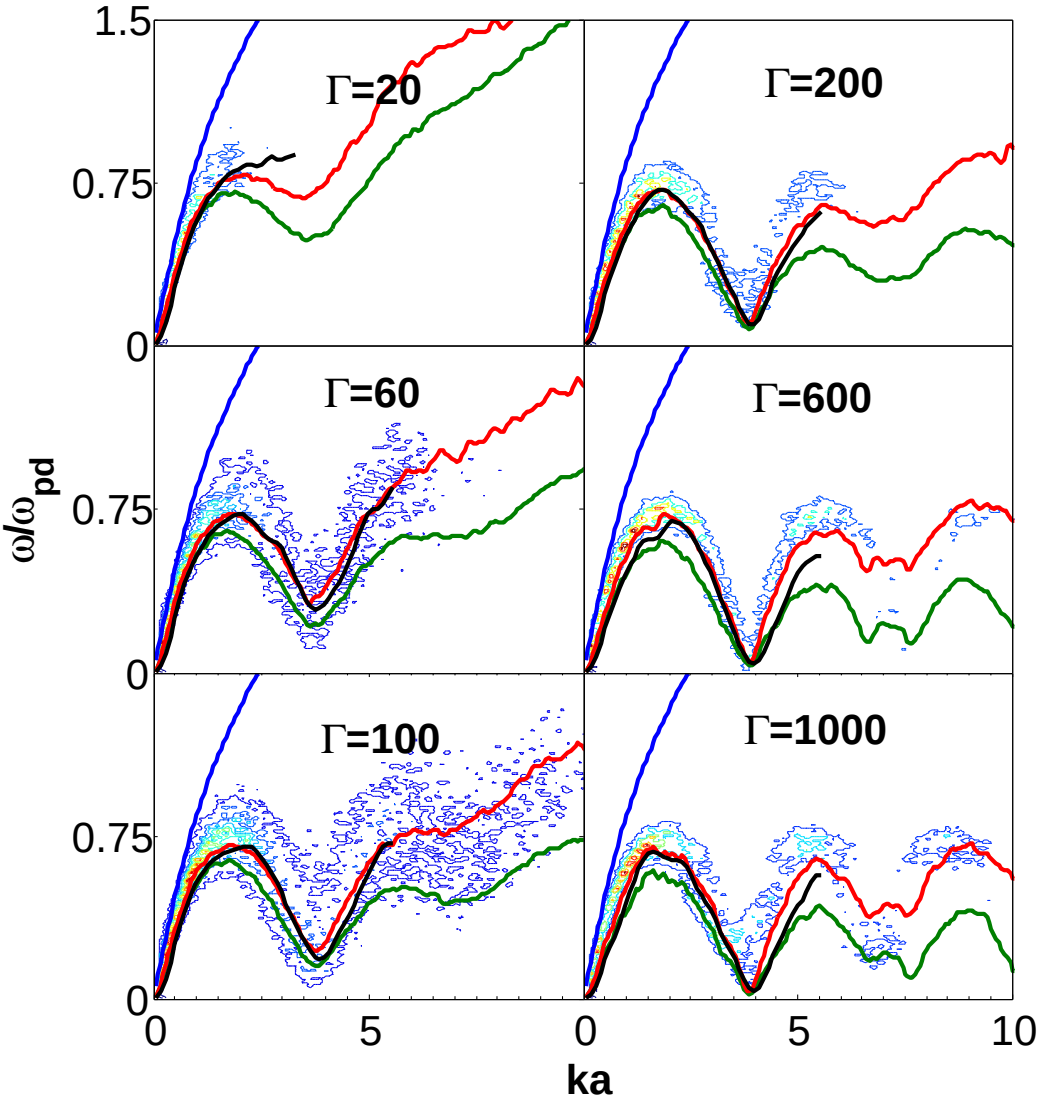

Figure 5.3: Longitudinal wave dispersion curves for $\Gamma = 20, 60, 100, 200, 600, 1000$, $\kappa = 1.0$ and $\gamma = 0.06$ against simulation data. Black curve represent Gaussian memory function model, red curve represents exponential memory function model (evaluated numerically) and green curve represents the delta memory function model, while the background contour plot is from simulation data. Also plotted is the prediction OH (blue).

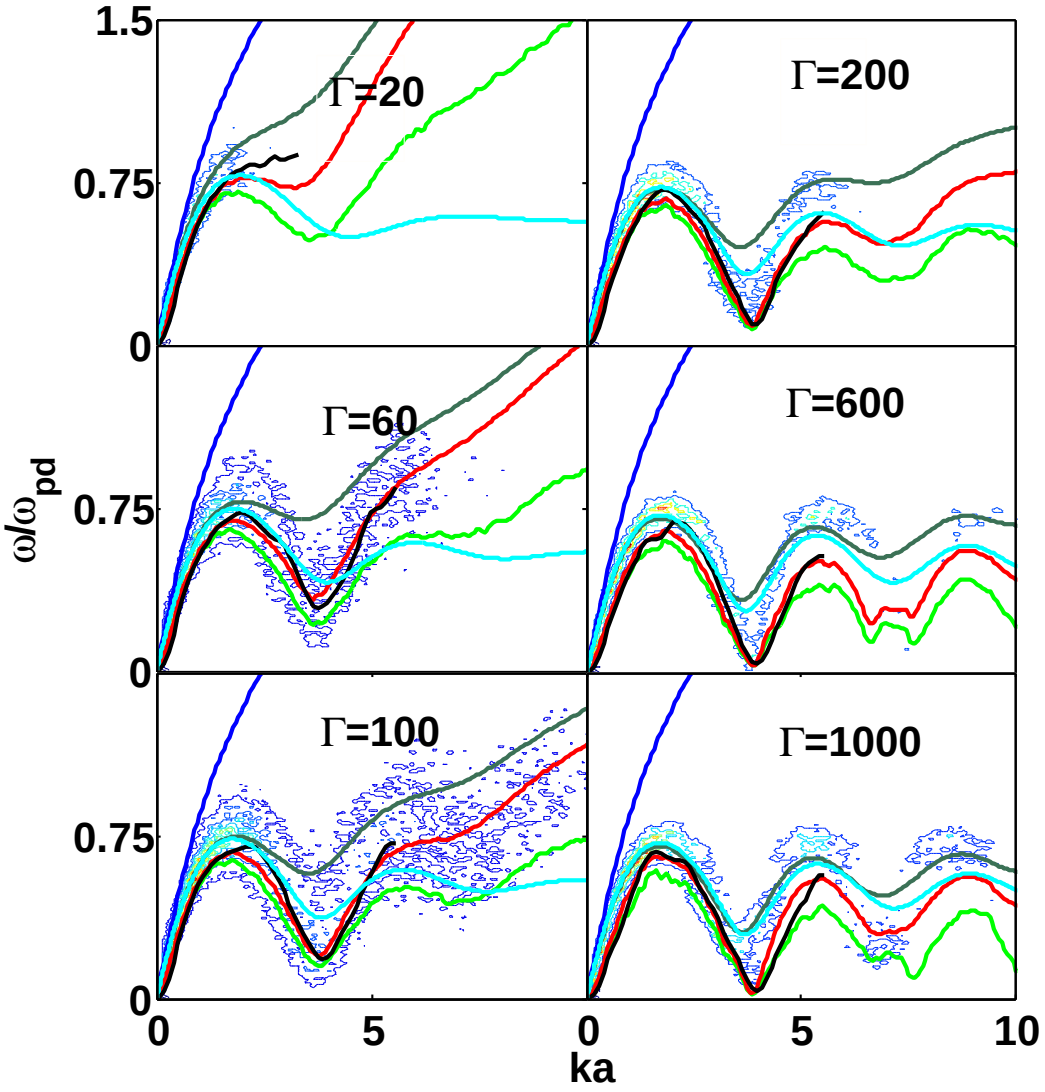

Figure 5.4: Longitudinal wave dispersion curves for $\Gamma = 20, 60, 100, 200, 600, 1000$, $\kappa = 1.0$ and $\gamma = 0.06$ against simulation data. Black curve represents Gaussian memory function model, red curve represents exponential memory function model (evaluated semi-analytically), light green curve represents the delta memory function model $\omega_0(k)$, dark green curve represents the $\omega_\infty(k)$ model while the background contour plot is from simulation data. Also plotted is the prediction from QLCA (cyan) and OH (blue).

lation is given by Eq. (4.51) and used in Figure 5.3[2]. The longitudinal second frequency moment $\langle\omega^2(k)\rangle$, required as the initial value for the exponential viscosity memory function has been evaluated numerically from the simulation data using Eq. (4.16b). As we can see, the model requires specifying the exponential relaxation time τ_l, which in our case we use as a fitting parameter. This has been found to show a weak dependence on the coupling strength Γ. Thus, for our purpose we model the relaxation time as $\tau_l = \tau_l(\Gamma)$, and this dependence has been observed to follow

$$\tau_l(\Gamma)\omega_{pd} = \begin{cases} 0.769 & \text{for } \Gamma < 60 \\ 1.000 & \text{for } 60 \leq \Gamma \leq 200 \\ 1.333 & \text{for } 200 < \Gamma \leq 1000. \end{cases} \tag{5.4}$$

From Figure 5.3 we notice a good improvement in the dispersion curves using the exponential model (red) for longitudinal viscosity memory function in comparison with that obtained from both OH and the delta function model, where the peak positions are better modeled even at higher wave-numbers and for higher coupling strengths.

In addition, as shown in Figure 5.4, a comparison of the exponential model for longitudinal viscosity memory function, this time showing exact peak positions of the power spectral density from Eqs. (4.40) and with second moment evaluated semi-analytically (implying that it will only require the radial distribution function from simulation for its evaluation, as explained in the footnote on page 10) using Eq. (A.1)[3] for a fairer comparison with QLCA, one notices a good agreement with the predictions from QLCA[4] where, in fact, we find that for lower coupling strengths, our model fares better, especially at higher wavenumber k, where it is able to model the rising dispersion curve. This is possibly because of the linear dependence of ω on k at higher wave-numbers, since the structure factor at large $k \gtrsim 2\pi$ and small Γ essentially becomes a constant due to the shorter range ordering.[5]

Further, from the exponential model dispersion relation Eq. (4.51), we notice that if $\omega\tau_l \gg 1$, i.e., in the large relaxation time limit, the dispersion relation takes the form $\omega = \omega_\infty(k)$, where

$$\omega_\infty^2(k) = \frac{\langle\omega^2(k)\rangle}{v_{th}^2}. \tag{5.5}$$

This has been plotted in Figure 5.4 and is seen to be very close to the predictions of QLCA for the crystalline states ($\Gamma > 200$) for $ka \lesssim 2\pi$. We thus have from GH two semi-analytic results, $\omega_0(k)$ and $\omega_\infty(k)$, that do not use any fitting parameters, yet are fairly good descriptions of the longitudinal wave dispersion relation.

[2]The difference in dispersion curves obtained by using Eq. (4.51) or Eq. (4.40) by extracting its peak positions is not very significant and we will use the exact peak positions in Figure 5.4

[3]We still use the same choice of relaxation time fitting parameter as when the second moment was evaluated numerically.

[4]QLCA data sets are courtesy Dr. L.J. Hou, Max-Planck-Institut für Extraterrestrische Physik, 85741 Garching, Germany. *e-mail*: ljhouwang@gmail.com

[5]The rise in dispersion curves at low Γ and for higher k is sometimes manually included in the QLCA model, in what is called the Extended QLCA (EQLCA) [8].

Next, to obtain results from the Gaussian model where the relevant coefficients are evaluated using Eq. (4.58), we proceed exactly the same way as before except that the Laplace transform of the Gaussian evaluated at $s = i\omega$ has to be computed numerically and used in Eq. (4.40). In addition, semi-analytic expressions for the fourth frequency moment are hard to evaluate and require as input the three particle distribution function. In order to proceed with this model, we therefore evaluate both the second and fourth moments directly from the simulation data using Eq. (4.16b) for the second moment and using

$$\frac{1}{2\pi}\int_{-\infty}^{\infty} d\omega\ \omega^4 P(k,\omega) = \langle \omega^4(k) \rangle, \tag{5.6}$$

for the fourth moment, where $P(k,\omega)$ is the power spectral density obtained from simulation.

From Figure 5.3 we see that the dispersion relation obtained from the Gaussian model (thick solid lines) also provides a reasonably good modeling of wave dispersion, especially up to the first dispersion peak. In fact, as can be seen for $\Gamma = 1000$, all three models are also able to recover the region where $\omega \to 0$, a characteristics of the crystalline state which is missing from the QLCA dispersion curves. In addition, the fairly close match between the Gaussian memory function model and the exponential model, not only lends confidence in our choice of the relaxation time fitting parameter used in the exponential model, it also provides us with a model that is independent of the use of any free parameters. These results are thus very encouraging.

Having discussed that the dispersion curves predicted by GH hold good against simulation data and also with respect to the existing model of QLCA[6], we next discuss the comparison of spectral widths as obtained from our models, against simulation data, thereby highlighting the main motivation for using this approach. In the following, all data sets pertain to the second frequency moment evaluated numerically.

5.2.2 Damping Estimates via Comparison of Spectral Widths

We plot in Figures 5.5-5.10, profiles curves[7] for the Gaussian (green) and exponential (red) model of the longitudinal viscosity memory functions for $\Gamma = 20$, 60, 100, 200, 600, and 1000, respectively, and compare them with the profile plots obtained directly from simulation data. In this way, we illustrate the advantage of using the memory function formalism within the GH model in tackling the difficult issue of wave-number dependent damping of the longitudinal collective modes in dusty plasma since the widths provide us with a measure of the full (or half) width at half maximum which is physically proportional to inverse of the damping.

A comparison of these plots reveals reasonably good fits over a range of k values for both models of

[6] In Appendix A we show a comparison of results for the second frequency moment obtained numerically as above and using the semi-analytic expressions (as used in the exponential model comparison with QLCA).

[7] By profile plots will be referring to wavenumber k dependent spectral widths, i.e., plots of the cross-sections of the power spectral densities as a function of ω for different values of k

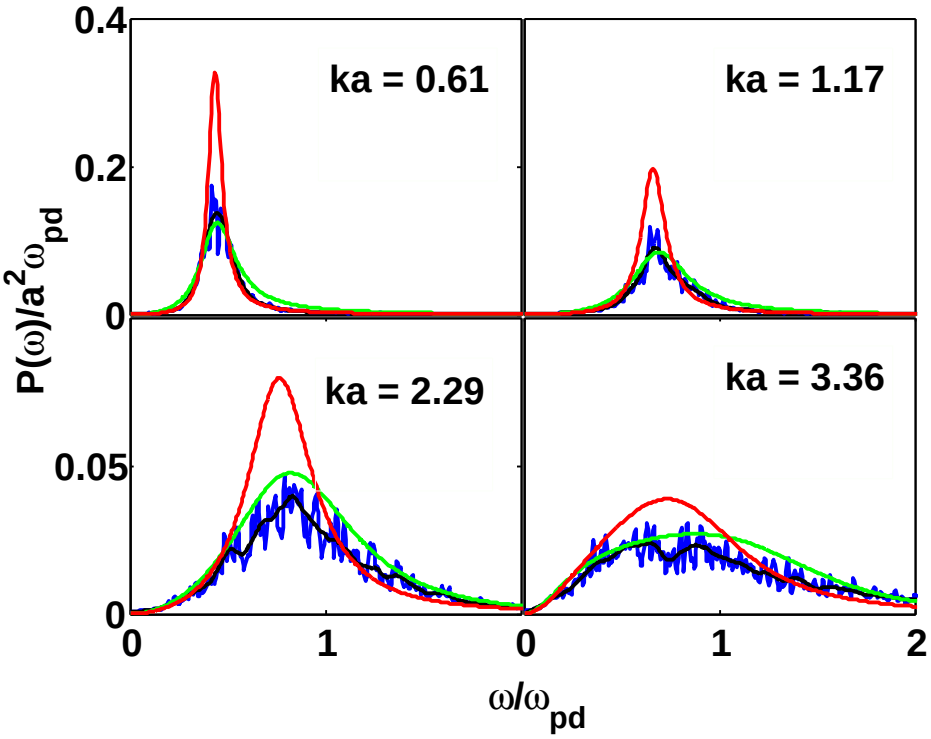

Figure 5.5: Reduced longitudinal spectral density profile curves versus reduced frequency ω/ω_{pd} from simulation (noisy curve), Gaussian model (green curve), and exponential model (red curve) for $\Gamma = 20$, $\kappa = 1.0$ and $\gamma = 0.06$ at different reduced wave-numbers. The black curve shown attempts to follow the envelope of the noisy simulation data.

longitudinal viscosity memory functions. These fits are especially good for lower Γ where the hydrodynamic regime is expected to be strongest while for very high values of Coupling strength, $\Gamma \geq 200$, the fits begin to deteriorate. However, the predictions may still be considered fairly reasonable, given that the hydrodynamic model has been stretched well into the crystalline state.

In order to more clearly illustrate the wave-number dependent damping rate estimates provided by this model, we next plot in Figure 5.11, the approximate half-widths evaluated at half the maximum value (HWHM) of the reduced power spectral density, and compare the results for exponential model HWHM (red dots) with simulation results (blue triangles). We notice a reasonable agreement in terms of the magnitude of widths predicted except for the large k regions for $\Gamma = 20$ and for the larger deviations in the estimated widths, for the weakly damped states, $\Gamma \geq 200$. A possible source of these deviations is the noise in the samples of the static structure factor $S(k)$, as further explained in our concluding remarks.

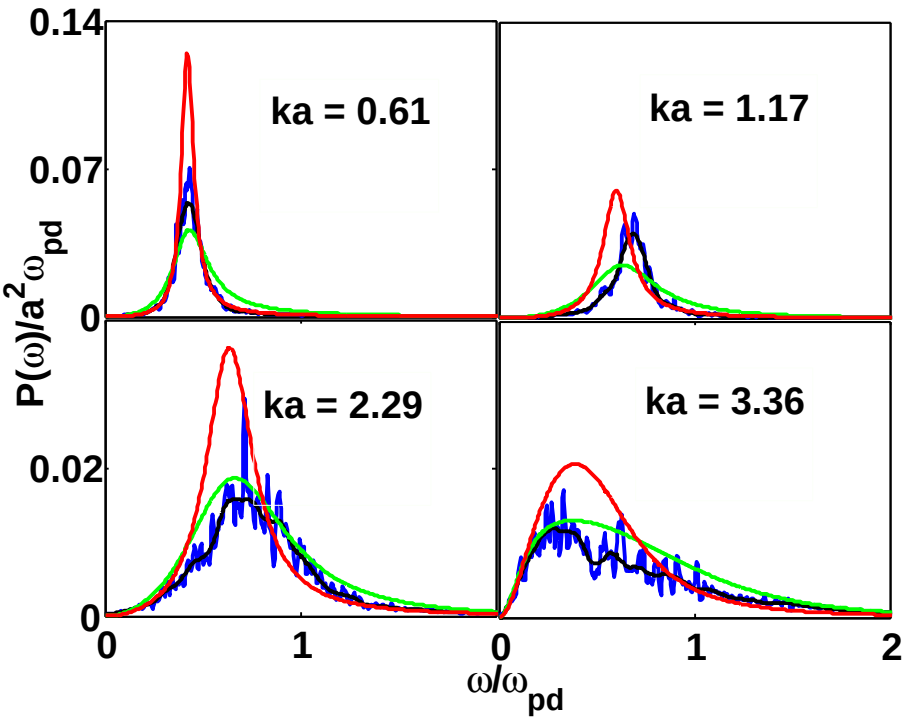

Figure 5.6: Reduced longitudinal spectral density profile curves versus reduced frequency ω/ω_{pd} from simulation (noisy curve), Gaussian model (green curves), and exponential model (red curve) for $\Gamma = 60$, $\kappa = 1.0$ and $\gamma = 0.06$ at different reduced wave-numbers. The black curve shown attempts to follow the envelope of the noisy simulation data.

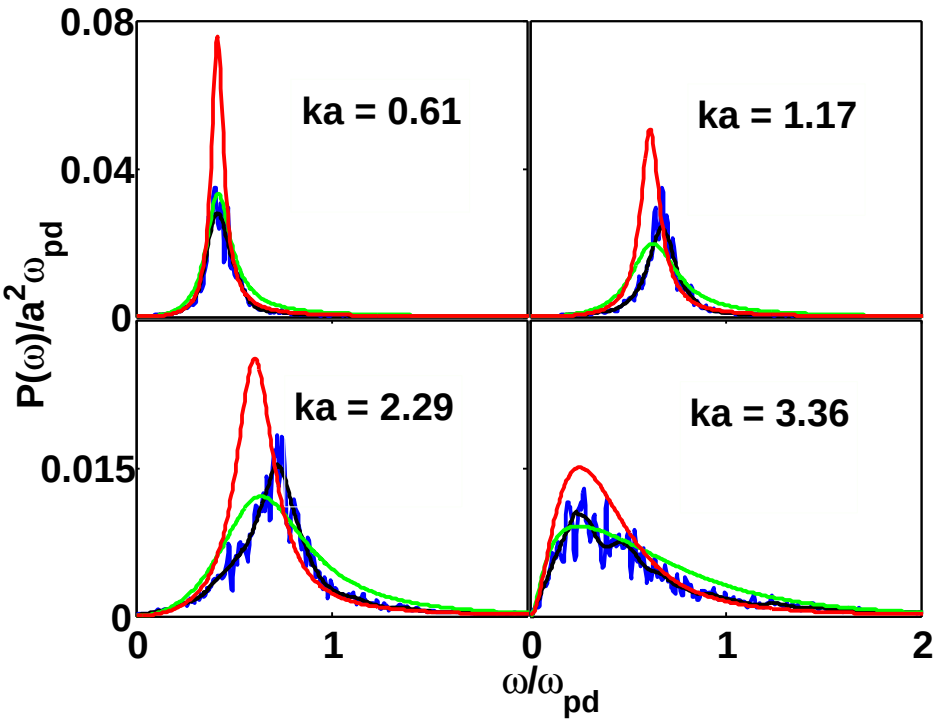

Figure 5.7: Reduced longitudinal spectral density profile curves versus reduced frequency ω/ω_{pd} from simulation (noisy curve), Gaussian model (green curves), and exponential model (red curve) for $\Gamma = 100$, $\kappa = 1.0$ and $\gamma = 0.06$ at different reduced wave-numbers. The black curve shown attempts to follow the envelope of the noisy simulation data.

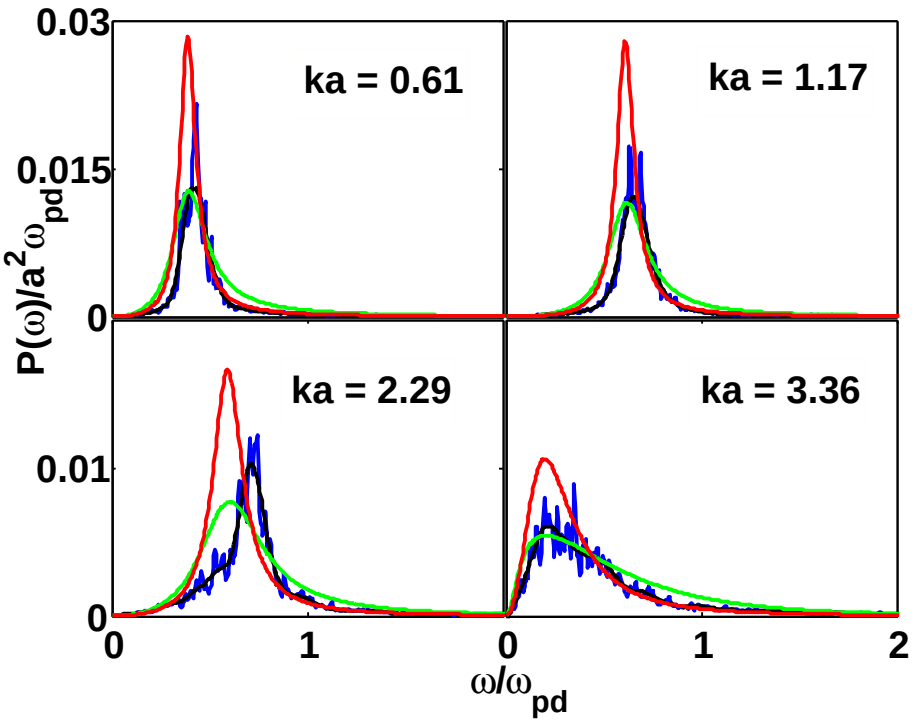

Figure 5.8: Reduced longitudinal spectral density profile curves versus reduced frequency ω/ω_{pd} from simulation (noisy curve), Gaussian model (green curve), and exponential model (red curve) for $\Gamma = 200$, $\kappa = 1.0$ and $\gamma = 0.06$ at different reduced wave-numbers. The black curve shown attempts to follow the envelope of the noisy simulation data.

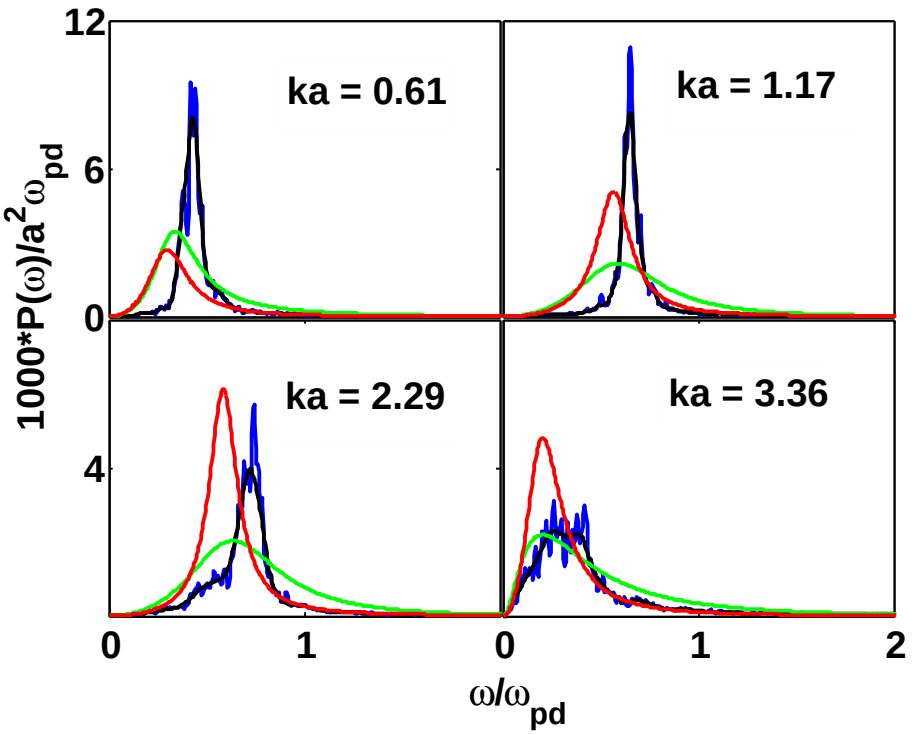

Figure 5.9: Reduced longitudinal spectral density profile curves versus reduced frequency ω/ω_{pd} from simulation (noisy curve), Gaussian model (green curve), and exponential model (red curve) for $\Gamma = 600$, $\kappa = 1.0$ and $\gamma = 0.06$ at different reduced wave-numbers. The black curve shown attempts to follow the envelope of the noisy simulation data.

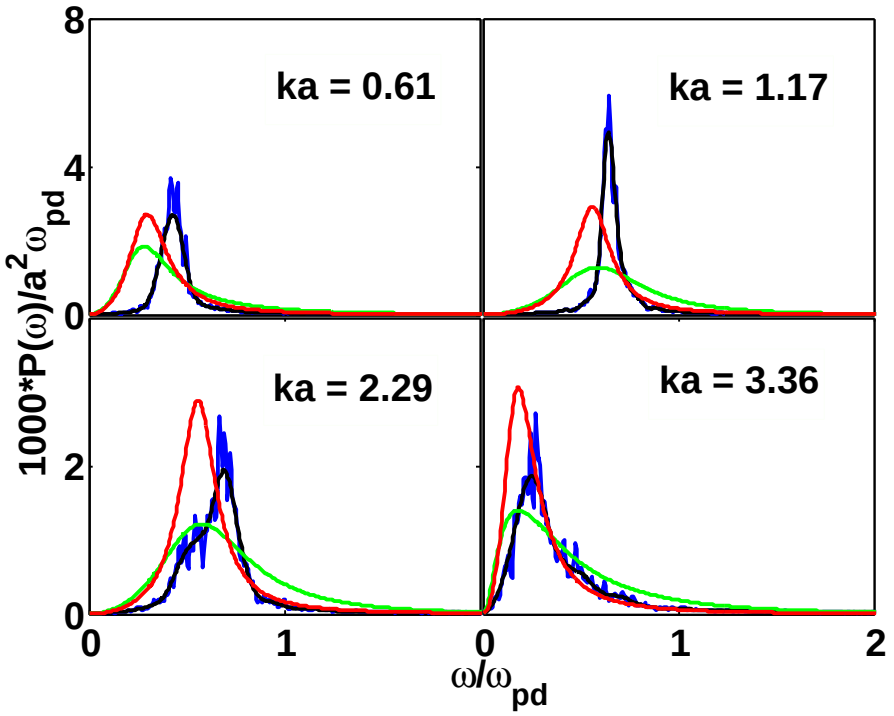

Figure 5.10: Reduced longitudinal spectral density profile curves versus reduced frequency ω/ω_{pd} from simulation (noisy curve), Gaussian model (green curve), and exponential model (red curve) for $\Gamma = 1000$, $\kappa = 1.0$ and $\gamma = 0.06$ at different reduced wave-numbers. The black curve shown attempts to follow the envelope of the noisy simulation data.

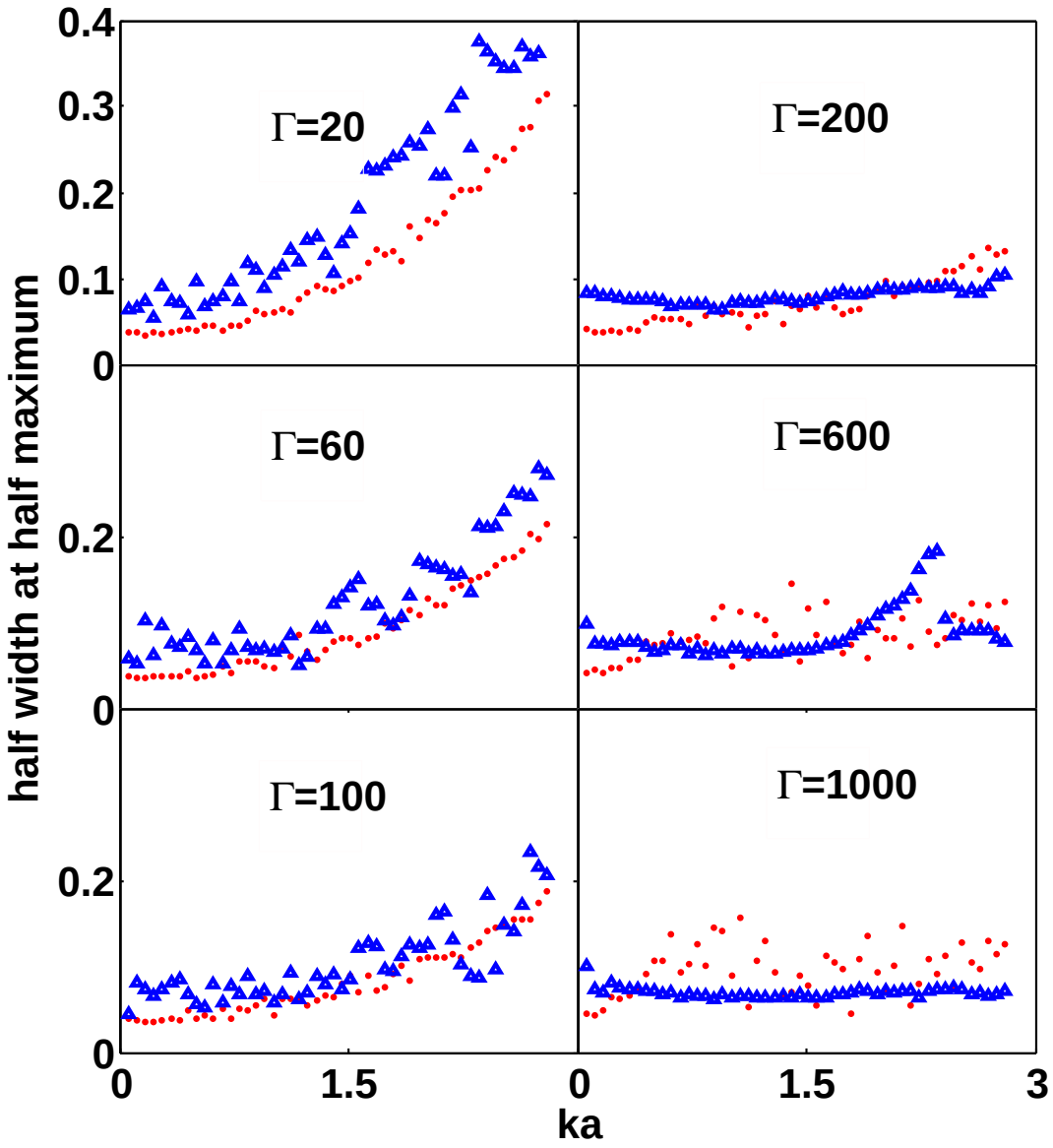

Figure 5.11: Longitudinal wave number dependent wave damping estimates via the evaluation of half-width at half maxiumum (HWHM) as a function of reduced wave-number ka computed using the exponential model for longitudinal viscosity memory function (red dots) and from BD simulation (blue triangles) for $\Gamma = 20, 60, 100, 200, 600, 1000$, $\kappa = 1.0$ and $\gamma = 0.06$.

Chapter 6

Effect of Ion Flow on Inter-Particle Potential

As discussed in the second chapter, we will now try to analyze the effect of ions streaming perpendicularly into the 2D layer of dusty plasma. The work in this section is mostly simulation based, and we will make use of the generalized inter-particle potential reported by Hou *et al.* [6] in our simulation to model the effect of ion flow into the layer of dusty plasma.

6.1 Inter-Particle Potential

The theoretical development of the generalized inter-particle potential between dust grains is carried by modeling the flow of ions using hydrodynamic continuity and momentum conservation equations for charged species. Based on Hou *et al.* [6] results, this interaction potential[1] can be split into two parts as $U(r,z) = U_D(r,z) + U_W(r,z)$. U_D represents the screened Coulomb potential

$$U_D(r,z) = U_0 \int_0^\infty dl\ lJ_0(l\frac{r}{\lambda_D})\frac{\eta_+}{\eta_+^2+\eta_-^2}e^{\frac{-\eta_+|z|}{\lambda_D}}, \tag{6.1}$$

while U_W, represents the long ranged oscillatory downstream wake potential

$$U_W(r,z) = U_0 \int_0^\infty dl\ lJ_0(l\frac{r}{\lambda_D})\frac{\eta_-}{\eta_+^2+\eta_-^2}\sin\left(\frac{\eta_-\,|z|}{\lambda_D}\right)H(-z). \tag{6.2}$$

Here $U_0 = \frac{q_d^2}{\lambda_D}$, l is a dimensionless variable of integration, $H(-z)$ is a unit step function and

$$\eta_\pm = \frac{1}{\sqrt{2}}\{[(1+l^2-M^{-2})^2+4M^{-2}l^2]^{\frac{1}{2}} \pm (1+l^2-M^{-2})\}^{\frac{1}{2}}, \tag{6.3}$$

[1] These expressions are in 3D.

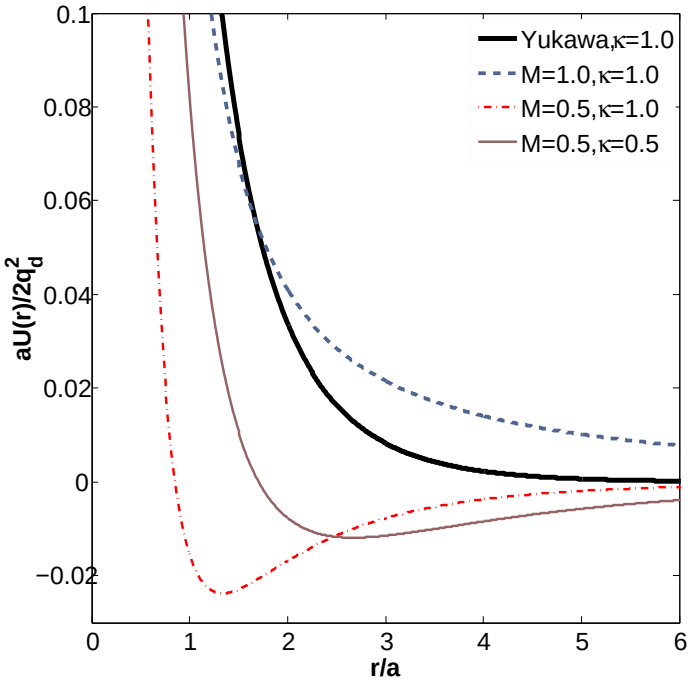

Figure 6.1: Reduced potential $\frac{aU_D}{2q_d^2}$ versus reduced distance r/a in a direction perpendicular to ion flow for several combinations of the Mach number $M = v_0/(\omega_{pi}\lambda_D)$ and the screening parameter $\kappa = a/\lambda_D$.

where $M = \frac{v_0}{v_s}$ is the Mach number, and $v_s = \sqrt{\frac{k_B T_e}{m_i}}$ is the ion sound velocity. If $M \to \infty$, it can be shown [6] that Eq. (6.1) yields

$$U_D(r,z) = \frac{q_d^2}{R} e^{-\frac{R}{\lambda_D}}, \tag{6.4}$$

where $R = \sqrt{r^2 + z^2}$, recovering the Yukawa potential. We can see that a finite M yields Eq. (6.1) as the inter-particle potential between dust grains, and the purpose of the following work is to analyze the effects of incorporating this form of the potential in our BD simulation.

6.2 Simulation Results

Since the 2D layer of dust particles is assumed to occupy the x, y plane, we can set $z = 0$ in the expression for U_D. Note that U_W vanishes for $z = 0$. Thus, the only modification needed in our simulation work described in previous sections, is to replace the Yukawa potential with the non-dimensional form of $\frac{a\bar{U}_D}{2q_d^2}$ in Eq. (2.48). The simulation with this modified potential[2] is run for a system of $N = 4000$ particles, for reduced time of the order of $\frac{10}{\gamma}$, after which we sample the equilibrium distribution of dust particles and evaluate the radial distribution function (RDF)(Appendix D). This is done for different values of coupling

[2]All the variables in the integrand in Eq. (6.1) are also non-dimensionalized and the resulting integral is evaluated numerically.

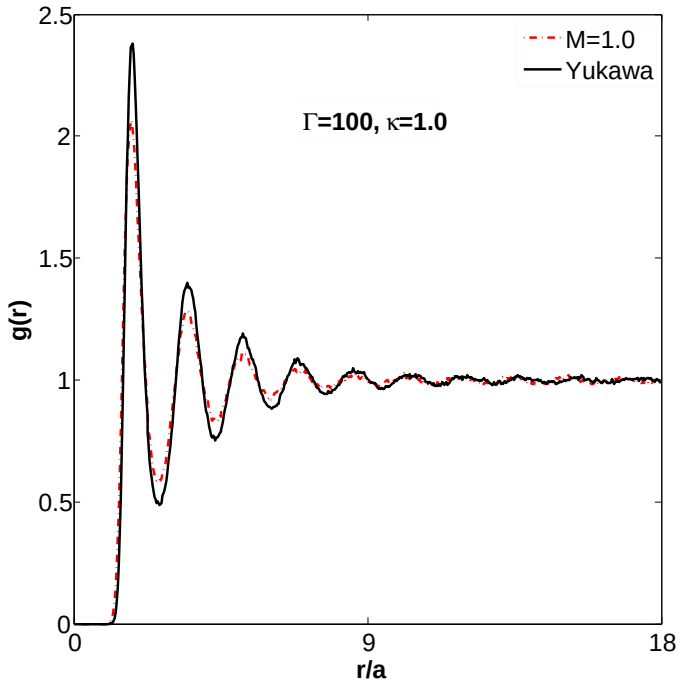

Figure 6.2: Radial distribution functions versus reduced distance r/a in 2D dust layer with coupling strength $\Gamma = 100$, screening parameter $\kappa = 1$, for Yukawa potential and the repulsive potential with Mach number $M = 1$.

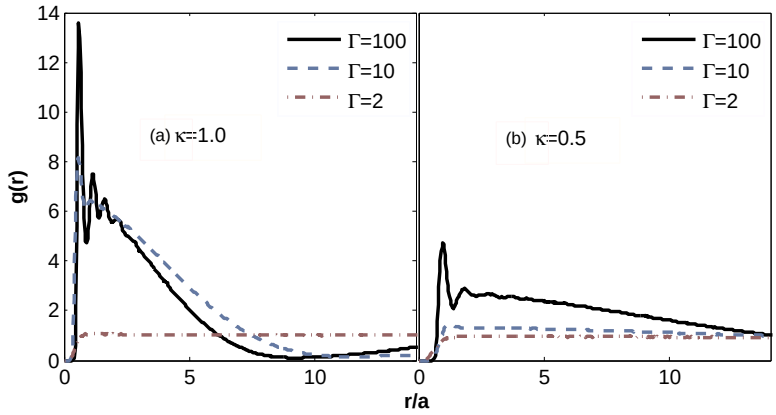

Figure 6.3: Radial distribution functions versus reduced distance r/a in 2D dust layers with attractive potentials corresponding to Mach number $M = 0.5$, for two screening parameters $\kappa = 1$ (a) and 0.5 (b), and for three coupling strengths, $\Gamma = 2$, 10 and 100.

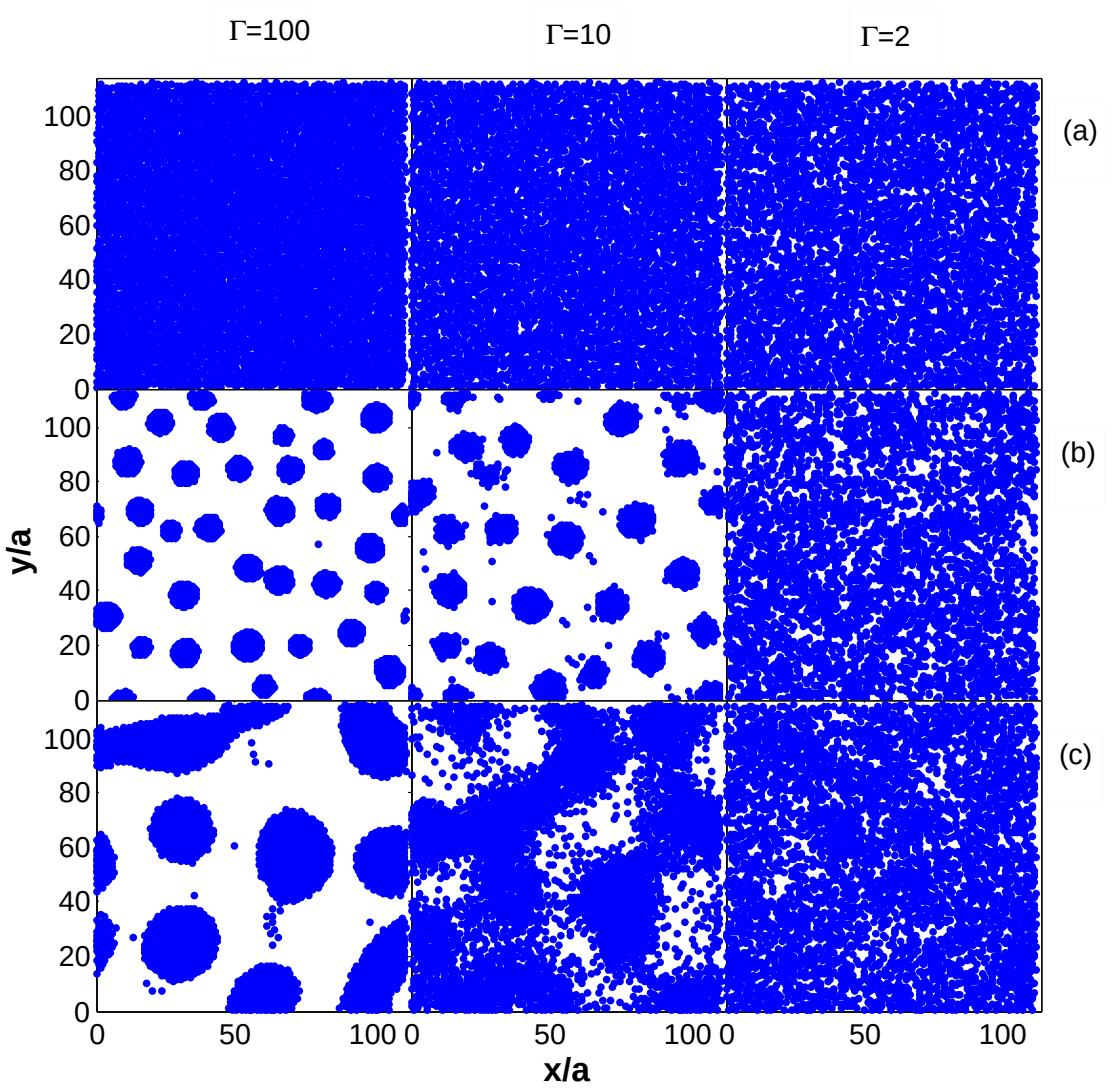

Figure 6.4: Two-dimensional dust particle layouts with Yukawa potential for screening parameter $\kappa = 1$ (row a), and with the two attractive potentials corresponding to Mach number $M = 0.5$, for $\kappa = 1$ (row b) and 0.5 (row c), and for three coupling strengths, $\Gamma = 2$, 10 and 100.

strength Γ, Mach numbers M and screening parameter κ, as discussed next.

In Figure 6.1 we show the interaction potential, evaluated from Eq. (6.1) for $M = 1$ and $\kappa = 1$ (dashed curve), $M = 0.5$ and $\kappa = 1$ (dash-dot curve), and $M = 0.5$ and $\kappa = 0.5$ (thin solid curve), along with the Yukawa potential ($M \to \infty$) for $\kappa = 1$ (thick solid curve). We note that, for $M \gtrsim 2$, Eq. (6.1) gives a potential that is very close to the Yukawa model, so we chose to show in Figure 6.1 the critical case $M = 1$ only, which is the smallest value of the Mach number that yields a purely repulsive interaction, with a potential that is seen in Figure 6.1 to be significantly softer than the Yukawa potential. More importantly, all subsonic cases are characterized by a potential well, so we chose $M = 0.5$ as a typical case for two screening parameters, $\kappa = 1$ and 0.5.

In order to make a comparison between the two repulsive potentials from Figure 6.1, Yukawa and $M = 1$, both with $\kappa = 1$, we perform BD simulations of the 2D dust layer for several coupling strengths Γ characterizing liquid state of the system. While our simulations showed no significant differences in the equilibrium layouts of dust particles between the two potentials (not shown here), we show in Figure 6.2 a comparison of the corresponding equilibrium RDFs, $g(r)$, for $\Gamma = 100$. The structures of the two RDFs are quite similar, with peaks sitting on top of each other, while the only difference noticeable is the small dampening of the amplitudes of oscillations in the $M = 1$ case. From these results, we may conclude that the Yukawa potential presents a well founded interaction model, at least for a 2D dust liquid in the sheath region with supersonic ion flows, $M \geq 1$.

Next, turning our attention to subsonic ion flows with $M = 0.5$, we show in Figure 6.3 results from our BD simulations for equilibrium RDFs for two screening parameters, $\kappa = 1$ and $\kappa = 0.5$, each for three coupling strengths, $\Gamma = 2$, 10, and 100. In the case of weak coupling with $\Gamma = 2$, one notices that RDFs are flat, characterizing a gas like disordered phase where the kinetic energy of dust particles is so high, that any signature of the presence of the attractive potential wells in the two corresponding potentials, shown in Figure 6.1, is lost. For stronger couplings, $\Gamma = 10$ and 100 and screening parameter $\kappa = 1$, one observes a decrease in the corresponding RDFs to zero at some finite distances r. One may infer that 2D clusters, or islands, are formed with an average diameter of about 10 (reduced units), corresponding to the radial distance r/a, where the RDFs in Figure 6.3(a)vanish. On the other hand, one can still notice oscillations in the corresponding RDFs at short distances, indicating that there exists a short-range, close-packed condensed structure within such clusters. When the screening length is doubled, giving $\kappa = 0.5$ in Figure 6.3(b), one may still infer that 2D clusters are formed at the strongest coupling of $\Gamma = 100$, with an average diameter of around 30 (reduced units), but the situation at intermediate coupling of $\Gamma = 10$ is not as clear. While the short-range order seems to have been largely lost for $\Gamma = 10$ with $\kappa = 0.5$, the non-uniform RDF at large distances are suggestive of early stages in dust coagulation.

Finally, in Figure 6.4 we show snapshots of equilibrium dust particle layouts for three coupling strengths, $\Gamma = 2$, 10, and 100, comparing the cases of attractive potentials, $M = 0.5$ discussed in Figure 6.3, with Yukawa potential ($\kappa = 1$). While for $\Gamma = 2$, all three potentials display similar gas like disordered phase,

one can clearly notice an aggregation of dust particles into clusters in the case of attractive potential for higher coupling strengths. It is interesting to further notice that the screening length plays an important role in this phenomenon. For shorter screening length, corresponding to $\kappa = 1$, one observes the formation of well defined clusters in the shape of circular discs, having a rather uniform distribution of diameters at $\Gamma = 100$, with a few dust particles left in the dispersed phase at $\Gamma = 10$. On the other hand, the case of longer screening length, corresponding to $\kappa = 0.5$, allows for some elongated islands, in addition to the disc-shaped clusters of larger size than in the case of $\kappa = 1$ with $\Gamma = 100$, whereas the structure at the intermediate coupling of $\Gamma = 10$ seems to be characterized by a diffuse network of connected dust islands separated by some void regions.

Chapter 7

Conclusions and Future Work

- The work done as part of this thesis has shown that the theory of GH given by Boon and Yip [20] for simple fluids can provide good agreements with the results obtained from the Brownian Dynamics (BD) simulation in describing the longitudinal dust wave modes for a 2-Dimensional layer of dusty plasma. Not only are we able to provide a description of the wave dispersion but, through the memory function formalism, we are also able to provide reasonably good estimates of wave number dependent wave damping, an issue hitherto not addressed very well [8]. In addition, the theory allows us to predict the propagation of shear waves, and obtain estimates of its dispersion and damping that can be compared against data obtained from BD simulation, though further work may need to be done in view of the simulation data being much more noisy than for longitudinal wave modes, thereby deteriorating the quality of predictions.

  In order to put this theory on stronger mathematical and physical grounds, we next enlist some possibilities for further research.

  - One of the main statistical inputs to the GH approach is the static structure factor $S(k)$, and in our case we have found it quite difficult to obtain clean samples of the same specially for higher coupling strengths. Typically, it is relatively easier to obtain smooth data sets for the radial distribution function, and therefore evaluate $S(k)$ as its Fourier transform using Eq. (D.6). However, for $\Gamma \geq 100$, it has been observed that this approach is not very reliable at low values of wave number $ka \lesssim 3.0$ where it shows pronounced oscillations and therefore, we have tried to evaluate $S(k)$ directly from simulation using its definition Eq. (D.5). Although, this provides much more reliable data at the lower k values indicated, the data sets are also much noisier. Thus, it will be very useful to find more reliable ways to obtain cleaner data sets for the static structure factor either from simulation or by using certain analytic expressions as obtained using the mean spherical approximations [21] for a Yukawa potential.
  - The relaxation time τ_l, used in the exponential model for the longitudinal viscosity memory function has been used as a fitting parameter. For a Lennard-Jones fluid, Boon and Yip [20] have

suggested that τ_l is in general a function of wavenumber k, and could be related to coefficients of elasticity for the fluid [37]. Thus, it will be very useful to either obtain analytic expressions for the relaxation time [32], or obtain it as a function of k, directly from simulation [38].

- Although our subsequent extension to a Gaussian model for the longitudinal viscosity memory function has allowed us to obtain good results without any free parameters, the fact that the frequency sum rules are evaluated numerically from the simulation data presents a possible source of weakness in our work. Although we have shown that the second moment obtained from simulation is in reasonable agreement with the second moment evaluated from the equilibrium radial distribution function especially for lower Γ and lower wave-number k, similar extensions to higher order moments can be quite intractable, necessitating the need for numerical evaluation from simulation data. Nonetheless, since our discussion has centered around the low frequency longitudinal dust wave modes which, as mentioned in the introduction, can be observed and video recorded during laboratory experiments, obtaining their power spectral density from the video recording and a subsequent computation of the moments should also be possible, thus validating to some extent, our use of this approach.
- Further, the use of GH model also allows us to predict the propagation of shear wave modes for higher Γ, with the relaxation time used in the exponential model found to be dependent upon both, Γ and γ. However, an extension to Gaussian model for transverse viscosity memory function has not proved to be very fruitful, since the predictions were only seen to deteriorate and this has so far been a drawback of the model, since we have not been able to validate our exponential model for the shear wave modes, as in the case of longitudinal wave modes.

- Another useful outcome of our simulation of the 2D layer of dusty plasma has been the study of the effect of ions streaming into the dusty plasma layer and its effect on the inter-particle potential between dust particles. From our simulations we have observed that the Yukawa potential is well suited for modeling the inter-particle potential in the supersonic regime $M \geq 1$, while in the sub-sonic regime, interesting new features have been observed. In particular, formation of dust particle aggregates due to the presence of attractive well in the inter-particle potential for sub-sonic ion flow speeds has been observed, although the exact physical mechanism leading to this observation is still not very clear. Some possibilities for future work could therefore be, to try and understand the physical behavior leading to an aggregation of dust particles, modeling the effects of finite-size dust particles, as well as obtaining analytic formulation of the dispersion relation, particularly in the subsonic regimes.

Appendices

Appendix A

Frequency Sum Rules

Frequency sum rules [20] essentially allow us to compute the short time behavior of time correlation functions. In theory, all the frequency moments can be expressed as integrals over the equilibrium particle distribution functions and the interaction potential [20]. For instance, the second frequency moment for the longitudinal current density auto-correlation can be expressed as

$$\langle \omega^2(k) \rangle = 3k^2 v_{th}^4 + \frac{\rho}{m_d} v_{th}^2 \int d^2\mathbf{r}\, g(r) \left[1 - \cos(kx)\right] \frac{\partial^2 U(r)}{\partial x^2}, \tag{A.1}$$

where $g(r)$ is the radial distribution function and $U(r)$ is the inter-particle potential. For the exponential model of longitudinal viscosity memory function, we can use either Eq. (4.20) with $n = 2$ or Eq. (A.1), although the choice of relaxation time as a fitting parameter may provide a better match with one or the other methods for computing the second moment. However, for the purpose of using the Gaussian model for longitudinal viscosity memory function, we have evaluated all the necessary frequency moments directly from simulation data, following the definition Eq. (4.20). This is because, analytic expressions for the moments of higher order become very cumbersome to handle, involving for instance, the three particle distribution function in the case of fourth frequency moment, and the three particle distribution function is usually not available as an input.

For the purpose of comparison though, we show in Figure A.1 the reduced second moments, $\langle \omega^2(k) \rangle / a^2 \omega_{pd}^4$, corresponding to the longitudinal wave mode cases $\Gamma = 20, 60, 100, 200, 600, 1000$, which are evaluated either from Eq. (A.1) (solid curve) or from Eq. (4.20) for $n = 2$ with the power spectral density $P(k, \omega)$ obtained from simulation (dashed curve). One notices a reasonably good agreement between the two types of calculations for dust layer in liquid state ($\Gamma < 200$), at least for wavelengths longer than the average inter-particle separation ($ka \lesssim 2\pi$), but significant discrepancies develop when the coupling strength grows well into the crystalline state. Similarly, we find that the dispersion curves obtained from the two models begin to show higher discrepancy for stronger coupling strength, $\Gamma \geq 200$ and at higher wave number k, as can be seen from Figure A.2.

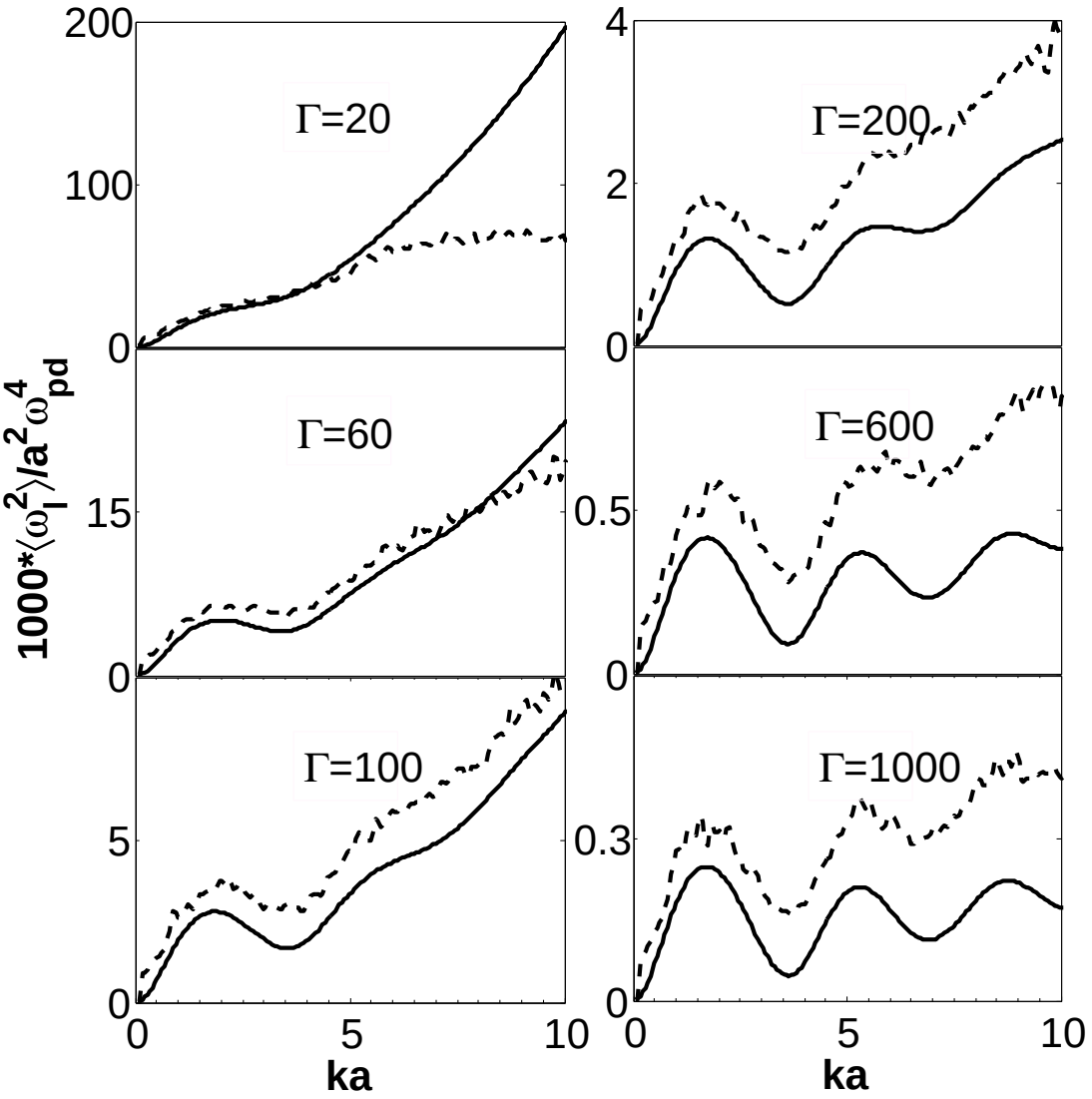

Figure A.1: Reduced second frequency moment $\langle\omega_l^2(k)\rangle/a^2\omega_{pd}^4$ for the longitudinal mode as a function of the reduced wave-number ka, obtained from the radial distribution function via Eq. (A.1) (solid curves) and from the simulation spectra via Eq. (4.20) with $n = 2$, for $\Gamma = 20, 60, 100, 200, 600, 1000$, $\kappa = 1.0$ and $\gamma = 0.06$.

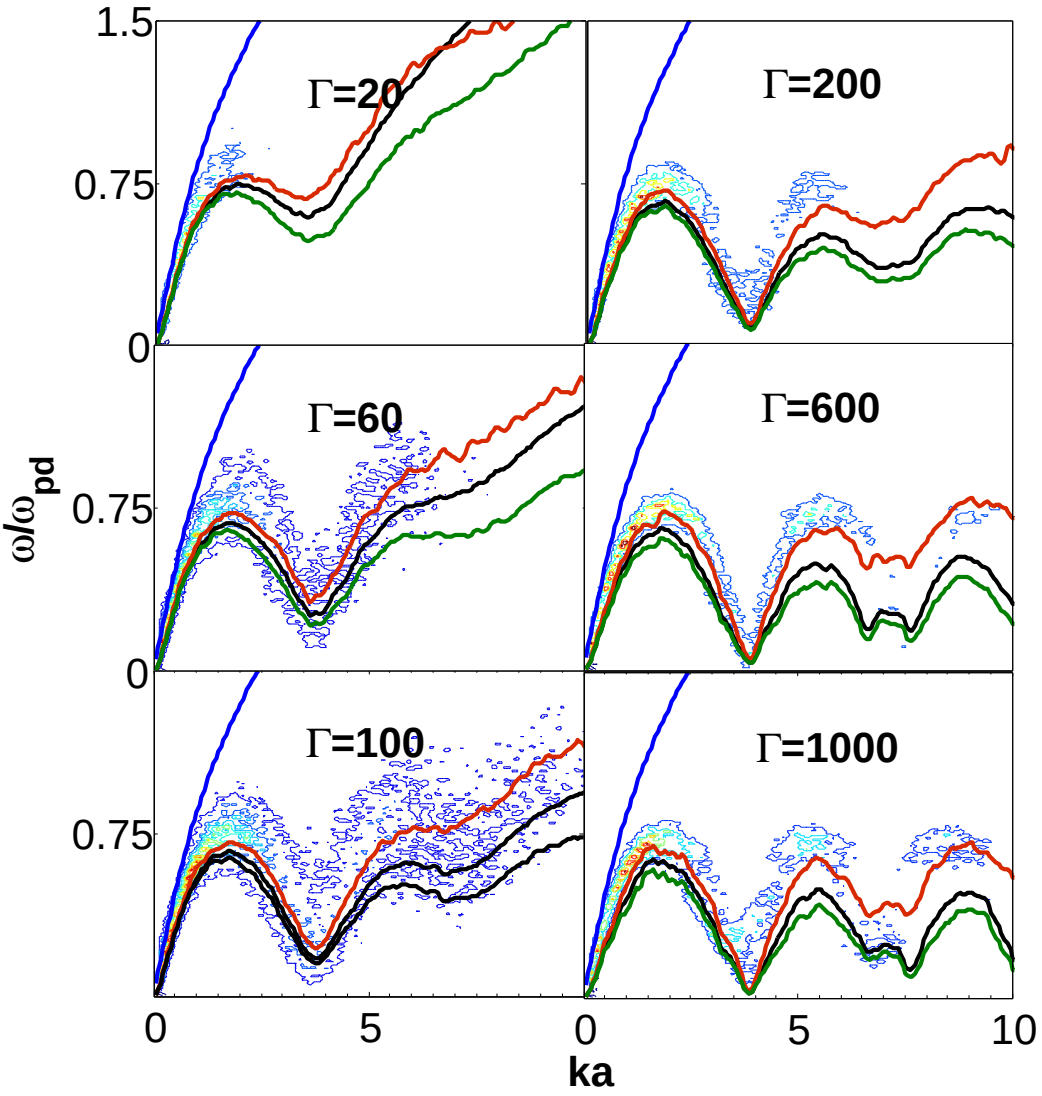

Figure A.2: Reduced longitudinal wave dispersion curves against simulation power spectral density. Green curves represent the delta function model, black curve represents the exponential model with second moment obtained from the radial distribution function via Eq. (A.1), red curve represents the exponential model with second moment evaluated numerically from simulation data and the blue curve represents the ordinary hydrodynamic model computed for for $\Gamma = 20, 60, 100, 200, 600, 1000$, $\kappa = 1.0$ and $\gamma = 0.06$.

Appendix B

Power Spectral Density

B.1 Power Spectrum from Auto-Correlation Function

Consider a deterministic function $x(t)$. The average power of the function is defined as

$$P = \lim_{T\to\infty} \frac{1}{T} \int_{-T/2}^{T/2} dt\ x(t)x^*(t). \tag{B.1}$$

Defining a truncated function as

$$x_T(t) = \begin{cases} x(t) & \text{for } |t| < \frac{T}{2}, \\ 0 & \text{otherwise,} \end{cases} \tag{B.2}$$

the power spectral density for $x_T(t)$ is defined as

$$S_X(\omega) = \lim_{T\to\infty} \frac{|X_T(\omega)|^2}{T}, \tag{B.3}$$

where $X_T(\omega)$ is the Fourier transform of $x_T(t)$. From Parseveal's theorem, we know that

$$P = \lim_{T\to\infty} \frac{1}{T} \int_{-T/2}^{T/2} dt\ x(t)x^*(t) = \frac{1}{2\pi} \int_{\infty}^{\infty} d\omega\ S_X(\omega). \tag{B.4}$$

An equivalent way of obtaining the power spectral density of the signal $x(t)$ is as follows. The time auto-correlation function is defined as

$$R_x(\tau) = \lim_{T\to\infty} \frac{1}{T} \int_{-T/2}^{T/2} dt\ x(t)x^*(t+\tau) = \lim_{T\to\infty} \frac{1}{T} \int_{-T/2}^{T/2} dt\ x(t)x^*(t-\tau). \tag{B.5}$$

In terms of the truncated signal $x_T(t)$,

$$\lim_{T\to\infty}\int_{-T/2}^{T/2} dt\ x(t)x^*(t+\tau) = \int_{-\infty}^{\infty} dt\ x_T(t)x_T^*(t+\tau). \tag{B.6}$$

The Fourier transform of the right side of the above equation can be obtained from convolution theorem as

$$\mathcal{F}[\int_{-\infty}^{\infty} dt\ x_T(t)x_T^*(t-\tau)] = X_T(\omega)X_T^*(\omega) = |X_T(\omega)|^2. \tag{B.7}$$

Therefore, we obtain

$$\mathcal{F}[R_x(\tau)] = \lim_{T\to\infty}\frac{|X_T(\omega)|^2}{T} = S_X(\omega). \tag{B.8}$$

Thus, the power spectral density is the Fourier transform of time auto-correlation function, which, by definition is the time average of $\overline{x(t)x(t+\tau)}$, where overline denotes a time average.

Now, for an ergodic process, time averages are the same as ensemble averages and therefore the time auto-correlation function of a sample $y(t)$, $\overline{y(t)y(t+\tau)}$ is equal to the auto-correlation function of ensemble. The power spectral density of a random process can be defined as the average power spectral density of each of its sample functions. For an ergodic process, this average is the same for each of its sample functions. Thus the power spectral density can be obtained from the time auto-correlation function as given by Eq. (B.8), or equivalently by the Fourier transform of auto-correlation function

$$S_y(\omega) = \mathcal{F}[\langle y(t)y(t+\tau)\rangle]. \tag{B.9}$$

B.2 Power Spectral Density from Laplace Transform

The following section reproduces the derivation of Hansen [21], relating the Laplace transform of an auto-correlation function to its power spectral density. Consider the time auto-correlation function of the fluctuations of a random process $A(t)$,

$$C(t) = \langle [A(t+t') - \langle A\rangle][A(t') - \langle A\rangle]\rangle. \tag{B.10}$$

Its power spectral density is obtained as

$$\overline{C}(\omega) = \frac{1}{2\pi}\int_{-\infty}^{\infty} dt\ C(t)e^{-i\omega t}, \tag{B.11}$$

and its Laplace transform is

$$\widetilde{C}(s) = \int_0^{\infty} dt\ C(t)e^{-st}. \tag{B.12}$$

Here $s = i\omega + \epsilon$ is the complex frequency. Using Eq. (B.11) into the above equation,

$$\begin{aligned}\widetilde{C}(s) &= \int_0^{\infty} dt\ e^{-st}\int_{-\infty}^{\infty} d\omega'\ \overline{C}(\omega')e^{i\omega' t},\\ &= \int_{-\infty}^{\infty} d\omega'\ \frac{\overline{C}(\omega')}{s - i\omega'}.\end{aligned} \tag{B.13}$$

Now, from complex analysis,

$$\lim_{\epsilon \to 0} \frac{1}{x - i\epsilon} = \mathcal{P}(\frac{1}{x}) + i\pi\delta(x), \tag{B.14}$$

where $\mathcal{P}$ denotes the principal part. Re-writing the above integral as

$$\widetilde{C}(s) = -i \int_{-\infty}^{\infty} d\omega' \ \frac{\overline{C}(\omega')}{\omega - \omega' - i\epsilon}, \tag{B.15}$$

and expanding $\frac{1}{(\omega - \omega') - i\epsilon}$ as suggested by Eq. (B.14), we have

$$\widetilde{C}(s) = -i \int_{-\infty}^{\infty} d\omega' \ \overline{C}(\omega') \mathcal{P}(\frac{1}{\omega - \omega'}) + \int_{-\infty}^{\infty} d\omega' \ \overline{C}(\omega') \pi\delta(\omega - \omega'). \tag{B.16}$$

Equating thus, from the real parts we obtain the following relation

$$\overline{C}(\omega) = \lim_{\epsilon \to 0} \frac{1}{\pi} \Re\{\widetilde{C}(s)\}. \tag{B.17}$$

Another way of obtaining this result is through the fact that a classical time auto-correlation function is a real and even function of time and thus $C^*(t) = C(t)$ and $C(-t) = C(t)$. Thus, its Fourier transform is also real and even function of ω i.e. $\overline{C}^*(\omega) = \overline{C}(\omega)$ and $\overline{C}(\omega) = \overline{C}(-\omega)$. Thus, $\overline{C}(\omega)$ may be written as a cosine transform

$$\begin{aligned} \overline{C}(\omega) &= \frac{1}{2\pi} \int_{-\infty}^{\infty} dt \ C(t) \cos(\omega t) \\ &= \frac{1}{\pi} \int_{0}^{\infty} dt \ C(t) \cos(\omega t) \\ &= \lim_{\epsilon \to 0} \frac{1}{\pi} \Re\{\widetilde{C}(s)\}. \end{aligned} \tag{B.18}$$

Appendix C

Simulation and Time Saving

C.1 Consistency Checks

During the course of simulation work, it is often useful to perform some consistency checks. Some of the checks that were performed during the course of this work are summarized below.

- *Kinetic Energy* From Eq. (2.48), we know that at thermal equilibrium, the Kinetic Energy(KE) per particle should reach $\frac{1}{2\Gamma}$. This is one of the principal tests that is performed with every simulation run. Figure C.1 shows a typical plot of the average KE per particle as a function of time for $\Gamma = 100$, $\gamma = 0.06$ and $\kappa = 1.0$. We can further note from this plot that fluctuations around the mean value of KE with time are fairly small, thus validating our assumptions of working in an isothermal system. For instance, typically after a long run (after $\approx \frac{10}{\gamma}$), we find that the mean= 0.0050 and standard deviation= 7.9 x 10^{-5}, both in reduced units.

- Another check is to plot the velocity distribution of dust particles in equilibrium. Figure C.1 clearly reveals a Maxwell distribution for the longitudinal component of velocity plotted at equilibrium.

- Another check is to calculate Eq. (4.16a) for the zeroth sum rule directly from the longitudinal current density auto-correlation function power spectrum. Since this sum rule is independent of the the particular nature of inter-particle potentials, it should evaluate to the thermal velocity, v_{th} providing another good consistency check, specially for any scaling related issues in the magnitude of the power spectral density.

C.2 Time Saving

As mentioned earlier, the most time consuming step of our simulation is that of force evaluation, since for a many-particle system interacting via pair-wise forces, visiting each particle and evaluating the resultant

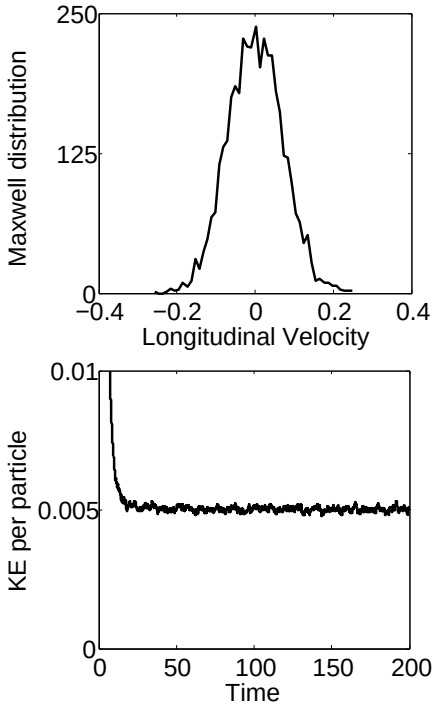

Figure C.1: Equilibrium velocity distribution(Top) of longitudinal component of velocity and the kinetic energy (Bottom) per particle showing the approach to equilibrium, both in reduced units.

force on it by every other particle could be very time consuming. There are however, some useful methods to reduce the overall simulation time and in the following we mention some of the methods that were used during the course of this work. An excellent reference for many more methods and for simulations in general is Allen [29].

- While evaluating the force on one particle, say the i-th particle, exerted by any other particle, say j-th particle, we can make use of Newton's third law and instead of just updating the resultant force on i-th particle, we can simultaneously do this for every j-th particle visited.

- The exponential term in the Yukawa force Eq. (2.9) decays as $\frac{1}{\kappa}$. Thus, we can expect that the force becomes virtually zero at around a cutoff distance $R_{cut} = \frac{10}{\kappa}$. Using this fact, we can divide our simulation grid into smaller cells with dimensions of the order of R_{cut} and maintain a list of neighboring particles. For instance, in this work, at every new step, particles were sorted according to the cell they were currently occupying, thus creating a list of neighboring particles. This can be done for instance, by using linked-lists in the C programming language. From this, the inter-particle forces were evaluated only for particles within a cell and occupying the nearest neighbor cells. Further, for every interaction whether it be within a cell or with particles in the neighboring cells, we used Newton's third law.

  This procedure has helped immensely in reducing the simulation time during the course of this work. For instance, for a system of $N = 2000$ particles, a full run to extract the longitudinal power

spectral density without this procedure takes around 3000-minutes CPU time, while with the aid of this procedure, we can reduce the time to around 45-50-minutes CPU time

C.3 Generation of Normal Random Variables in C Language

Since there is no built-in routine to generate normal random variables in C programming language, we use the following method as proposed by Gillespie [25].

- Generate two uniform random variables, U_1 and U_2.
- Normal random variable $N1 = \sqrt{[-2.00\log(U_1)]}\cos(2\pi U_2)$
- Normal random variable $N2 = \sqrt{[-2.00\log(U_1)]}\sin(2\pi U_2)$

C.4 Computation of Radial-Distribution Function and Static Structure Factor

- Being an isotropic homogenous system, the radial distribution function (RDF) Eq. (D.4), $g(|\mathbf{r}-\mathbf{r}'|)$ only depends upon the inter-particle separation distance r. Thus, starting with any given particle as center, we move in small steps of $dr \sim 0.02$ (in reduced units, as used in this work) and keep a count of the number of particles within the radial distance r to $r+dr$ as r is varied. This is followed by averaging over all particles in the system and over several time runs. The result is then normalized by the total number of particles within a differential area element $2\pi r dr$, i.e., $\sigma 2\pi r dr$ where σ is the area density of our 2D system. In Figure C.2 we show plots of the RDF for several values of coupling strength Γ.
- The static structure factor $S(k)$ is computed directly from simulation using its definition Eq. (D.5). Once the system reaches equilibrium, we compute this in steps of $dk = \frac{2\pi}{l}$, where l is the length of simulation cell in longitudinal direction, in reduced units. This is followed by a long time average of the same.

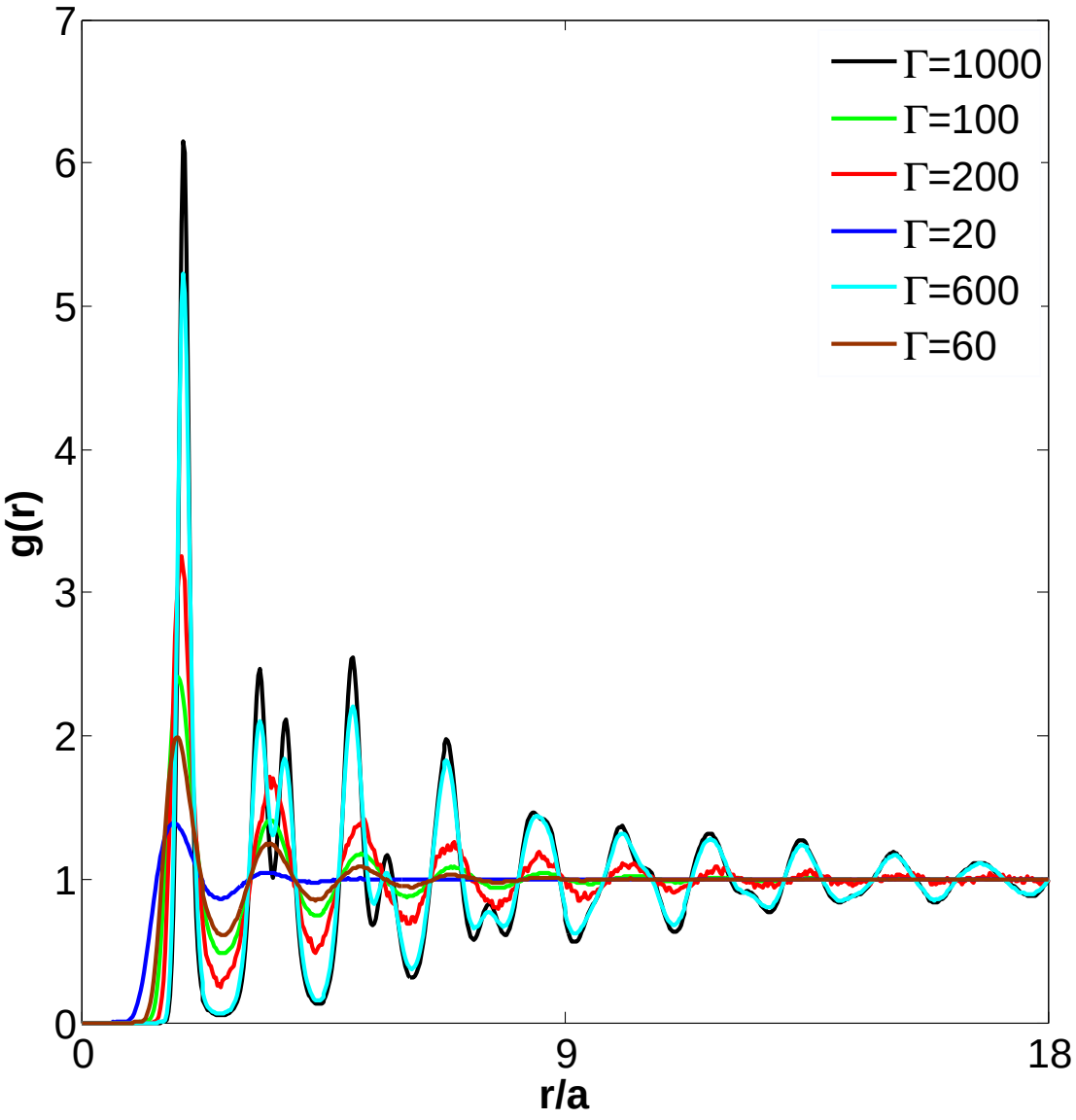

Figure C.2: Radial distribution function $g(r)$ as a function of the reduced distance r/a for Γ =20,60,100,200,600 and 1000 computed at $\kappa = 1.0$ and $\gamma = 0.06$.

Appendix D

Definitions from Statistical Mechanics

The following are some of the definitions used during the course of this work [39, 21, 11].

D.1 Dynamic Functions

- *Local Particle Density*

$$\rho(\mathbf{r},t) = \frac{1}{\sqrt{N}} \sum_{i=1}^{N} \delta(\mathbf{r} - \mathbf{r}_i(t)), \tag{D.1}$$

where N is the total number of particles in the system. Denoting the Fourier transform of local particle density as $\mathcal{F}[\rho(\mathbf{r})] = \rho_{\mathbf{k}}$, we have

$$\rho_{\mathbf{k}}(t) = \frac{1}{\sqrt{N}} \sum_{i=1}^{N} e^{-i\mathbf{k}\cdot\mathbf{r}_i(t)}. \tag{D.2}$$

- *Current Density*
  The particle current density is defined as

$$\mathbf{j}(\mathbf{r},t) = \frac{1}{\sqrt{N}} \sum_{i=1}^{N} \mathbf{v}_i(t)\delta(\mathbf{r} - \mathbf{r}_i(t)). \tag{D.3}$$

D.2 Static Functions

In this section we will focus only on static functions obtained once the system has reached equilibrium so that one may drop the time dependence from their definitions while explicitly using angular brackets to

denote ensemble averaging. For their practical use during the course of this work, this implies that these functions are evaluated at one instance of time, while the angular brackets are replaced by time averages by invoking the ergodic hypothesis. For the present, all derivations and definitions are theoretical though.

- *Pair Distribution Function*
  The pair distribution function, $g(\mathbf{r}, \mathbf{r}')$, is defined as

$$\rho^2 g(\mathbf{r}, \mathbf{r}') = \left\langle \sum_{i \neq j}^{N} \delta(\mathbf{r} - \mathbf{r}_i)\delta(\mathbf{r}' - \mathbf{r}_j) \right\rangle . \tag{D.4}$$

  For an isotropic homogenous system, $g(\mathbf{r}, \mathbf{r}') = g(|\mathbf{r} - \mathbf{r}'|)$ and is called the radial distribution function (RDF) in that case.

- *Static Structure Factor*
  The static structure factor, $S(\mathbf{k})$, can be measured experimentally and is related to the Fourier transform of RDF [21] as shown below.

$$\begin{aligned}
S(\mathbf{k}) &= \langle \rho_{\mathbf{k}} \rho_{-\mathbf{k}} \rangle , \\
&= \frac{1}{N} \left\langle \sum_{i=1}^{N} \sum_{j=1}^{N} e^{-i\mathbf{k}\cdot\mathbf{r}_i} e^{i\mathbf{k}\cdot\mathbf{r}_j} \right\rangle , \\
&= 1 + \frac{1}{N} \left\langle \sum_{i \neq j}^{N} e^{-i\mathbf{k}\cdot(\mathbf{r}_i - \mathbf{r}_j)} \right\rangle , \\
&= 1 + \frac{1}{N} \left\langle \sum_{i \neq j}^{N} \int\int d^2\mathbf{r} d^2\mathbf{r}' \; e^{-i\mathbf{k}\cdot(\mathbf{r}-\mathbf{r}')} \delta(\mathbf{r} - \mathbf{r}_i)\delta(\mathbf{r}' - \mathbf{r}_j) \right\rangle , \\
&= 1 + \frac{\rho^2}{N} \int\int d^2\mathbf{r} d^2\mathbf{r}' \; e^{-i\mathbf{k}\cdot(\mathbf{r}-\mathbf{r}')} g(\mathbf{r}, \mathbf{r}'),
\end{aligned} \tag{D.5}$$

  where in the last step we have interchanged the order of integration and angular ensemble averaging. Further, for an isotropic homogenous system, the last equation may be expressed as

$$\begin{aligned}
S(\mathbf{k}) &= 1 + \frac{\rho^2 A}{N} \int d^2\mathbf{r} \; e^{-i\mathbf{k}\cdot(|\mathbf{r}-\mathbf{r}'|)} g(|\mathbf{r} - \mathbf{r}'|), \\
&= 1 + \rho \int d^2\mathbf{r} \; e^{-i\mathbf{k}\cdot\mathbf{r}} g(\mathbf{r}) \\
&= 1 + \rho \int d^2\mathbf{r} \; e^{-i\mathbf{k}\cdot\mathbf{r}} \left[g(\mathbf{r}) - 1 \right] + (2\pi)^2 \rho \delta(\mathbf{k}).
\end{aligned} \tag{D.6}$$

  where in the last step we separated $[g(\mathbf{r}) - 1]$ out to ensure convergence. For all $\mathbf{k} \neq 0$, Eq. (D.6) can be taken as the working definition of the static structure factor.

- *Isothermal Compressibility*
  From thermodynamics, the isothermal compressibility is defined as

$$\chi_T = -\frac{1}{A} \left[\frac{\partial A}{\partial P} \right]_{N,T} , \tag{D.7}$$

where A is the area, P is the pressure and T is the temperature. Further, from statistical mechanics calculations in the grand canonical ensemble for a homogenous system, the isothermal compressibility can be expressed [21] as

$$k_B T \rho \chi_T = 1 + \rho \int d^2\mathbf{r} \ \left[g(\mathbf{r}) - 1 \right]. \tag{D.8}$$

From Eq. (D.6), it then follows that

$$S(\mathbf{k} \to 0) = k_B T \rho \chi_T. \tag{D.9}$$

Appendix E

Time Derivatives of Auto-Correlation Functions

These results are a reproduction of standard results for derivatives of time auto-correlation functions in references [21, 20] needed during the course of this work. Consider the derivative of a general auto-correlation function (for a stationary process) $C(t) = \langle A(t+s)A^*(s)\rangle$ with respect to t i.e.

$$\frac{d}{dt}C(t) = \frac{d}{dt}\left\langle A(t+s)A^*(s)\right\rangle .$$

But this vanishes from Eq. (4.20) for odd n.

Consider now the second derivative of an auto-correlation function for a stationary process with respect to the time difference t. Since the process is stationary, $\langle A(t+s)A^*(s)\rangle$ only depends upon the time difference. Using the dot notation for derivatives and following the derivation in[21]

$$\frac{d^2}{dt^2}\left\langle A(t+s)A^*(s)\right\rangle = \left\langle \frac{d^2}{dt^2}A(t+s)A^*(s)\right\rangle = \left\langle \ddot{A}(t+s)A^*(s)\right\rangle . \tag{E.1}$$

For an ergodic process, ensemble averaging is the same as time averaging. Thus, writing the above ensemble average as a time average,

$$\frac{d^2}{dt^2}\left\langle A(t+s)A^*(s)\right\rangle = \lim_{\tau\to\infty}\frac{1}{\tau}\int_0^\tau dt'\ \ddot{A}(t+t')A^*(t'). \tag{E.2}$$

Noting that $\left\langle \frac{d^2}{dt^2}A(t+s)A^*(s)\right\rangle = \left\langle \left[\frac{d^2}{dt^2}A(t)\right]_{t=s}A^*(s-t)\right\rangle$ allows us to integrate by parts giving,

$$\frac{d^2}{dt^2}\langle A(t+s)A^*(s)\rangle = \lim_{\tau\to\infty}\frac{1}{\tau}[\dot{A}(t+t')A^*(t')]_0^\tau - \lim_{\tau\to\infty}\frac{1}{\tau}\int_0^\tau dt'\ \dot{A}(t+t')\dot{A}^*(t'). \tag{E.3}$$

The first term on the right will evaluate to 0 since it is essentially the difference in the values of a time correlation function evaluated with origin at $t' = 0$ and $t' = \tau$, but with the same time difference t. Thus

we find,

$$\frac{d^2}{dt^2}\langle A(t+s)A^*(s)\rangle = -\langle \dot{A}(t+s)\dot{A}^*(s)\rangle. \tag{E.4}$$

Appendix F

Transverse Waves

The study of transverse wave propagation for dusty plasma has also aroused a lot of interest [8, 9], specially since ordinary fluids cannot support shear stress, and thus, there are no shear wave modes predicted from OH. Since our focus during the course of this work was mostly on longitudinal wave modes, we will not attempt to discuss transverse wave modes in much detail[1]. However, since the transverse wave modes can be observed easily from our simulation, and the theory of GH is capable of predicting their propagation, in this section we briefly outline their description along with some of the results we obtain from simulation.

The derivation of power spectral density for transverse waves proceeds exactly the same way as for longitudinal waves[2]. Beginning with Eq. (4.8c), we define the transverse current density auto-correlation function as

$$C_t(k,t) = \langle j_k^t(0)^* j_k^t(t) \rangle. \tag{F.1}$$

The time evolution of transverse current density auto-correlation is thus

$$\frac{\partial}{\partial t} C_t(k,t) = -\nu_1 k^2 C_t(k,t). \tag{F.2}$$

Eq. (F.2) thus suggests a purely dissipative behavior. Now, following the same derivation as for longitudinal wave modes, we introduce a transverse viscosity memory function, whereby Eq. (F.2) is modified to

$$\frac{\partial}{\partial t} C_t(k,t) = -k^2 \int_0^t dt' \; K_t(k, t-t') C_t(k,t'), \tag{F.3}$$

where $K_t(k, t-t')$ is the transverse viscosity memory function. Differentiating Eq. (F.3) once, we see that the initial value of the transverse viscosity memory function must satisfy the condition

$$K_t(k, t=0) = \frac{\langle \omega_t^2(k) \rangle}{k^2 v_{th}^2}, \tag{F.4}$$

[1] In particular, we will avoid any analysis of the cut-off wave-number predicted for their propagation [9].

[2] All quantities are assumed to be in reduced units.

where $\langle\omega_t^2(k)\rangle = -\left[\frac{\partial^2}{\partial t^2}C_t(k,t)\right]_{t=0}$ is defined as the second moment of the transverse current density auto-correlation function. Solving Eq. (F.3) by taking its Laplace transform and setting $s = i\omega$, we get the power spectral density as the real part of the aforementioned Laplace transform

$$P_t(k,\omega) = 2v_{th}^2 \frac{k^2 K_t'(k,\omega)}{[\omega + k^2 K_t''(k,\omega)]^2 + [k^2 K_t'(k,\omega)]^2}, \tag{F.5}$$

where we have defined the real and imaginary parts of Laplace transformed transverse viscosity memory function as

$$\mathcal{L}[K_t(k,t)]_{s=i\omega} = K_t'(k,\omega) + iK_t''(k,\omega). \tag{F.6}$$

Inclusion of neutral friction in the above model can be accomplished analogously to the longitudinal wave mode power spectral density as

$$P_t(k,\omega) = 2v_{th}^2 \frac{k^2 K_t'(k,\omega) + \xi}{[\omega + k^2 K_t''(k,\omega)]^2 + [k^2 K_t'(k,\omega) + \xi]^2}. \tag{F.7}$$

We next compare results for an exponential model of $K_t(k,t)$ with simulation data.

F.1 Simulation Results

Transverse or shear wave modes only exist for higher coupling strengths Γ. This is because, low Γ typically characterizes fluid like behavior, and fluids cannot resist any shear stress. Thus, wave propagation will only be supported at higher Γ. In the following we will try and compare simulation results with the model from GH for a typical case of $\Gamma = 100$, $\kappa = 1.0$, and for a value of neutral friction γ=0.06 and try to discuss the trend.

We first define an exponential model for the transverse viscosity memory function as

$$K_t(k,t) = K_t(k,0)e^{-\frac{t}{\tau_t}}, \tag{F.8}$$

where $K_t(k,0)$ is given by Eq. (F.4) and τ_t, is the relaxation time assumed to be independent of k. A typical dispersion plot evaluated from Eq. (F.5) for $\Gamma = 100$ and for neutral friction $\gamma = 0.06$ with a corresponding value of $\tau_t = 5.0$ chosen to match the simulation data is given in Figure F.1. Further, some profile plots with $\Gamma = 100, \gamma = 0.06$ are shown in Figure F.2.

We can see that by choosing the appropriate fitting parameter, reasonably good fits with the dispersion curve and also to some extent, for the profile plots may be obtained. Further, analogous to the high relaxation time limit for the longitudinal wave dispersion relation, if $\omega\tau_t \gg 1$, the dispersion relation again takes the form $\omega = \omega_\infty(k)$, where

$$\omega_\infty^2(k) = \frac{\langle\omega_t^2(k)\rangle}{v_{th}^2}. \tag{F.9}$$

This has been shown as the green curve in Figure F.1 and is seen to be a good semi-analytical approximation.

An attempt to further improve on the model and circumvent the use of a free parameter for the relaxation time by evaluating the fourth moment (analogous to the case of the longitudinal wave dispersion modes) and subsequently use a Gaussian model for the transverse viscosity memory function was also made. However, the Gaussian model was seen to have much flatter profile curves at small values of wave number k (showing no peaks in the profile plots), and the model in general displayed poorer performance in comparison to the exponential model described above.

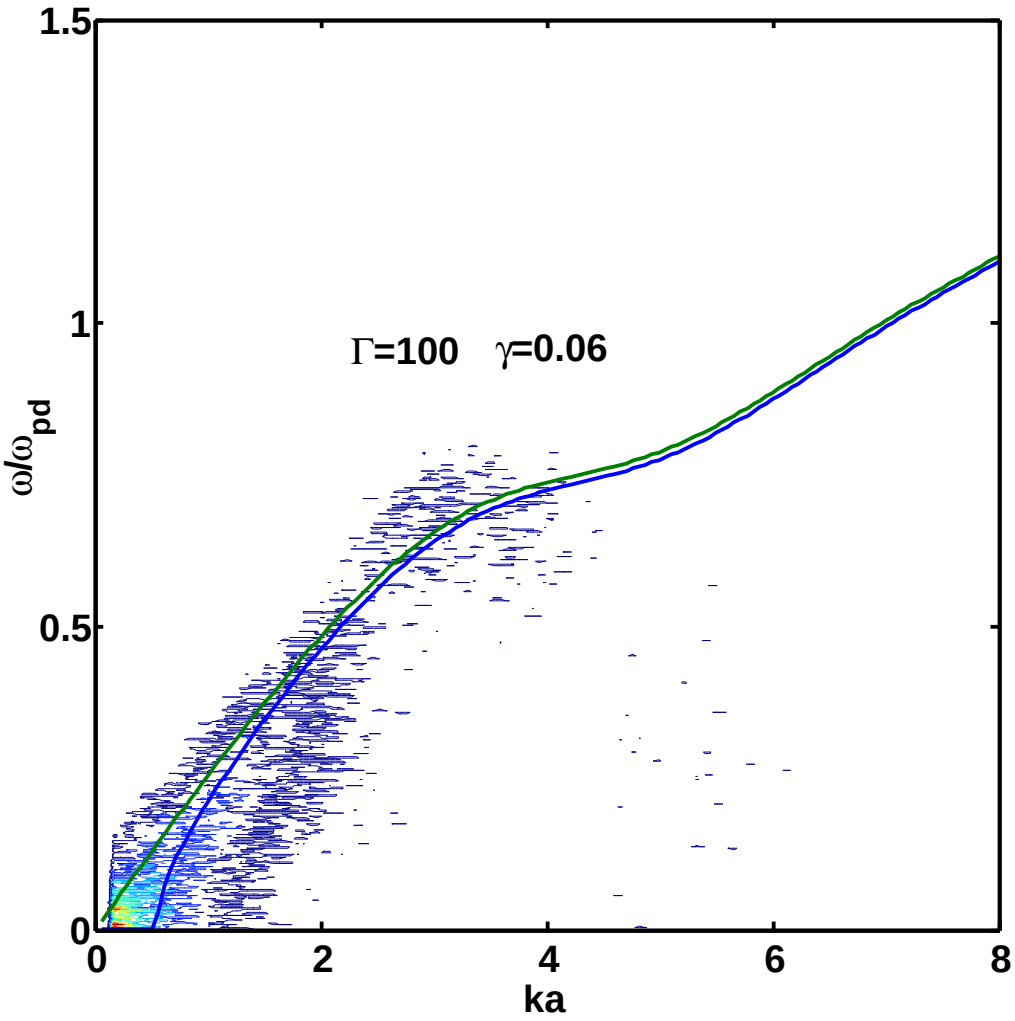

Figure F.1: Reduced transverse wave dispersion curves against simulation data for $\Gamma = 100$, $\kappa = 1.0$ and $\gamma = 0.06$. Blue curve represents the exponential model for the transverse viscosity memory function with $\tau_t = 5.0$, the green curve represents the dispersion curve evaluated in the limit of large relaxation time $\omega_\infty(k)$, while the background noisy plot is from simulation.

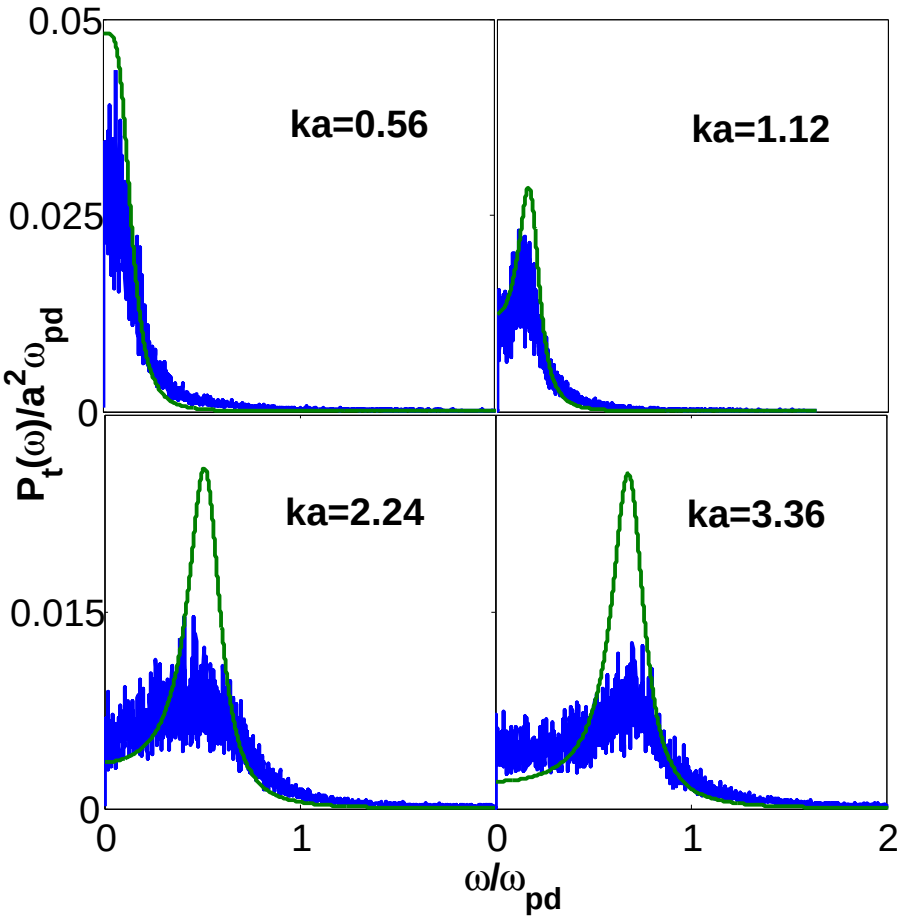

Figure F.2: Reduced transverse spectral density profile curves versus reduced frequency ω/ω_{pd} from simulation (noisy curves) and exponential model (dashed curves) for $\Gamma = 100$, $\kappa = 1.0$ and $\gamma = 0.06$ at different reduced wave-numbers.

Appendix G

Gear Like Predictor Corrector Time Stepping Algorithm

In direct analogy with simulations in deterministic systems, the Gear-like Predictor-Corrector (PC) methods for BD simulation also include three stages, namely, predicting, force evaluating, and correcting [27]. The difference is that one has to add random displacements of the velocity and position by using Eq. (3.46) at the end of a time step to complete the BD simulation. The basic procedure goes as follows.

G.1 Prediction Stage

In this stage, one has:

$$\begin{aligned}
\mathbf{r}^P &= \mathbf{r}_0 + c_1\mathbf{v}_0 t + c_2\mathbf{a}_0 t^2 + c_3\dot{\mathbf{a}}_0 t^3 + c_4\ddot{\mathbf{a}}_0 t^4 + c_5\dddot{\mathbf{a}}_0 t^5 \\
\mathbf{v}^P &= c_0\mathbf{v}_0 + c_1\mathbf{a}_0 t + c_2\dot{\mathbf{a}}_0 t^2 + c_3\ddot{\mathbf{a}}_0 t^3 + c_4\dddot{\mathbf{a}}_0 t^4 \\
\mathbf{a}^P &= \mathbf{a}_0 + \dot{\mathbf{a}}_0 t + \frac{1}{2!}\ddot{\mathbf{a}}_0 t^2 + \frac{1}{3!}\dddot{\mathbf{a}}_0 t^3 \\
\dot{\mathbf{a}}^P &= \dot{\mathbf{a}}_0 + \ddot{\mathbf{a}}_0 t + \frac{1}{2!}\dddot{\mathbf{a}}_0 t^2 \\
\ddot{\mathbf{a}}^P &= \ddot{\mathbf{a}}_0 + \dddot{\mathbf{a}}_0 t \\
\dddot{\mathbf{a}}^P &= \dddot{\mathbf{a}}_0,
\end{aligned} \tag{G.1}$$

where as usual bold-face letters indicate a vector representation of position, velocity, acceleration and higher-order derivatives of acceleration and the superscript P is to indicate that these are quantities in the predicting stage. (For simplicity, we have written $a^n(0) = a_0^n$ from Eq. (3.7) and dropped derivatives of $\mathbf{a}(t)$ higher than the third order, but extensions to higher orders are quite straightforward.) One may notice in Eq. (G.1) that we have used in Eq. (3.32) and Eq. (3.17) the means of the position and velocity instead of using Taylor series of the position and velocity, as is normally done in the Gear method for MD

simulation [27]. Other than that, the remaining parts of this stage (derivatives of the force) are essentially the same as those in the MD simulation.

G.2 Force Evaluation

In this stage, the predicted position $\mathbf{r}^P(t)$ is used to obtain a new force, that is, new acceleration $\mathbf{a}(t)$, and a difference between the predicted acceleration $\mathbf{a}^P(t)$ and the new acceleration $\mathbf{a}(t)$ is formed:

$$\Delta\mathbf{a} = \left[\mathbf{a}(t) - \mathbf{a}^P(t)\right]. \tag{G.2}$$

It can be seen that this step is exactly the same as in MD simulation [29].

G.3 Correction

In this stage, the above difference term is used to correct all predicted positions and their "derivatives", as follows:

$$\begin{aligned}
\mathbf{r}^C &= \mathbf{r}^P + 2c_2\alpha_0\Delta\mathbf{R2} \\
\mathbf{v}^C t &= \mathbf{v}^P t + c_1\alpha_1\Delta\mathbf{R2} \\
\frac{\mathbf{a}^C t^2}{2!} &= \frac{\mathbf{a}^P t^2}{2!} + \alpha_2\Delta\mathbf{R2} \\
\frac{\dot{\mathbf{a}}^C t^3}{3!} &= \frac{\dot{\mathbf{a}}^P t^3}{3!} + \alpha_3\Delta\mathbf{R2} \\
\frac{\ddot{\mathbf{a}}^C t^4}{4!} &= \frac{\ddot{\mathbf{a}}^P t^4}{4!} + \alpha_4\Delta\mathbf{R2} \\
\frac{\dddot{\mathbf{a}}^C t^5}{5!} &= \frac{\dddot{\mathbf{a}}^P t^5}{5!} + \alpha_5\Delta\mathbf{R2}
\end{aligned} \tag{G.3}$$

with

$$\Delta\mathbf{R2} \equiv \frac{\Delta\mathbf{a}t^2}{2!}, \tag{G.4}$$

and the coefficients α_i are given in the following table:

α_i	3th-order	4th-order	5th-order
α_0	$\frac{1}{6}$	$\frac{19}{120}$	$\frac{3}{16}$
α_1	$\frac{5}{6}$	$\frac{3}{4}$	$\frac{251}{360}$
α_2	1	1	1
α_3	$\frac{1}{3}$	$\frac{1}{2}$	$\frac{11}{18}$
α_4	0	$\frac{1}{12}$	$\frac{1}{6}$
α_5	0	0	$\frac{1}{60}$

This table is simply a reproduction of those in Refs. [27, 29], and is provided here for completeness. By using parameters in different columns, one may realize 3rd-, 4th-, and 5th-order (or 4-, 5- and 6-value) Gear-like algorithms for BD simulation. Note that the first two lines in Eq. (G.3) are slightly different from those in MD simulation, in order to restore the damping effect on deterministic acceleration, and to keep the consistency with the corresponding terms in Eq. (3.32) and Eq. (3.17) [or the first two lines in Eq. (G.1)].

G.4 Adding Random Displacements

The above three stages are the same as those of Gear's algorithm for MD simulation. However, to complete the BD simulation, we have to use the updating formulae Eq. (3.46) to add random displacements of the velocity and position. It should be noted that now the corrected values $\mathbf{r}^C$ and $\mathbf{v}^C$ should be used in the places of $\langle \mathbf{r} \rangle$ and $\langle \mathbf{v} \rangle$ in Eq. (3.46) respectively. Also note that, to implement the simulation, one needs the initial conditions, $\mathbf{r}_0$, $\mathbf{v}_0$, $\mathbf{a}_0$, $\dot{\mathbf{a}}_0$, $\ddot{\mathbf{a}}_0$ and $\dddot{\mathbf{a}}_0$, at $t = 0$. This poses a problem for the very first several steps of simulation, because $\dot{\mathbf{a}}_0$, $\ddot{\mathbf{a}}_0$ and $\dddot{\mathbf{a}}_0$ are undefined. The simplest way to get around this issue is to set all of them to be zero at the very first step, which is what we do in this work. Subsequent updates of higher derivatives are obtained as

$$\begin{aligned}
\frac{d}{dt}\left[e^{-\gamma t}\frac{d\langle \mathbf{v}\rangle'}{dt}\right] &= \dot{\mathbf{a}}(t) = \dot{\mathbf{a}}_0 + \ddot{\mathbf{a}}_0 t + \frac{1}{2!}\dddot{\mathbf{a}}_0 t^2 + \cdots \\
\frac{d^2}{dt^2}\left[e^{-\gamma t}\frac{d\langle \mathbf{v}\rangle'}{dt}\right] &= \ddot{\mathbf{a}}(t) = \ddot{\mathbf{a}}_0 + \dddot{\mathbf{a}}_0 t + \cdots \\
\frac{d^3}{dt^3}\left[e^{-\gamma t}\frac{d\langle \mathbf{v}\rangle'}{dt}\right] &= \dddot{\mathbf{a}}(t) = \dddot{\mathbf{a}}_0 + \cdots
\end{aligned} \tag{G.5}$$

The above are the basic procedures for the Gear-like PC method for BD simulation. It should be restated that these formulae and the simulation stages are quite similar to those in the Gear method for MD simulation of Newton's equations [27, 29], except for the expressions for the velocity and position in Eq. (G.1) and Eq. (G.3), and for the addition of random displacement at the end of every time step. When $\gamma \to 0$, the Gear-like method goes over to the Gear method for MD simulation.

Glossary

$C_{l,t}(k,t)$	longitudinal, transverse current density auto-correlation function in wave number and time space
$F(r)$	magnitude of inter-particle central force
N	total number of particles
$N(0,1)$	normal random variable with mean 0 and variance 1
$P_{l,t}(k,w)$	longitudinal, transverse current density auto-correlation function power spectrum (power spectral density)
R	magnitude of inter-particle separation in three-Dimensions
$S(k)$	Static-structure factor
T	Temperature
$U(r)$	Potential Energy
Γ	Coupling strength
β	$\sqrt{\frac{\gamma}{\Gamma}}$
γ	neutral drag coefficient in reduced units
κ	screening length
λ_D	Debye length
$\mathbf{R}$	vector inter-particle separation in three-Dimensions
$\mathbf{j}(\mathbf{r},t)$	current density in position and time space
$\mathbf{j}_k^{l,t}(t)$	longitudinal, transverse current density in wave number and time space
$\mathbf{k}$	vector in wave number space
$\mathbf{r}$	vector inter-particle separation in two-Dimensions
∇	Gradient operator
ν	viscosity

ω	frequency
ω_{pd}	plasma dust natural frequency
ϕ	electrostatic potential
ρ	number density of dust particles in continuum description
ξ	neutral drag coefficient
a	characteristic length scale, average separation between dust particles
$g(r)$	radial distribution function
k	magnitude of wave number
k_B	Boltzmann constant
$m_{e,i,d}$	mass of electron, ion or dust particle
n_α	number density of specie α
q_α	charge on specie α
r	magnitude of inter-particle separation in two-Dimensions
v	velocity
v_{th}	Thermal velocity=$\sqrt{\frac{k_B T}{m}}$

Table of Relevant Reduced Variables

Dimensional Variable/Parameters	Scaling Factor
t	$1/\omega_{pd}$
r	a
v	$a\omega_{pd}$
k	$1/a$
ξ	ω_{pd}
$U(r)$	$2\frac{q_d^2}{a}$
$P(k,\omega)$	$a^2\omega_{pd}$

Most other variables of interest maybe derived from these.

Bibliography

[1] G.E. Morfill and H. Thomas. *Plasma crystal. J. Vac. Sci. Technol. A*, 14(2) (1995) 490. ix, 4

[2] P.K. Shukla and A.A. Mamun. *Introduction to dusty plasma Physics.* Institute of Physics Publishing, Bristol, (2002). 1, 2, 8

[3] P.K. Shukla and B. Eliasson. *Colloquium: Fundamentals of dust-plasma interactions. Rev. Mod. Phys.*, 81 (2009) 25. 2

[4] H. Thomas et al. *Plasma Crystal: Coulomb crystallization in Dusty Plasma. Phys. Rev. Lett*, 73 (1994) 652. 2

[5] S.V. Vladimirov and M. Nambu. *Attraction of charged particulated in plasma with finite flows. Phys. Rev. E*, 52 (1995) R2172. 3

[6] L.J. Hou, Y.N. Wang and Z. L. Mišković. *Interaction potential among dust grains in a plasma with ion flow. Phys. Rev. E.*, 64 (2001) 046406. 3, 7, 55, 56

[7] N. Upadhyaya, L.J. Hou and Z. L. Mišković. *Structure of 2D dusty plasmas in the presence of perpendicular ion flow. Phys. Lett. A*, (2010) 19507. 3

[8] L.J. Hou, Z. L. Mišković, A. Piel, and M.S. Murillo. *Wave spectra of two-dimensional dusty plasma solids and liquids. Phys. Rev. E*, 79 (2009) 046412. 4, 8, 10, 38, 40, 46, 61, 79

[9] M. S. Murillo. *Critical Wave Vectors for Transverse Modes in Strongly Coupled Dusty Plasmas. Phys. Rev. Lett.*, 85 (2000) 2514. 4, 29, 35, 79

[10] P.K. Kaw and A. Sen. *Low frequency modes in strongly coupled dusty plasmas. Physic of Plasmas*, 5 (1998) 3552. 4, 10, 12, 35, 36

[11] H.B. Callen. *Thermodynamics and Introduction to Thermostatistics.* John Wiley and Sons, Inc. Singapore, (1985). 4, 17, 74

[12] M. Scott. *Applied Stochastic Processes in Science and Engineering, University of Waterloo*, (2009). 4, 18, 32

[13] A. Zee. *Quantum Field Theory in a Nutshell.* Princeton University Press, USA, (2009). 7

[14] L.J. Hou, Y.N. Wang and Z. L. Mišković. *Theoretical study of laser excited Mach cones in dusty plasma. Phys. Rev. E*, 70 (2004) 056406. 8

[15] N.N. Rao, P.K. Shukla and M.Y. Yu. *Dust acoustic waves in dusty plasmas. Planet. Space Sci.*, 38 (1990) 543. 8

[16] Z. Donko, J. Goree, P. Hartmann and K. Kutasi. *Shear viscosity and shear thinning in Two-Dimensional Yukawa Liquids. Phys. Rev Lett.*, 96 (2006) 145003. 10

[17] B. Liu and J. Goree. *Shear Viscosity of Two-Dimensional Yukawa Systems in the Liquid State. Phys. Rev Lett.*, 94 (2005) 185002. 10

[18] K.I. Golden and G.J. Kalman. *Quasilocalized charge approximation in strongly coupled plasma physics. Physics of Plasmas*, 7 (1999) 14. 10

[19] D. Chandler. *Introduction to Modern Statistical Mechanics.* Oxford University Press, New York, (1987). 11, 38

[20] J.P. Boon and S. Yip. *Molecular Hydrodynamics.* McGraw-Hill, (1980). 11, 14, 30, 31, 33, 34, 35, 40, 61, 64, 77

[21] J.P. Hansen and I.R. McDonald. *Theory of simple liquids.* Academic Press Inc, London, (1986). 11, 14, 29, 30, 31, 32, 34, 36, 61, 68, 74, 75, 76, 77

[22] F.S. Crawford. *Berkley Physics Course - volume 3.* Mcgraw Hill Book Company, New York, (1968). 12, 13

[23] I.Z. Fisher. *Statistical Theory of Liquids.* University of Chicago Press, Chicago and London, (1964). 14

[24] S. Chandrashekhar. *Brownian Motion, Dynamical Friction and Stellar Dynamics. Rev. Modern Phys.*, 21 (1949) 383. 16

[25] D.T. Gillespie. *Markov Processes: An introduction for physical scientists.* Academic Press, Inc. USA, (1992). 17, 18, 26, 72

[26] D.S. Lemons. *An Introduction to Stochastic Processes in Physics.* The John Hopkins University Press, USA, (2002). 18, 20, 24, 25, 26

[27] L.J. Hou and Z. L. Mišković. *A Gear-like Predictor-Corrector method for Brownian Dynamics Simulation. http://arxiv.org/abs/0806.3912v2*, (2008). 20, 21, 25, 26, 84, 85, 86

[28] R.J. Leveque. *Finite Difference methods for Differential Equations, University of Washington*, (2005). 26

[29] M.P. Allen and D.J. Tildesley. *Computer Simulation of Liquids.* Oxford University Press, New York, (1989). 26, 27, 41, 71, 85, 86

[30] L.D. Landau and E.M. Lifshitz. *Fluid Mechanics - Volume 6 of course of Theoretical Physics.* Pergamon Press, Great Britain, (1987). 28, 29

[31] V. Nosenko and J. Goree. *Shear Flows and Shear Viscosity in a Two-Dimensional Yukawa System (Dusty Plasma). Phys. Rev. Lett.*, 93 (2004) 155004. 28

[32] J.L. Barrat, J.P. Hansen and H. Totsuji. *Collective modes and single-particle motion in Yukawa fluids near freezing. J. Phys. C.*, 21 (1988) 4511. 29, 36, 37, 62

[33] Z.Donko, J.Goree, P. Hartmann and B. Liu. *Time-correlation functions and transport coefficients of two-dimensional Yukawa liquids. Phys. Rev E.*, 79 (2009) 026401. 30

[34] W. Hess and R. Klein. *Generalized hydrodynamics of systems of Brownian particles. Adv. Phys.*, 32 (1983) 173. 35, 36, 38

[35] S. Toxvaerd. *Solution of the Generalized Langevin equation. J. Chem Phys.*, 82 (1985) 5658. 38

[36] B.P. Lathi. *An introduction to Random signals and Communication theory.* International Textbook Company, Pennsylvania, (1968). 41

[37] C. Kittel. *Introduction to Solid state Physics.* John Wiley and Sons, Inc. New York, (1953). 62

[38] N. Ailawadi, A. Rahman and R. Zwanzig. *Generalized Hydrodynamics and Analysis of Current Correlation Functions. Phys. Rev. A*, 4 (1971) 1616. 62

[39] R. Wickham. *Statistical Mechanics Lecture Notes - Physics 704, University of Waterloo*, (2009). 74